

# The Influence of Temperature on Dynamic Membrane Structure

By  
Bochao Xu

Supervisor: Dr. Wa Gao  
Co-Supervisor: Dr. Baoqiang Liao

A thesis  
Presented to Lakehead University in partial fulfilment of the requirements for Master of Science  
in Environmental Engineering

Department of Environmental Engineering  
Lakehead University  
Thunder Bay, Ontario, Canada  
P7B 5E1

## ABSTRACT

This study investigates the influences of cold source-water temperatures and warm temperature recoveries on the dynamic changes of membrane structure. The morphology of membrane pores on the membrane surface was firstly compared through SEM images. The visual comparisons of the images show that the shrinkage of membrane pores occurred in the cold-water (0.3, 5, 10°C) treatments and could then be recovered in the warm-water (room temperature and 35°C) remediation. Furthermore, the dynamic changes in membrane pore sizes during cold temperature and recovery treatments were illustrated by the percentile membrane diameters — d10, d50 and d90. The membrane pore sizes in cold-water treatment at 0.3°C shrank faster and were smaller than those of 5 and 10°C. The recovery treatment at 35°C, which fully recovered the membrane pore sizes to those of virgin membrane, was much more effective than room temperature treatment. Room temperature recovery only restored the membrane pores close but not exceeding the original sizes under tested conditions. Both cold temperature treatments and warm water recoveries stabilized the membrane pore sizes after around 24 hours. Finally, membrane structure changes over time have been modelled. It implied that warm water cleaning could retrieve the membrane structure losses affected by cold source water.

**Keywords:** Ultrafiltration, membrane structure, dynamic membrane structure, pore size, cold water temperature, warm water temperature, pore size shrinkage, pore size expansion.

## ACKNOWLEDGMENTS

I would like to sincerely thank my supervisor Dr. Wa Gao and my co-supervisor Dr. Baoqiang Liao, for their invaluable supervision and support in forming this thesis. Their profound and sophisticated knowledge of water treatment and membrane technology helped me accomplish the experiment and the dissertation. I also wish to thank Dr. Guosheng Wu from the instrumentation lab for the guidance in utilizing SEM.

I would appreciate the industrial advisor Mr. Walter Turek, process engineer from the Bare Point Drinking Water Membrane Filtration Plant, City of Thunder Bay, for his guidance, support, and help in this study. I also acknowledge the financial support of NSERC, City of Thunder Bay, and Lakehead University for this study.

Finally, I am grateful to my parents and family, who have supported me throughout my life. In addition, I want to thank my friends for their company in this exceptional adventure. 😊

# TABLE OF CONTENTS

<b>ABSTRACT.....</b>	<b>I</b>
<b>TABLE OF CONTENTS .....</b>	<b>III</b>
<b>LIST OF FIGURES .....</b>	<b>V</b>
<b>LIST OF TABLES .....</b>	<b>VII</b>
<b>LIST OF NOMENCLATURE .....</b>	<b>VIII</b>
<b>CHAPTER 1 INTRODUCTION .....</b>	<b>1</b>
<b>CHAPTER 2 LITERATURE REVIEW .....</b>	<b>5</b>
2.1 OVERVIEW OF MEMBRANE FILTRATION .....	5
2.2 MEMBRANE MATERIALS.....	6
2.3 MEMBRANE FOULING.....	7
2.3.1 <i>Fouling characteristics</i> .....	8
2.3.2 <i>Factors impacting membrane fouling</i> .....	11
2.4 TEMPERATURE IMPACTS ON MEMBRANE FILTRATION .....	15
2.4.1 <i>Temperature impacts on fouling</i> .....	15
2.4.2 <i>Impacts on permeability and performance</i> .....	23
2.4.3 <i>Impacts on structure and integrity</i> .....	26
2.4.4 <i>Impacts of temperature on membrane cleaning</i> .....	29
<b>CHAPTER 3 METHODOLOGY .....</b>	<b>35</b>
3.1 MATERIALS AND APPARATUS.....	35
3.2 EXPERIMENT PROCEDURES.....	35
3.3 SAMPLE COLLECTION AND ANALYSIS.....	37
3.4 DATA ANALYSIS .....	38

<b>CHAPTER 4 RESULTS .....</b>	<b>42</b>
4.1 TEMPERATURE IMPACTS ON MEMBRANE PORE SIZE DISTRIBUTION .....	42
4.1.1 <i>Morphology of membrane surface from SEM images</i> .....	42
4.1.2 <i>Temperature effects on membrane pore size and size distribution</i> .....	46
4.1.3 <i>Effects of recovery temperature on membrane pore size and size distribution</i> .....	48
4.2 DYNAMIC CHANGES IN MEMBRANE PORE SIZES .....	50
4.2.1 <i>Dynamic changes in membrane pore sizes during cold temperature treatment</i> .....	50
4.2.2 <i>Dynamic changes in membrane pore size during recovery treatments</i> .....	54
4.3 MODELLING OF DYNAMIC CHANGES IN MEMBRANE PORE SIZES .....	60
4.3.1 <i>Modelling for cold temperature treatment</i> .....	60
4.3.2 <i>Modelling for recovery treatment</i> .....	67
<b>CHAPTER 5 DISCUSSION .....</b>	<b>74</b>
<b>CHAPTER 6 CONCLUSION.....</b>	<b>82</b>
<b>REFERENCE.....</b>	<b>83</b>

## LIST OF FIGURES

Figure 2.1.1 Pressure-driven membrane process application guide (Edzwald 2011).....	6
Figure 3.4.1 Effect of the counted number of pores on the randomization of the measured MPSD. (a) percentile pore diameters d10, d50 and d90 expressed as “average $\pm$ standard deviation for three data sets” and (b) accumulated frequency of pore diameters (sample origin from 5CT-ET-24h).....	39
Figure 4.1.1 SEM images of membranes: a) 0.3CT-VM, b) 0.3CT-14d, c) 5CT-VM, d) 5CT-15d, e) 10CT-VM and e) 10CT-14d.....	43
Figure 4.1.2 SEM images of membranes: a) 0.3CT-VM, b) 0.3CT-RT-4d, c) 0.3CT-ET-4d, d) 5CT-VM, e) 5CT-RT-6d, f) 5CT-ET-6d, g) 10CT-VM h)10CT-RT-4d and i)10CT-ET-4d. .....	45
Figure 4.1.3 Membrane pore size distributions (accumulative frequencies) in the steady states of cold temperature treatments (0.3CT, 5CT and 10CT).....	47
Figure 4.1.4 Membrane pore size distributions (accumulative frequencies) in the steady states of recovery treatments (0.3CT-RT/ET, 5CT-RT/ET and 10CT-RT/ET) .....	49
Figure 4.2.1 Dynamic changes in membrane pore size during 0.3°C (0.3CT), 5°C (5CT) and 10°C (10CT) cold temperature treatments.....	51
Figure 4.2.2 Recovery of membrane pore sizes at room temperature (RT) and 35°C (ET) following 0.3°C cold temperature .....	55
Figure 4.2.3 Recovery of membrane pore sizes at room temperature (RT) and 35°C (ET) following 5°C cold temperature .....	56
Figure 4.2.4 Recovery of membrane pore sizes at room temperature (RT) and 35°C (ET) following 10°C cold temperature .....	57

Figure 4.3.1 Fitting curves for Nd10, Nd50 and Nd90 versus time in 0.3°C cold temperature treatment .....	62
Figure 4.3.2 Fitting curves for Nd10, Nd50 and Nd90 versus time in 5°C cold temperature treatment .....	63
Figure 4.3.3 Fitting curves for Nd10, Nd50 and Nd90 versus time in 10°C cold temperature treatment .....	64
Figure 4.3.4 Comparison of CT effects on Nd10 vs. Time .....	66
Figure 4.3.5 Comparison of CT effects on Nd50 vs. Time .....	66
Figure 4.3.6 Comparison of CT effects on Nd90 vs. Time .....	66
Figure 4.3.7 Fitting curves for Nd10, Nd50 and Nd90 versus time in recovery treatments in the subsequence of 0.3CT treatment .....	68
Figure 4.3.8 Fitting curves for Nd10, Nd50 and Nd90 versus time in recovery treatments in the subsequence of 5CT treatment .....	69
Figure 4.3.9 Fitting curves for Nd10, Nd50 and Nd90 versus time in recovery treatments in the subsequence of 10CT treatment .....	70
Figure 4.3.10 Comparison of recovery temperature effects on Nd10 vs. Time .....	72
Figure 4.3.11 Comparison of recovery temperature effects on Nd50 vs. Time .....	73
Figure 4.3.12 Comparison of recovery temperature effects on Nd90 vs. Time .....	73

## LIST OF TABLES

Table 2.4.1 Summary of the impacts of temperature on membrane fouling.....	20
Table 2.4.2 Summary of the impacts of temperature on permeability and performance.....	25
Table 2.4.3 Summary of the impacts of temperature on structure and integrity .....	28
Table 2.4.4 Summary of the impacts of temperature on cleaning .....	33
Table 3.2.1 Measuring periods of cold temperature treatment.....	36
Table 3.2.2 Measuring periods of recovery treatment .....	37
Table 4.2.1 Summary of the d10, d50, and d90 in different cold temperature treatment conditions at 0h, 5h and 24h. ....	52
Table 4.2.2 Membrane pore size changing rates during initial 5 hours of cold temperature treatment .....	52
Table 4.2.3 ANOVA and student t-test results (p-values) of d10, d50 and d90 for temperature factor after 24h treatment at cold temperatures.....	53
Table 4.2.4 Recovery of d10, d50, and d90 after 0, 5h and 24h with warm water (room temperature and 35°C) treatments .....	57
Table 4.2.5 Membrane pore size changing rates during initial 5 hours of warm water (room temperature and 35°C) treatments .....	59
Table 4.2.6 ANOVA and student t-test results (p-values) of d10, d50 and d90 for temperature factor after 24h treatment at warm temperatures .....	59

## LIST OF NOMENCLATURE

AFM	Atomic force microscopy
AnMBR	Anaerobic membrane bioreactor
ANOVA	Analysis of Variance
BSA	Bovine serum albumin
CA	Cellulose acetate
CN	Cellulose nitrates
COD	Chemical oxygen demands
CT	Cold temperature
CTA	Cellulose triacetate
CTS	Climate testing systems
d	Day
d 10 / 50 / 90	Percentile diameter 10% / 50% / 90%
DCAA	Dichloroacetic acid
EDTA	Ethylenediamine tetra-acetic acid
EPS	Extracellular polymeric substances
ET	Elevated temperature
FO	Forward osmosis
GO	Graphene oxide
h	Hour
HAAs	Haloacetic acids
HANs	Haloacetonitriles
HKs	Haloketones
HRT	Hydraulic retention time
MBR	Membrane bioreactor
MF	Microfiltration
MPSD	Membrane pore size distribution
Nd 10 / 50 / 90	Normalized percentile diameter 10% / 50% / 90%
NF	Nanofiltration

NOM	Natural organic matter
PAA	Poly acrylic acid
PAC	Poly aluminum chloride
PAN	Polyacrylonitrile
PE	Polyethylene
PES	Polyethersulfone
PI	Polyimide
PP	Polypropylene
PS	Polysulphone
PSU	Polysulfone
PTFE	Polytetrafluoroethylene
PVA	Polyvinyl alcohol
PVDF	Polyvinylidene fluoride
PVP	Polyvinylpyrrolidone
RO	Reverse osmosis
RT	Room temperature
SAnMBR	Submerged anaerobic membrane bioreactor
SBR	Sequencing batch reactor
SDS	Sodium dodecyl sulphate
SEM	Scanning electron microscope
SMP	Soluble microbial products
TCM	Trichloromethane
TCNM	Trichloronitromethane
THMs	Trihalomethanes
TMP	Transmembrane pressure
UF	Ultrafiltration
VM	Virgin membrane
WWTP	Wastewater treatment plant

## CHAPTER 1 Introduction

Drinking water treatment is essential in sustaining the daily life of human beings, and economical and efficient technologies are always the target in the development of producing safe drinking water (Canada 2004). Membrane technology has been widely applied to purify water and acquired several merits, such as high impurity removal rate, saving space, less attentive operation and few chemical usages (Pearce 2007). Many factors would impact the efficiency of membrane filtration, including source water characteristics, membrane characteristics, operating conditions, fouling and cleaning methods (Wang et al. 2010, Krzeminski et al. 2012, Woo et al. 2013, Chun et al. 2017). However, one of the issues for membrane filtration is flux decline, which could be induced by fouling and membrane structure change (Wang et al. 2008, Cui et al. 2017). Numerous academic works have investigated the fouling problem in the operation of membrane filtration, but limited research has been done regarding the subtle changes in membrane structure during filtration.

Water temperature is one of the crucial source water characteristics in water treatment membrane filtration, and the variation of temperature could interact with membrane fouling and structural changes to affect filtration processes. Cold source water temperature has been found to increase the membrane fouling rate and the natural organic matter retention rate and decrease filtration flux and cleaning efficiency in microfiltration and ultrafiltration operations (Ma et al. 2013a, Alresheedi and Basu 2019). For reverse osmosis membranes, the decrement of influent temperature could promote a thicker biofilm, a lower rate of biofilm formation, a lower permeate flux, a higher rejection rate and a higher transmembrane pressure (Jawor and Hoek 2009, Jin et al. 2009, Farhat et al. 2016). Besides increasing rejection rate, Ma et al. (2013) attributed the

permeability loss with cold source water to fouling problems, potentially overlooking the feed temperature impacts on membrane structure.

Only a few studies were conducted regarding the influence of source water temperature on membrane structure. Sharma et al. (2003) were the first to reveal the thermal expansions of pore sizes for two commercial nanofiltration membranes. In addition, it was reported that low temperature could cause the increment of tortuosity and the loss of pore size and integrity for membranes (Farahbakhsh and Smith 2006). After raising the source water temperature by 20°C from 20°C, the average pore diameters could vary from 0.78 to 0.88nm, and the deficiency of removing the pollutant occurred with a nanofiltration reactor (Dang et al. 2014). Another study revealed that two nanofiltration operations had membrane pore sizes from 0.48 and 0.46 to 0.56 and 0.51, respectively, in switching feed water temperatures from 5°C to 25°C (Xu et al. 2020). Furthermore, with an extremely cold source water temperature (0.3°C), the membrane pore shrinkage and the significant deteriorations of membrane performance have been disclosed, and the warm water cleaning was conformed to be functioning to remediate the degradation (Cui et al. 2017, Tikka et al. 2019).

Cleaning is inevitable during the operation of membrane filtration. Elevating the physical cleaning temperature could increase the cleaning efficiency and decrease the irreversible fouling of membrane filtration (Zhao and Zou 2011, Lintzos et al. 2018, Hube et al. 2021). Although chemical cleanings in various temperatures had no effect on membrane surface charge and zeta potential (Al-Amoudi et al. 2007, Simon et al. 2013), changing the cleaning temperature from 2°C to 23°C led to an increasing permeation for polyvinylidene fluoride (PVDF) hollow fibre membrane (Woo et al. 2013). Additionally, Rabuni et al. (2015) found that chemical cleaning at 50°C recovered the membrane permeation to above 100% and considered it was caused by the

property alteration but ignored the pore expansion of the flat-sheet PVDF membrane. However, the cleaning temperature cannot be increased infinitely, and 50 to 60°C were examined to be the optimal chemical cleaning temperatures as the higher cleaning temperatures could erode and disintegrate the membranes (Almecija et al. 2009, Ahmad et al. 2014).

In cold regions, such as North America, Asia and Europe, the membrane filtration for water treatment could be operated with extremely low feed water temperatures during winters. Cold source/feed water temperature effects on membrane filtration and cleaning have been studied by Tikka et al. (2019) with specific time points and temperatures. However, the changing of membrane structures under cold source water and recovery of membrane structure under warm cleaning temperatures have not been explored. In this research, the influences of cold source water temperatures on the dynamic changes of membrane structures and the impacts of warm temperature cleanings on the membrane structure recoveries will be investigated. Specific objectives are:

1. Investigating the influences of cold temperatures on the dynamic changes of membrane structure,
2. Exploring the effects of warm water on the membrane structure recoveries.

The thesis is arranged in the following orders: Chapter 1 presents an introduction to the importance, rationale and objectives of this research; Chapter 2 comprehensively reviews the literature on the topics of membrane materials, characteristics, fouling and, more importantly, the temperature effects on membrane performance, fouling, structure and cleaning; Chapter 3 introduces the experimental apparatus, methods and analyzing procedures; Chapter 4 shows the cold feed water temperature impacts on dynamic membrane structures, the effects of warm recovery temperatures on dynamic membrane structures; Chapter 5 discusses the impacts of membrane structure changes

with cold source water and warm remediation on membrane filtration operations; finally, Chapter 5 summarizes the conclusions from this study and the perspectives for future research.

## CHAPTER 2 LITERATURE REVIEW

### 2.1 Overview of Membrane Filtration

Membrane filtration implements a membrane as a filter. Membrane filters are applied to repel contaminants and produce clean water in water treatment. In this circumstance, water flows through the membrane as it permeates, then pollutants are blocked by the membrane and retentates in the filtration process. Membranes can be morphologically categorized as flat sheet, hollow fibre and spiral wound membranes (Randtke and Horsley 2012). A flat sheet membrane has the simplest structure, with the water flowing from one side to another. A hollow fibre membrane is like a tiny tube formed by porous materials, typically polymers, which the water permeates from outside the fibre wall to inside or inside to outside. Within the fibre tube, pressure can be driven to both ends of the fibre as “crossflow” or only one end with another “dead end.” A hollow fibre membrane could be either symmetrical, in which the structures of the feed side and the filtrate side are uniform, or asymmetrical with the different surfaces on the two sides (Childress et al. 2005). Numerous membrane fibres bundled in parallel become hollow fibre membrane modules. In addition, multiple-layer flat-sheet membranes rolling up on a collector tube forms a spiral-wound membrane module, and series-connected modules covered by a pressure vessel construct a whole spiral-wound membrane vessel.

With the increasing sequences of equivalent membrane pore sizes, reverse osmosis (RO), nanofiltration (NF), ultrafiltration (UF) and microfiltration (MF) are identified as the pressure-driven membrane filtration processes (Bruggen et al. 2003). The membrane with a smaller equivalent pore size has less permeability. Therefore, based on Darcy’s law, more significant transmembrane pressure (TMP) would be demanded to maintain the desired flux for the membrane with less permeability. Therefore, RO and NF membranes are high-pressure-driven membranes,

while MF and UF membranes only require low pressure to be operated. Additionally, these kinds of membranes also have different geometrical features. For example, MF and UF membranes are always applied as hollow fibre, while RO and NF membranes have both hollow fibre and spiral wound configurations in the water treatment industry (Edzwald 2011). Figure 2.1.1 shows the application guide for various membrane filtration processes.

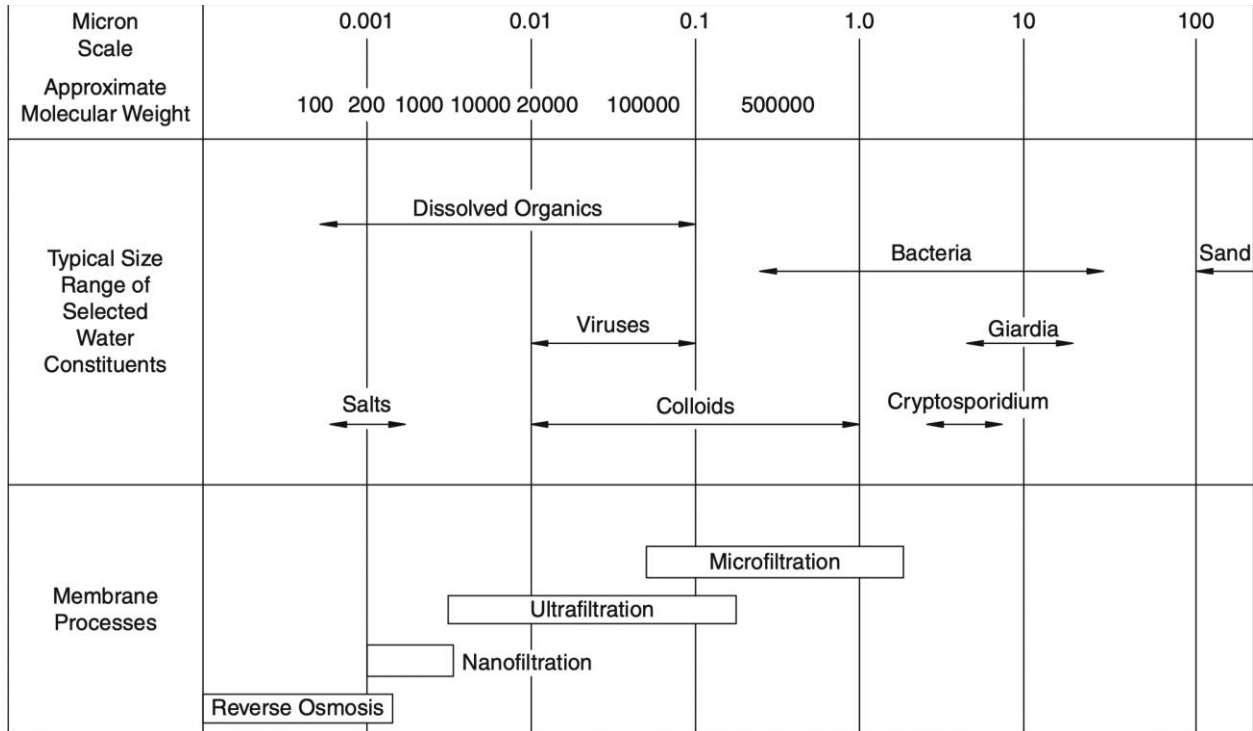


Figure 2.1.1 Pressure-driven membrane process application guide (Edzwald 2011).

## 2.2 Membrane Materials

Membrane materials determine the specific properties of membranes in treatment process design. Generally, all membranes are fabricated with inorganic and organic materials. Inorganic materials, including ceramics and zeolites, recently attracted considerable attention because of their admirable thermal, chemical and mechanical natures (Lee et al. 2016). For instance, the combination of graphene oxide, a material with outstanding mechanical strength, and  $\text{TiO}_2$ , which had the photocatalytic function of degrading organic pollutants under UV light, formed a

remarkable membrane with high flux and recoverability (Zhu et al. 2017). Although inorganic materials have been researched more than in the past, organic materials still dominate commercial membrane treatment processes.

Organic materials for membranes commonly are synthetic polymers. Polymer materials possess a great diversity of structures and properties. Widely utilized polymer materials include cellulose acetate (CA) and cellulose nitrates (CN), polyacrylonitrile (PAN), polyethersulfone (PES), polyimide (PI), polypropylene (PP), polysulfone (PSU), polytetrafluoroethylene (PTFE), polyvinyl alcohol (PVA) and polyvinylidene fluoride (PVDF) (Lee et al. 2016). Among these membranes, PI and PES had the highest mechanical property and maximum served temperature (Bassyouni et al. 2019). In another study, the PES membrane was found that has higher permeability and energy economy than PVDF and PAN membranes resulting from its outstanding hydrophilicity, porous uniformity and thermal stability (Fan et al. 2016). Various membranes present distinct features, such as hydrophobicity or hydrophilicity, pH tolerance, oxidant tolerance, mechanical strength and flexibility. Membrane material selection depends significantly on feed water characteristics, operating conditions and cleaning chemicals (Lee et al. 2016).

### 2.3 Membrane fouling

One principal problem that impedes the development of membrane filtration is fouling (Peña et al. 2013, Chun et al. 2017). Fouling during membrane treatment processes derives from the retentate precipitates and accumulates within the pores and on the surface of the membrane. According to Matyka et al. (2008), fouling occurrence declined the porosity and raised the tortuosity of the membrane, which leads to the decrement of permeability.

Membrane foulants can be categorized into four types. Regarding membrane fouling's reversibility, there are hydraulically reversible and irreversible fouling (Alresheedi and Basu 2019). Hydraulically irreversible fouling could be chemically reversible and chemically irreversible. Physical cleaning could wash off the hydraulically reversible fouling, while chemically reversible means that the fouling part can be detached by cleaning agents after physical cleaning. Typically, if the reversibility has not been specified hydraulically or chemically, it would be hydraulic reversibility. In addition, inorganic fouling, organic fouling, and biofouling are based on categorizing foulant composition (Chun et al. 2017). Source water, membrane materials and structures, operating conditions, and their interaction could influence membrane fouling and should attract significant attention.

### 2.3.1 Fouling characteristics

Organic fouling is formed by depositing organic matter on/in a membrane. In water treatment, natural organic matter (NOM) dominates the organic part of membrane fouling. Among NOM foulants, the prevalent fractions are the humic substances, which originate from the degradations of animal residues and plants, including proteins, carbohydrates, and lignin (Nyström et al. 1996, Yuan and Zydney 1999, 2000, Srisurichan et al. 2005). In an experiment operated by Pramanik et al. (2017) implementing a 0.1 $\mu$ m pore size PVDF membrane as the material, it was found that carbohydrates are more reversible than proteins and dissolved organic carbon contents. The interaction of different organic foulants is crucial in determining the fouling rate due to their intermolecular adhesion. The intermolecular bonding was proved by observing adhesive sites on membrane surfaces in adhesion force measurement (Mi and Elimelech 2008). Some studies also researched the correlation of different organic foulants contributing to membrane fouling. For

example, in the source water containing two oppositely charged substances, such as lysozyme and alginate, flux decline and mass foulant accumulation were severer than fouling caused by either single component (Gu et al. 2013). In another research, feed water consisting of humic acid and lysozyme solution deteriorated the fouling reversibility but not the hydraulic resistance for the membrane (Shao et al. 2019).

The sieving mechanism dominates the organic fouling formation in membrane filtration. Size exclusion was related to the properties of organic substance and membrane surface, which are membrane pore size and distribution, NOM's molecule size, distribution and shapes (Ghosh and Schnitzer 1980, Yuan and Zydney 1999, 2000). The magnitude and outline of NOM molecules significantly depend on the ionic strength and pH in the aquatic environment (Ghosh and Schnitzer 1980). Moreover, membrane fouling conditions and performance were dramatically impacted by the hydrophobic and hydrophilic fractions of NOM in feed water (Sun et al. 2013, Liu et al. 2015).

Organic fouling is generally predominant among the fouling segments in membrane water treatment (Yamamura et al. 2014). Its properties determine the flux decline and cleaning regimes during the operating processes.

Besides organic membrane foulants, inorganic foulants are also a crucial part of the membrane fouling layer. Inorganic fouling is the precipitant of the ions in the influent water for membrane treatment. The dominant cations in drinking water include  $Mg^{2+}$ ,  $Ca^{2+}$ ,  $K^+$ , and  $Na^+$ , while  $HCO_3^-$ ,  $Cl^-$ ,  $SO_4^{2-}$  and  $NO_3^-$  are the primary anions (Jackson 2001).

The inorganic fouling is also widely called the 'mineral scale' induced by particulate deposition and crystallization. Particulate deposition relates to the convective movement between the aqueous environment and membrane surface, and the high concentrations of inorganic ions exceeding the vicinity solubility of the membrane surface contribute to the fundamental

mechanism of the inorganic scaling formation(Lee and Lee 2000). Dissolved ions could potentially be concentrated 4 to 10 times near the membrane surface during the permeation in nanofiltration and reverse osmosis systems (Shirazi et al. 2010). Al-Amoudi (2010) reported that some particles on the membrane surface, such as aluminum oxide, inorganic salts, clays, sands and microbes, aggregated the inorganic fouling crystallization as the substrates. The compositional complexity in the raw water facilitates the fouling precipitation. The coalescence of foulants potentially exaggerated the difficulty in dealing with the membrane fouling problem (Al-Amoudi 2010).

There are numerous kinds of microorganisms in the aqueous environment. These microbes could be sieved and then become foulants during drinking water purification by membrane technology. For instance, the microorganisms in the raw water were capable of reproduction and metabolism, of which products, including soluble microbial products (SMP) and extracellular polymeric substances (EPS), significantly impacted membrane fouling (Liao et al. 2004). Moreover, the periodical application of chlorine cleaning plausibly restrained the duplication of the microorganisms and further alleviated membrane fouling (Gao et al. 2011a).

Microbial cells attach to the membrane surface and become fouling through several steps. Electrokinetic and hydrophobic interactions first prompted microbes' attachment; these microbes, such as bacteria, fungi, protozoa and algae, then consumed the nutrients from water or membrane surface to propagate and grow; the reproduction of microbes produced SMP and EPS as supplementary foulants in occupying the surface and inner pores of the membrane (Nguyen et al. 2012). In addition, biofouling not only plugs the membrane pores but also deteriorates the membrane structure. Hilal et al. (2004) claimed biofouling could degrade the membrane polymer and introduce pathogens onto the membrane surface.

### 2.3.2 Factors impacting membrane fouling

Under the fouling problem in membrane filtration, it is pressing to reveal the fouling mechanisms to mitigate the impacts of the fouling. However, multiple factors are decisive for membrane fouling, and even their interactions play crucial roles in the fouling formation. Therefore, these mechanisms should be continuously studied, explored and revealed. Furthermore, several factors, such as membrane materials, configuration, NOM and water temperature, have been unfolded in affecting membrane fouling (Yoon et al. 2005, Rosenberger et al. 2006, Jung et al. 2006, Howe et al. 2007).

Membranes are special polymers with pretty low orders of magnitudes of pore sizes. The tiny pores equipped with a membrane repel the impurities in the raw water, which the property is excellent for producing drinking water. The cutting-off capacity of particles, microbes and even soluble substances depends significantly on the membrane materials and properties (Jung et al. 2006).

Membranes can be fabricated with many different materials, which decide the properties of the membrane. For the two top categories of membranes, ceramic membrane and polymeric membrane, fouling situations seem identical, but physical cleaning can remove most fouling for ceramic membranes, while the polymeric membrane requires chemical cleaning to recover the permeability (Dashtban Kenari and Barbeau 2016). Hofs et al. (2011) investigated four ceramic membranes composited by  $\text{Al}_2\text{O}_3$ ,  $\text{ZrO}_2$ ,  $\text{TiO}_2$  and SiC and their fouling status during surface water filtration. They found SiC membrane, the exceptionally hydrophilic one, had the lowest transmembrane pressure increment and the least reversible and irreversible foulants (Hofs et al. 2011).

A crucial property deciding the membrane choice for filtrations is the hydrophobicity/hydrophilicity of the membrane (Jönsson and Jönsson 1995, Jung et al. 2006, Hofs et al. 2011, Yamamura et al. 2014). Hydrophilic materials have acute contact angles with water and small capillary resistance, while hydrophobic materials repel water and are more likely to bond with organics. A study by Jönsson and Jönsson (1995) claimed that hydrophilic and hydrophobic properties, membrane pore size and pollutant concentration could affect the fouling situation in membrane filtration, and hydrophilic membranes were less pronounced to be fouled. In addition, compared with hydrophilic membranes, hydrophobic membranes were prone to adsorb more hydrophobic organics and had a higher adsorption ratio and flux decline rate (Jung et al. 2006, Hofs et al. 2011). Another study contrasted four kinds of polymer membranes composed of PE, PVDF, PAN and PES. The study concluded that PE and PAN membranes were hydrophilic and predisposed organic matter to foul the membranes than PVDF and PES membranes, which were hydrophobic (Yamamura et al. 2014).

A variety of novel membrane materials were utilized to alleviate the membrane fouling problem. For example, Zhu et al. (2017) blended TiO<sub>2</sub> on the graphene oxide membrane surface. Graphene oxide is a perfect hydrophilic material, and the combination of graphene oxide and TiO<sub>2</sub> could photodegrade the fouling caused by organic matter on the membrane surface to retrieve up to 96% of the transmembrane flux (Zhu et al. 2017). In another study, a modified polysulfone hollow fibre membrane was invented. This membrane was attached by 3-(3,4-dihydroxyphenyl)alanine and N-TiO<sub>2</sub>-NH<sub>2</sub> on the surface and was capable of photocatalysing humic acids to reduce membrane fouling (Wan et al. 2019). Whatsmore, ZnO embedded in polysulfone was capable of increasing the membrane hydrophilicity, porosity, NOM resistance rate, fouling resistance and bacterial killing rate (Sarihan and Eren 2017). Moreover, Yang et al.

(2019) integrated porous carbon with carbon nanotubes to be the membrane, and this membrane could generate hydroxyl radical around the membrane surface to oxidize the organic foulants. In summary, choosing membrane material is vital to relieve the fouling problem of water treatment membrane filtration (Yang et al. 2019).

Membranes with different configuration modes have distinctive surface properties, porosities, pore morphology and layer density (Howe et al. 2007). Water treatment commonly implements flat sheet and hollow fibre membranes. The membrane fouling with flat sheet configuration is much severer than in hollow fibre configuration in the same circumstance, and coagulation pretreatment in some cases could mitigate the fouling problem with hollow fibre membrane but deteriorate the situation with flat sheet membrane (Howe et al. 2007). The submerged configuration had a thicker but looser fouling layer than the sidestream configuration for the forward osmosis bioreactors. The differences could be owing to the different scouring methods: hydraulic and air scouring for sidestream and submerged designs, respectively (Morrow et al. 2018). Furthermore, membrane packing density is crucial for membrane fouling control. Therefore, the manufacturers should consider the optimal density for the membrane module since the increasing packing density enhances the crossflow velocity but boosts the fouling problem (Liao et al. 2004).

Natural organic matter is the essential portion that must be eliminated from the water and the inevitable fraction of the fouling problem on membrane water treatment (Metsämuuronen et al. 2014). There are innumerable organic substances in the natural water. Researchers are still working on identifying NOM and its roles in contributing to membrane fouling. Humic acids are the prevalent group belonging to NOM in surface water (Nyström et al. 1996, Yuan and Zydney 1999, 2000). Back to an early study, Hong and Elimelech (1997) compared several humic acid

substances and concluded that one of the three humic acids with higher hydrophilicity, more negative charges and lower molecular weight created much less fouling on the membrane surface after being filtrated. Interestingly, Yamamura et al. (2014) presented a discrepancy and argued that hydrophilic organic matter dominated the physically irreversible fouling. They revealed that the essential ingredient of the hydrophilic NOM in surface water was biopolymers, which included carbohydrates and proteins, and the irreversible fouling was unrelated to the size of NOM. In addition, the concentrations of biopolymers in the influent regulated the irreversible fouling levels with a PVDF membrane (Yamamura et al. 2014). Another research by Liu et al. (2020) reported that the neutral hydrophilic components in NOM in the surface water contribute most to chemically irreversible fouling for membrane filtration, while the protein-like and humic-like substances do not evidently participate in it. The same study also announced that chemically irreversible fouling consists of constituents with low molecular weights of less than 1kDa and polysaccharide-like substances.

The intermolecular interaction between NOM and different contaminants considerably affects membrane fouling (Mi and Elimelech 2008, Li et al. 2010, Kim and Jang 2016). For example, the coalescence of kaolinite and humic acid as foulants less severely fouls the membrane than the pollutant of solo inclusion with humic acid (Li et al. 2010). Furthermore, alginate, Aldrich humic acid and bovine serum albumin were in descending order of the severity of inducing fouling based on the bonding between NOM and calcium cations (Mi and Elimelech 2008). However, Kim and Jang (2016) argued that sodium alginate has the highest fouling potential, while bovine serum albumin and humic acid have the secondary and slightest tendencies to foul the membrane. This inconsistency may be because the former study used cellulose acetate membrane, and the latter study adopted ceramic membrane as experimental objects, according to Kim and Jang (2016).

Cui and Choo (2014) indicated that NOM formed the membrane fouling by pore blocking in the first step; then, NOM aggregated as gel and deposited on the membrane surface; finally, NOM integrated with other particles to create a dense and less permeable fouling layer. NOM fouling could be controlled by the size and charge density of NOM and has correlations with the membrane surface charge, hydrophilicity and pore sizes (Yoon et al. 2005). In addition, ionic strength, pH, divalent concentration and hydrodynamic conditions in the feeding water also crucially impact the membrane fouling by NOM (Zularisam et al. 2006, de la Rubia et al. 2008, Cui and Choo 2014).

## 2.4 Temperature impacts on membrane filtration

In membrane water and wastewater treatments, the water temperature differences have significant impacts, especially in cold regions with extraordinary seasonal temperature variations (Sharma et al. 2003, Farahbakhsh and Smith 2006, Lyko et al. 2008, Cui et al. 2017, Tao et al. 2021). The impacts of temperature on membrane filtration are from several aspects, such as fouling, permeability, structure and cleaning. Furthermore, temperature influences not only membrane material properties but also feed water characteristics. For example, Ma et al. (2020) reported that low water temperature would cause a thicker cake layer of foulants and severer membrane fouling. Therefore, it is nonnegligible that the temperature impacts should be considered in the daily operation of water treatment plants.

### 2.4.1 Temperature impacts on fouling

As mentioned previously, fouling is a crucial hindrance to water treatment using membrane filtration. Therefore, numerous studies have studied the temperature effects on membrane fouling

(Table 2.4.1). Temperature either facilitates or mitigates the problem of fouling due to the foulant property shifting incurred by temperature fluctuation.

For instance, low temperature dramatically increased EPS, SMP, proteins, polysaccharides and soluble chemical oxygen demands (COD) in the supernatants for the MBR system, and these biopolymers caused membrane fouling (Wang et al. 2010, Ma et al. 2013b). As a result, the capillary suction and diluted sludge volume index were also higher with lower temperatures, making the pollutants hard to settle and dewater. Thus, higher membrane fouling rates were reported at low temperatures (8.7~10°C) than at high temperatures (19.7~20°C) (Ma et al. 2013a, 2013b). Van den Brink et al. (2011) presented the four factors increasing the resistance of membrane bioreactors at low temperatures of 7°C: 1) The water viscosity increment reduced the shear stress around the membrane surface; 2) the sludge deflocculation created small particles and released the extracellular polymeric substances to aggravate the membrane fouling condition; 3) back transport velocity would be decreased; 4) COD biodegradation would be restrained.

Gao et al. (2011b) concluded that microbial species and richness in the sludge were diverse in the different operating temperatures, and high temperature stimulates the sludge layer accumulation but declines the layer thickness and total biomass aggregation. They found that high/warm-temperature shock benefited the submerged anaerobic membrane bioreactor (SAnMBR) and promoted the biogas-producing rate, but increasing water temperature from 37°C to 45°C resulted in breaking the sludge flocs into small pieces and then forming the cake layer in the bulk sludge, while the sludge flocs became larger with the increasing cake age. In addition, the colloidal particles, SMPs and bound EPSs were accumulated, and there was additional fouling resistance with high-temperature shock (Gao et al. 2012).

On the contrary, although biomass has lower growth rates at lower temperatures, the sludge layer is thicker and detrimental to the permeation flux and salt retention ability (Farhat et al. 2016). A pair of abnormal temperatures, 40°C and 60°C, was tested to distinguish biofouling developments in a membrane distillation system researched by Liu et al. (2019). They found that high temperature (60°C) caused significant flux decline and deposited protein-like matter and salt crystals on the membrane surface. Notably, the structures of microbial communities within the foulants at 60°C dramatically differed from that at 40°C (Liu et al. 2019).

Rong et al. (2022) claimed that when an anaerobic membrane bioreactor (AnMBR) was implemented to purify municipal wastewater, the membrane fouling condition deteriorated at a low temperature of 15°C, resulting from the accumulation of microbial products and inorganic foulants accompanied by increasing water viscosity. Hube et al. (2022) investigated the temperature impact on a gravity-driven microfiltration membrane reactor treating domestic wastewater and revealed that foulants at a room temperature of 22°C accumulated more on the surface of the membrane and had larger sizes within the cake layer. They concluded that the membrane had similar cake resistance in the two temperatures (8, 22°C) since no cleaning was presented, while the membrane at the room temperature had remarkably higher cake resistance than at low temperature of 8°C when there was periodic cleaning with the water at 50°C. However, the temperature variance did not influence foulant contents and the quality of permeates in this reactor. Tao et al. (2022) reported that polysaccharides positively correlated with hydraulically reversible resistance, while polysaccharides and low molecular weight substances induced hydraulically irreversible resistance in the ZeeWeed-1000 hollow fibre ultrafiltration membrane reactors treated municipal wastewater. Furthermore, Tao et al. (2022) claimed that the total

membrane resistance increases caused by fouling and intrinsic resistance were 55% and 122% at 14°C and 8°C, respectively, compared to the resistance at 20°C.

When a forward osmosis (FO) membrane system purified feed water with an elevated temperature (50°C), the decreased internal concentration polarization and the declined viscosity resulted in the increment of permeable flux. The FO membrane also encountered less fouling due to the existence of more soluble organic substances and the boosted back diffusion of organics on the membrane surface (Kim et al. 2015). Alresheedi and Basu (2019) examined a ceramic ultrafiltration system and found that the filtration fluxes were lower at 5°C and higher at 35°C compared to 20°C owing to the shifts in water viscosity and membrane material resistances. The NOM retention rates were 10% higher at 5°C and 16% lower at 35°C compared to the rate of 78% at 20°C because the lower temperature changed the fouling layer structures and enlarged NOM size. Besides higher flux decreasing rates and NOM retention rate, lower temperature led to lower hydraulic and chemical cleaning efficiencies (Alresheedi and Basu 2019). Both high viscosity and exacerbated fouling conditions contribute half to the increase of transmembrane pressure at the low temperature (5°C) for ceramic ultrafiltration. The low temperature induces more irreversible foulants, which block the inside of membrane pores, than the room and higher temperatures (Alresheedi and Basu 2020).

In a distillation study with graphene oxide (GO) coated calcium sulphate RO membrane, Ashfaq et al. (2020) suggested that the high temperatures in warm regions like Arabian countries resulted in severe membrane scaling and high resistance by boosting the precipitation reaction. They also revealed that the morphology of the scaling was distinctive under different temperatures, and the membrane tended to be more hydrophilic after scaling. Among scaling foulants, calcium

sulphate is more likely to form a sizeable needle-shaped crystal at high temperatures up to 80°C and severely foul the membrane (Elcik et al. 2020).

Table 2.4.1 Summary of the impacts of temperature on membrane fouling

Membrane type and material	Reactor	Temperature (°C)	Summary	Reference
Hollow fibre PVDF membrane	Full-scale municipal MBR	8~24	Lower temperature caused <ul style="list-style-type: none"> <li>• lower sludge stabilization, settleability, dewaterability</li> <li>• adjustments in cleaning frequency</li> </ul>	(Lyko et al. 2008)
RO membrane	Bench-scale reactor	15, 25, 35	Low temperature (15°C) caused <ul style="list-style-type: none"> <li>• high TMP</li> <li>• high solute rejection</li> </ul>	(Jawor and Hoek 2009, Jin et al. 2009)
Flat-sheet polyethersulfone (PES) membrane	Pilot-scale MBR	8~26	Low temperatures (8~15°C) caused <ul style="list-style-type: none"> <li>• increasing EPS, COD, polysaccharides and protein in supernatants</li> <li>• low sludge settleability, dewaterability</li> <li>• high membrane fouling rate</li> </ul>	(Wang et al. 2010)
PE microfiltration (MF) membrane	Bench-scale PAC-MBRs	10, 20		(Ma et al. 2013a)
Hollow fibre PVDF membrane	Pilot-scale MBR	8.7~19.7		(Ma et al. 2013b)
Hollow fibre PVDF MF membrane	Pilot-scale SAnMBR with real municipal wastewater as influent	15, 20, 25		(Rong et al. 2022)
Flat-sheet PVDF membrane	Lab-scale submerged anaerobic membrane bioreactor (SAnMBR)	37, 42, 47, 45, 50, 55	High-temperature shock (37 to 42°C, 37 to 47°C, 45 to 50°C, 45 to 55°C) caused <ul style="list-style-type: none"> <li>• biogas producing</li> <li>• smaller pieces sludge flocs</li> <li>• temporarily decreasing and then increasing fouling resistance</li> <li>• no influence on microbial community structure</li> <li>• diverse microbial species and richness</li> </ul>	(Gao et al. 2011b, 2012)
Flat-sheet PVDF membrane	Pilot-scale MBR	7, 15, 25	Mechanisms of membrane resistance increase at low temperature (7°C) <ul style="list-style-type: none"> <li>• water viscosity increment</li> <li>• sludge deflocculation</li> </ul>	(van den Brink et al. 2011)

Table 2.4.1 Summary of the impacts of temperature on membrane fouling

Membrane type and material	Reactor	Temperature (°C)	Summary	Reference
			<ul style="list-style-type: none"> <li>• decreased back transport velocity</li> <li>• restrained COD biodegradation</li> </ul>	
Forward osmosis (FO) membrane	Lab-scale reactor	20, 35, 50	High temperature (50°C) caused <ul style="list-style-type: none"> <li>• increasing permeable flux</li> <li>• less fouling</li> </ul>	(Kim et al. 2015)
Spiral wound RO membrane	Lab-scale reactor	10, 20, 30	Low temperatures (10, 13°C) caused <ul style="list-style-type: none"> <li>• low biomass growth rate</li> <li>• decreasing salt retention ability</li> </ul>	(Farhat et al. 2016)
Hollow fibre PVDF ultrafiltration (UF) membrane	Bench-scale reactor	13~20, 20~30	<ul style="list-style-type: none"> <li>• thick fouling layer</li> <li>• decreasing permeation flux</li> </ul>	(Ma et al. 2020)
Tubular ceramic UF membrane	Lab-scale reactor	5, 20, 35	Low temperature (5°C) caused <ul style="list-style-type: none"> <li>• high flux decreasing rates</li> <li>• high NOM retention rates</li> <li>• low hydraulic and chemical cleaning efficiencies</li> </ul>	(Alresheedi and Basu 2019)
Flat-sheet polytetrafluoroethylene (PTFE) membrane	Bench-scale direct contact membrane distillation	40, 60	High temperature (60°C) caused <ul style="list-style-type: none"> <li>• significantly flux decline</li> <li>• fouling microbial structure changed</li> </ul>	(Liu et al. 2019)
Ceramic UF membrane	Bench-scale reactor	5, 20, 35	<ul style="list-style-type: none"> <li>• Low temperature (5°C) induces more irreversible foulants</li> <li>• Both high viscosity and exacerbated fouling conditions contribute half to the increase of transmembrane pressure at the low temperature</li> </ul>	(Alresheedi and Basu 2020)
Graphene oxide (GO) coated calcium sulphate RO membrane	Bench-scale RO desalination	5, 15, 25, 35	High temperatures (25, 35°C) caused <ul style="list-style-type: none"> <li>• severe membrane scaling and high resistance</li> <li>• different scaling morphologies</li> </ul>	(Ashfaq et al. 2020)

Table 2.4.1 Summary of the impacts of temperature on membrane fouling

Membrane type and material	Reactor	Temperature (°C)	Summary	Reference
PTFE microfiltration membrane	Bench-scale direct contact membrane distillation	50, 60, 70, 80	High temperatures (70, 80°C) caused <ul style="list-style-type: none"> <li>calcium sulphate is more likely to form a sizeable needle-shaped crystal and severely foul the membrane</li> </ul>	(Elcik et al. 2020)
Hollow fibre PVDF MF membrane	Lava stone biocarrier facilitated gravity-driven membrane reactors	8, 22	High temperature caused <ul style="list-style-type: none"> <li>foulants accumulated more and had a large size</li> <li>no change in cake resistance without cleaning</li> <li>higher cake resistance with periodic cleaning</li> <li>no influence in foulant content and permeate quality</li> </ul>	(Hube et al. 2022)
Zeeweed-1000 hollow fibre UF membrane	Bench-scale SBRs with municipal wastewater as influent	8, 14, 20	Low temperatures (8, 14°C) caused high membrane resistance from fouling and intrinsic resistance.	(Tao et al. 2022)

#### 2.4.2 Impacts on permeability and performance

In membrane filtration, permeability is the decisive parameter for filtration performance. Several particle exclusion mechanisms influence the membrane permeability, but not all the mechanisms correlate with temperature changes. For example, Chae and Shin (2007) reported that when municipal wastewater was treated between 13°C and 25°C in a vertical submerged membrane bioreactor, there was no distinction in pollutant removal efficiency among different temperature environments, with all acceptable removal efficiencies achieved. Another article examined ten pilot and full-scale municipal membrane bioreactors, the temperatures of 9.7°C to 27.4°C did not affect active sludge's apparent viscosity (Moreau et al. 2009).

However, more researchers found that temperature variation did impact membrane performance in multiple respects. Temperatures impact the membrane permeability by more than changing aqueous viscosity (Sharma et al. 2003). For instance, higher temperatures caused the decrement of biomass quantity and sludge settleability and the increment of supernatant turbidity at 45°C compared to 25°C and 35°C. In addition, at 45°C, soluble microbial products were increasing while extracellular polymeric substances were decreasing in the reactor. Interestingly, COD removal rates by biological degradation and filtration were remarkably declined at the high temperature (45°C), accompanied by the ascending transmembrane pressure and backwash pressure during the operation. Thus, the overall performance of the membrane bioreactor was deteriorated by a much higher temperature of 45°C in treating synthetic-municipal wastewater (Al-Amri et al. 2010). On the other hand, Zheng et al. (2019) claimed that biodegradation was boosted during summer time, and the cold weather in the winter prompted slightly better antibiotic rejection than the warm temperature in membrane bioreactors.

In addition, even temperatures between 14°C and 26°C could dramatically influence the efficiency of a 40L lab-scale anaerobic membrane bioreactor with actual wastewater influent reported by Plevri et al. (2021). They claimed that with more than one day of hydraulic retention time (HRT), the effluents' COD in wintertime was almost twice as in summertime, while 35% less COD in the permeates during the summertime than during the wintertime was revealed at HRT of 12h. Furthermore, low temperatures would engender the effluent with more organic matter from a sequencing batch reactor (SBR). A tertiary ultrafiltration system treating this SBR's effluent was fabricated and had lower hydraulically irreversible permeability with lower operating temperatures. Lower temperatures narrowed the pore size to intercept the more significant amount of organic matter, and increased water viscosity played the leading role in decreasing hydraulically irreversible permeability (Tao et al. 2021).

With a bench-scale crossflow forward osmosis system, the temperature increasing from 20°C to 40°C promoted permeability because of the increasing thermal convection and decreasing water viscosity (Xie et al. 2013). In a fertilizer-driven forward osmosis reactor, the decreasing viscosity, the increasing water flux, the decreasing reverse ion flux, and the increasing specific reverse ion flux were revealed at 45°C, which the declined reverse salt flux can mitigate fouling potential (Karunakaran et al. 2021). Table 2.4.2 presents the collection of articles on the temperature impacts on membrane permeability and performance.

Table 2.4.2 Summary of the impacts of temperature on permeability and performance

Membrane type and material	Reactor	Temperature (°C)	Summary	Reference
Polyethersulfone (PES) hollow fibre MF membrane	Lab-scale submerged MBR treated synthetic-municipal wastewater	25, 35, 45	<p>High temperatures (45°C) caused</p> <ul style="list-style-type: none"> <li>• low biomass quantity and sludge settleability</li> <li>• high supernatant turbidity</li> <li>• increasing SMP, decreasing EPS</li> <li>• low COD removal rates</li> <li>• decreasing TMP and backwash pressures</li> <li>• decreasing overall performance</li> </ul>	(Al-Amri et al. 2010)
Asymmetric cellulose triacetate FO membrane and thin-film composite polyamide FO membrane	Bench-scale crossflow FO system	20, 40	Increasing temperatures promoted membrane permeability.	(Xie et al. 2013)
Unknown	Full-scale WWTP MBR	spring, summer, autumn, winter	<p>Low temperatures during wintertime caused</p> <ul style="list-style-type: none"> <li>• slow biodegradation</li> <li>• slightly better antibiotic rejection</li> </ul>	(Zheng et al. 2019)
FO membrane	Lab-scale fertilizer-driven FO	25, 30, 35	<p>High temperatures (30, 35°C) caused</p> <ul style="list-style-type: none"> <li>• decreasing water viscosity</li> <li>• decreasing reverse salt flux</li> <li>• increasing waster flux</li> <li>• increasing specific reverse salt flux</li> </ul>	(Karunakaran et al. 2021)
Flat sheet membrane	Lab-scale submerged AnMBR with real wastewater	14-26	Low temperatures caused high effluent CODs with different HRTs.	(Plevri et al. 2021)
Zeeweed-1000 hollow-fibres ultrafiltration membrane	Filtration of the effluent of bench-scale SBRs treating real municipal wastewater	8, 14, 20	<p>Low temperatures (8, 14°C) caused low hydraulically irreversible permeability by</p> <ul style="list-style-type: none"> <li>• altering influent organic matter features</li> <li>• decreasing water viscosity</li> <li>• narrowing membrane pores</li> <li>• membrane foulants' interactions</li> </ul>	(Tao et al. 2021)

### 2.4.3 Impacts on structure and integrity

Only a few studies have been done on the temperature impacts on the structure and integrity of membranes. Table 2.4.3 summarizes the published research findings on the cold temperature effects on membrane integrity and structure and membrane filtration operations. Membrane materials could encounter physical and chemical changes in various temperatures. For example, the low temperature at  $-10^{\circ}\text{C}$  compared to  $20^{\circ}\text{C}$  could reduce PVDF material's porosity (Lairinandrasana et al. 2009). The membrane with lower porosity has lower transmembrane flux and higher transmembrane pressure during the operation, which are vital for evaluating the membrane performance.

Pore size change is the microscopic manifestation of the membrane structure distinction under different temperatures. Sharma et al. (2003) first revealed the pore size differences for nanofiltration membranes in various thermal conditions. They found that the reflection rates of intermediate-size solute molecules, such as dextrose, ethanol, ethylene glycol, glycerol, t-butyl alcohol and xylose, were higher at lower temperatures ( $5, 15^{\circ}\text{C}$ ). Furthermore, the average pore sizes of the two commercial nanofiltration membranes were increased by 21% and 12% when the temperature varied from  $5$  to  $41^{\circ}\text{C}$  (Sharma et al. 2003). In another nanofiltration study by Dang et al. (2014), a pore-hindrance model showed that the membrane pores of a polyamide membrane were enlarged by 13% when the temperatures elevated from  $20^{\circ}\text{C}$  to  $40^{\circ}\text{C}$ . The authors also claimed that the increased membrane pore size and solute diffusion adversely impacted the pollutant rejection, and the membrane pore sizes were not correlated with the charge repulsion effect under changing temperatures. Xu et al. (2020) elucidated a similar trend with the membrane pore size variation in different temperatures ( $5, 10, 15, 20, 25^{\circ}\text{C}$ ), and they found that the two kinds of the membrane, loose and tight nanofiltration membranes, expressed 14% and 10% of pore

size shrinkages and 42% and 50% of pure water permeability loss, respectively, when the curing temperatures were changed from 25°C to 5°C. Declined temperatures increased the rejection of neutrally and positively charged micro-substances. However, the low temperatures (5~25°C) had no influence on the rejection of negatively charged micro-pollutants, such as clofibric acid, nalidixic acid, ibuprofen, mefenamic acid, diclofenac, indomethacin, bezafibrate and candesartan, because the negative electrostatic repulsion compensated for the weaker hindrance induced by pore expansion in higher temperatures between the membrane and contaminants both with negative charges (Xu et al. 2020). Xiao et al. (2014) applied pore-filling of several polymers on the PVDF membrane to create a sensitive temperature-responsive membrane which changed water fluxes up to 15 times between 30°C and 34°C. The SEM images showed dramatically distinctive pore sizes under 25°C and 40°C.

Cui et al. (2017), the first study exploring the membrane structures impacted by an extremely cold temperature at 0.3°C, revealed that the cold source water temperature could deteriorate the membrane performance, e.g., the shrinkage of the membrane pores. Another comparative research by Tikka et al. (2019) also reported the compromise of membrane filtration performance and membrane structure in extremely cold water.

Membrane integrity is rarely researched in low-temperature operating membrane filtration. Farahbakhsh and Smith (2006) revealed that low temperature reduced the diffusive air flow rates and the pressure decay rates of the microfiltration membrane, and the extremely low water temperature (around 0°C) might conceal membrane deflection.

Table 2.4.3 Summary of the impacts of temperature on structure and integrity

Membrane type and material	Reactor	Temperature (°C)	Summary	Reference
Zeeweed-500 hollow fibre MF membrane	Lab-scale filtration	0-30	<p>Low temperatures caused</p> <ul style="list-style-type: none"> <li>• reducing the diffusive air flow rates</li> <li>• reducing the pressure decay rates</li> <li>• membrane deflection</li> </ul>	(Farahbakhsh and Smith 2006)
Two commercial PI thin-film NF membranes	Lab-scale filtration	5, 15, 23, 35, 41	<p>Low temperatures (5, 15°C) caused</p> <ul style="list-style-type: none"> <li>• high reflection rate of intermediate-size solute molecules</li> <li>• membrane pore shrinkage</li> </ul>	(Sharma et al. 2003)
NF270 flat-sheet NF membranes	Lab-scale filtration	20, 30, 40	<ul style="list-style-type: none"> <li>• no impact on charge repulsion</li> <li>• permeability loss</li> </ul>	(Dang et al. 2014)
A loose and a tight NF membrane	Lab-scale cross-flow filtration	5, 10, 15, 20, 25	<ul style="list-style-type: none"> <li>• increasing the rejection of neutrally and positively charged micro-substances</li> </ul>	(Xu et al. 2020)
PVDF MF membranes and flat-sheet PAA-PVDFHE membrane	Lab-scale filtration	25, 30, 34, 40, 48	<p>Pore-filling several polymers on the PVDF membrane formed a sensitive temperature-responsive membrane.</p> <ul style="list-style-type: none"> <li>• dramatically distinctive pore sizes between 25°C and 40°C</li> <li>• fluxes varied up to 15 times between 30°C and 34°C</li> </ul>	(Xiao et al. 2014)
PVDF hollow fibre MF membrane	Lab-scale filtration	0.3, 21	<p>Extremely cold temperatures at 0.3 °C deteriorated membrane performance and led to membrane pore shrinkage</p> <ul style="list-style-type: none"> <li>• The deterioration could be almost recovered under room temperatures</li> </ul>	(Cui et al. 2017)
PVDF hollow fibre MF membrane	Lab-scale filtration	0.3, 21, 35	<ul style="list-style-type: none"> <li>• a higher remediated temperature recovered more permeability for the membrane</li> </ul>	(Tikka et al. 2019)

#### 2.4.4 Impacts of temperature on membrane cleaning

Membrane cleaning is necessary for maintaining the filtration flux and restoring the membrane performance during membrane filtration operation. Cleaning temperatures did not affect some membrane properties. For example, the cleaning temperatures of 20°C to 34°C had no profound impact on the membrane zeta potential and surface charge, while cleaning agents and pH did pronouncedly (Al-Amoudi et al. 2007). However, membrane structure could be altered during the cleaning at different water temperatures. After treating the cold water at 0.3°C, the deteriorated membrane structures could be recovered under the cleaning with warm water (23, 35°C), and a higher cleaning temperature at 35°C recovered more membrane permeability, but a longer cleaning time may result in a lower recovery rate than the optimal time (Cui et al. 2017, Tikka et al. 2019).

Membrane cleaning consists of physical and chemical cleanings. Chemical cleaning is applying the chemical properties of cleaning agents, such as oxidation, acidity, alkalinity and chelation, to decompose, solute, and detach the foulants adhering to the fouled membrane surface and inside pores (Edzwald 2011). Temperature considerably influences the chemical reaction kinetics, especially the chemical cleaning mainly relies on chemical reactions. Therefore, increasing membrane cleaning temperature generally raises the cleaning effectiveness by promoting mass transport processes and the solubility of solids (Al-Amoudi and Lovitt 2007).

Chen et al. (2003) conducted factorial designs to explore the main factors influencing membrane cleaning with UF and RO membranes in municipal wastewater treatment and showed that the higher temperature at 50°C compared to at 25°C significantly facilitated the chemical cleaning efficiencies. They found that the chemical cleaning at 50°C mitigated the importance of chemical dosages, and the high cleaning efficiencies can still be achieved at the elevated temperature of 50°C with the low concentration of the cleaning agent (Chen et al. 2003). In another

study, Almecija et al. (2009) examined a ceramic membrane implemented for protein separation, and the membrane was cleaned at different temperatures of 30, 50 and 60°C. 50°C was the optimal temperature for membrane chemical cleaning and productivity reinstatement, while cleaning at 30°C developed irreversible fouling around the first filtration cycle, but 60°C cleaning deteriorated and eroded the membrane pores. Rabuni et al. (2015) reported that higher temperature chemical cleaning incurs a higher flux recovery rate with a bench-scale PVDF ultrafiltration membrane filtration. They revealed that at 50°C, flux recovery rates could be more than 100% compared to at 25°C, potentially resulting from the membrane property alteration and degradation (Rabuni et al. 2015). However, the authors failed to consider that the increasing flux could be the effect of pore expansion, which is potentially invertible.

Membrane cleaning not only restores the permeability and performance of membranes but also generates by-products. The cleaning temperature is one of the influential factors for by-product formation (Ding et al. 2020, Wang et al. 2021). For example, NaOCl was applied to clean an ultrafiltration membrane fouled with an algal solution, and the increment of cleaning temperatures from 15°C to 25 and 35°C significantly boosted the generation of halogenated by-products, such as dichloroacetic acid (DCAA), trichloronitromethane (TCNM) and trichloromethane (TCM) (Ding et al. 2020). On the other hand, Wang et al. (2021) suggested that the different temperatures could stimulate or waken the generation of cleaning by-products. They found that the concentrations of trihalomethanes (THMs) and haloacetic acids (HAAs) at 35°C were 168% and 248% higher than those at 15°C, respectively, during the membrane chemical cleaning process, while haloacetonitriles (HANs) and haloketones (HKs) were 75% and 35% less in the corresponding circumstances.

The cleaning temperature cannot be infinitely increasing as the membrane has a threshold with material tolerance, and the better the cleaning temperature is not higher (Madaeni and Samieirad 2010, Ahmad et al. 2014). For example, a polyamide membrane used to treat industrial wastewater was cleaned at 15°C, 25°C, 35°C and 45°C in the research conducted by Madaeni and Samieirad (2010). Their experimental results presented that a low temperature at 15°C had low chemical cleaning strength in flux recovery, but the cleaning at 45°C presented an identical cleaning efficiency to that at 35°C. Therefore, it suggests that applying membrane cleaning temperatures higher than 35°C is unnecessary, and the optimized cleaning temperature should be determined to balance the membrane cleaning efficiency and energy consumption in industrial applications. However, the experiment of a cellulose acetate flat-sheet microfiltration membrane fouled with *Chlorella* cells revealed a different optimal cleaning temperature. Ahmad et al. (2014) claimed that after the third time of cleaning the fouled membrane at 60°C with NaOCl as the cleaning agent, it decreased by 7% of filtration flux, but the decrements were 52%, 38% and 17% with the cleaning at 25°C, 40°C and 80°C, respectively. Therefore, the authors argued that 60°C was the best chemical temperature for *Chlorella* cell fouled membranes.

Additionally, Simon et al. (2013) researched how cleaning water temperature influences the virgin membrane during chemical cleaning. They revealed no distinct temperature impact on the virgin membrane at various cleaning temperatures (20, 35, 50°C), which was consistent with the result presented by Al-Amoudi et al. (2007). Simon et al. (2013) also found that the elevated temperature caustic and acidic cleanings significantly increased the membrane surface roughness and resulted in higher hydrophobicity. The virgin membranes cleaned with citric acid expressed lower permeability, while caustic cleaned virgin membranes achieved higher permeabilities at 50°C. Chemical cleaning at excessive temperatures with ethylenediaminetetraacetic-acid (EDTA),

sodium dodecyl sulphate (SDS) or citric acid caused a better rejection of pharmaceutically active compounds and inorganic salts for membranes, but cleaning with caustic did not (Simon et al. 2013).

A limited number of study has been done on the cleaning temperatures close to the freezing point because the temperature can only be encountered in some cold regions during winters. One study by Woo et al. (2013) indicated that the chemical cleaning at 2°C had an 11.6% less permeation recovery rate than at 23°C.

Besides chemical cleaning, physical cleaning is more routine in daily operation and maintenance for membrane filtration water treatment. Physical cleaning employs hydraulic shear force to separate the connections between foulants and membrane physically, and the unattached foulants fall back into the bulk wash water. Temperature variation also has an impact on the effectiveness of physical cleaning. Zhao and Zou (2011) reported that although more severe membrane fouling occurred at the warm temperatures of 35°C and 45°C, warm cleaning water achieved greater efficiency than 25°C during physical cleaning in a forward osmosis desalination system. In an MBR treating synthetic wastewater, Lintzos et al. (2018) discovered that increased back wash temperatures to 38°C presented better performance and prolonged the intervals of physical cleanings. The article also elucidated that higher back wash temperatures led to much lower permeability decreasing rates, though the low-temperature (8°C) cleaning did not compromise the effluent quality. Hube et al. (2021) also claim that compared to at 25°C, physical cleaning at 50°C significantly mitigated intermediate pore blocking and physically irreversible membrane fouling with the filtration of the effluent of the primary settling process from a wastewater treatment plant.

Table 2.4.4 collects the impacts of cleaning water temperature on membrane cleaning.

Table 2.4.4 Summary of the impacts of temperature on cleaning

Membrane type and material	Fouled membrane origin	Cleaning method	Temperature (°C)	Summary	Reference
Spiral wound thin-film polyethersulfone (PES) UF and Polyamide RO membranes from Fluid Systems	Filtrated by Secondary effluent collected from a local sewage treatment	Physical: forward flush, backwash Chemical: TriClean 212F	25, 50	High cleaning temperatures (35, 45, 50°C) caused: <ul style="list-style-type: none"> <li>• high efficiency</li> <li>• chemical dosage economy</li> <li>• at 50°C, flux recovery rates can be more than 100%</li> </ul>	(Chen et al. 2003)
Flat-sheet cellulose triacetate (CTA) FO membranes	Treating real and simulated brackish water	Physical	25, 35, 45		(Zhao and Zou 2011)
Flat-sheet UF PVDF membrane	Fouled with bovine serum albumin (BSA)	Chemical: NaOH, NaOCl	25, 50		(Rabuni et al. 2015)
Three commercial NF membranes	Saline water desalination	Chemical: HCl, NaOH, SDS, Mixed agent of EDTA, TSP and STP, NaOH followed by HCl	20, 23, 25, 30, 34	Cleaning temperature had no impact on membrane surface charge and zeta potential.	(Al-Amoudi et al. 2007)
Tubular ceramic Céram Inside membrane made of ZrO <sub>2</sub> -TiO <sub>2</sub>	Fouled by protein solution containing β-lactoglobulin and bovine serum albumin	Chemical: sodium hydroxide and sodium dodecyl sulphate solution	30, 50, 60	<ul style="list-style-type: none"> <li>• 50°C is the optimal temperature</li> <li>• 30°C developed irreversible fouling</li> <li>• 60°C eroded the membrane</li> </ul>	(Almecija et al. 2009)
FT-30 polyamide membrane	Treated industrial wastewater	Chemical: HCl, HNO <sub>3</sub> , H <sub>2</sub> SO <sub>4</sub> , NaOH, EDTA, SDS	15, 25, 35, 45	<ul style="list-style-type: none"> <li>• 35 and 45°C had the same cleaning efficiency</li> <li>• Lower temperatures (2, 15°C) recovered less flux</li> </ul>	(Madaeni and Samieirad 2010)
PVDF hollow fibre membrane	Pilot plant treating river water	Chemical: NaOH, NaOCl, H <sub>2</sub> SO <sub>4</sub> , HNO <sub>3</sub> , citric acid and oxalic acid	2, 23		(Woo et al. 2013)
NF270 NF membrane with “a semi-aromatic piperazine-based polyamide skin layer on top of a microporous” polysulphone (PS) backing layer	Virgin membrane	Chemical: citric acid, NaOH, EDTA and SDS	20, 35, 50	<ul style="list-style-type: none"> <li>• Temperatures had no impact on the virgin membrane cleaning</li> <li>• High-temperature cleaning increased membrane roughness and hydrophobicity</li> </ul>	(Simon et al. 2013)

Table 2.4.4 Summary of the impacts of temperature on cleaning

Membrane type and material	Fouled membrane origin	Cleaning method	Temperature (°C)	Summary	Reference
				<ul style="list-style-type: none"> <li>• Different cleaning agents combined with various temperatures express distinctive effects</li> </ul>	
Cellulose acetate flat-sheet MF membrane	Fouled with <i>Chlorella</i> cells	Chemical: NaOH, NaOCl, nitric acid and citric acid	25, 40, 60, 80	<ul style="list-style-type: none"> <li>• 60°C is the optimal temperature</li> <li>• Other temperatures had lower flux recovery rates</li> </ul>	(Ahmad et al. 2014)
Hollow fibre UF R-PVDF membrane	Fouled with synthetic wastewater	Physical: backwash	8, 18, 28, 38	<p>Increasing back wash temperature to 38°C</p> <ul style="list-style-type: none"> <li>• presented better performance</li> <li>• prolonged the intervals of physical cleanings</li> <li>• led to much lower permeability-decreasing rates</li> </ul>	(Lintzos et al. 2018)
Flat-sheet PES ultrafiltration membrane	Fouled with algal solution	Chemical: NaOCl	15, 25, 35	<p>Increasing the cleaning temperature to 35°C significantly boosted the generation of halogenated by-products</p>	(Ding et al. 2020)
PVDF ultrafiltration membrane	Fouled with real wastewater	Physical	25, 50	<p>High cleaning temperature mitigated intermediate pore blocking and physically irreversible fouling</p>	(Hube et al. 2021)
PVP/SiO <sub>2</sub> modified hollow fibre PVDF ultrafiltration membrane	Fouled with simulated domestic sewage	Chemical: NaOCl	15, 25, 35	<p>Cleaning temperatures could impact the generation of disinfecting by-products</p>	(Wang et al. 2021)

## CHAPTER 3 Methodology

### 3.1 Materials and apparatus

In this study, distilled water was implemented for the experimental testing. Sodium metabisulphite ( $\text{Na}_2\text{S}_2\text{O}_5$ , supplied by Anachemia) was dissolved and then diluted to 1% (w/w) solution, which formed the repository and experimental environment for submerging the tested membranes. The virgin membrane was fabricated with polyvinylidene fluoride (PVDF), which has a 0.1  $\mu\text{m}$  pore size and is from Jiangsu Dafu Membrane Technology Co., Ltd (PRChina).

A cold room CTS (Climate Testing Systems Inc., Warminster, PA) was used for the cold temperature testing, and the temperature fluctuation of the cold room was  $\pm 0.5^\circ\text{C}$ .

### 3.2 Experiment procedures

The virgin membrane was cleaned with a bleach solution (200ppm hypochlorite) to eliminate potential microbial and organic pollutants on the membrane surface. After pre-cleaning in bleach, the membranes were then flushed with distilled water to eliminate the residual bleach solution and transferred to a glass holding tank (30 $\times$ 15 $\times$ 5cm). The holding tank was filled with the 1% (w/w) sodium metabisulfite ( $\text{Na}_2\text{S}_2\text{O}_5$ ) solution, which could suppress the microorganism growth on the membrane during the several-months experimental process (Xu et al. 2010, Cui et al. 2017). 1L beakers filled with the  $\text{Na}_2\text{S}_2\text{O}_5$  solution were used to create the various thermal aqueous environments to control solution temperatures for membrane testing. Each testing temperature had one beaker in the environment with the  $\text{Na}_2\text{S}_2\text{O}_5$  solution, which was pre-cooled/heated to the target temperature.

The cleaned virgin membranes submerged in the holding tank were first transferred to the beaker in the cold room at a cold temperature (CT; 0.3 $^\circ\text{C}$ , 5 $^\circ\text{C}$  or 10 $^\circ\text{C}$ ) for two weeks. After the

cold temperature treatment, the membranes were taken out of the cold environment and shifted to the two beakers at room temperature (RT) at around 23°C and an elevated temperature (ET) at 35°C, respectively, for several days of recovery treatment. During both cooling and warming periods, membrane pore sizes were intermittently measured. The dynamic changes in membrane pore structure can be reflected through the variations of the membrane pore sizes with respect to the treatment times. The details of measuring periods are shown in Table 3.2.1 for cold temperature treatment and Table 3.2.2 for recovery treatment. In the following of this article, the abbreviation of a specified treatment condition will be used. For example, 48 hours of cold temperature treatment at 5°C will be expressed as “5CT-48h”, and “0.3CT-ET-5h” represents the sample being treated at 35°C for 5 hours after 0.3°C of cold temperature treatment.

*Table 3.2.1 Measuring periods of cold temperature treatment*

Cold temperature (°C)	0.3 (CT)	5 (CT)	10 (CT)
	0	0	0
	0.5	2	2
	1.5	5	5
	3	8	8
	5	24	24
	8	48	48
Cold temperature treatment time (hour)	12	96	96
	24	168	168
	48	240	240
	96	360	336
	168		
	240		
	336		

Table 3.2.2 Measuring periods of recovery treatment

Cold temperature (°C)	0.3 (CT)		5 (CT)		10 (CT)	
Recovery temperature (°C)	23 (RT)	35 (ET)	23 (RT)	35 (ET)	23 (RT)	35 (ET)
	0	0	0	0	0	0
	0.5	0.5	0.5	0.5	0.5	0.5
	1.5	1.5	1.5	1.5	1.5	1.5
	3	3	3	3	3	3
Recovery treatment time (hour)	5	5	5	5	5	5
	8	8	8	8	8	8
	12	12	10	10	12	12
	24	24	24	24	24	24
	48	48	48	48	48	48
	96	96	144	144	96	96

The cold temperature examined were selected considering the water temperatures that some water treatment plants operating in cold regions during winter and springtime, while the two recovery temperatures were potentially used for cleaning.

### 3.3 Sample collection and analysis

Three replicate runs were performed for each experimental treatment. For each trial run, a large piece of the membrane was first to cut into small strips of 1cm×4cm. About 40 membrane strips were then placed into the beaker in the cold room. One membrane strip was taken out from the temperature-controlling beaker as each time point sample for examination. After two weeks of cold temperature treatment, the remainder of the membrane strips were divided into two sets and placed in the beakers containing Na<sub>2</sub>S<sub>2</sub>O<sub>5</sub> solution to start recovery treatments. The recovery treatments were conducted in two independent temperatures: lab room temperature (RT) and the elevated temperature (ET) of 35°C. One beaker with the Na<sub>2</sub>S<sub>2</sub>O<sub>5</sub> solution was set in the lab room as the RT control, while another maintained the ET with the beaker in a water bath. Beakers were sealed with plastic wrap to avoid solution evaporation. Several treatment time points were chosen

for both cold and warm temperature treatments to measure the dynamic change of the membrane pore size.

After being taken out, the sampled membrane strips were immediately soaked in liquid nitrogen for 10 minutes to dry and stabilize the membrane structure. Each dried membrane strip sample was cut into two pieces of 0.5×0.5 cm and pasted onto two metal holders by carbon tapes. For the measurement of membrane pore distribution, a Scanning Electron Microscope (SEM, SU70, Hitachi, Japan) was used, and before testing in SEM, the samples were coated with carbon powers using a Sputter Coater (Model 12560, Fullam, USA) on the membrane surface. The magnification was selected at 100k, where the pores can be clearly identified, and an adequate number of pores was on one image. The measurement of equivalent pore diameters determines the pore sizes on the membrane surface. The images of membrane surfaces were measured by ImageJ (Version from 1.53f to 1.53s, National Institutes of Health, USA).

### 3.4 Data analysis

Large numbers of pores were measured to verify the reproducibility concerning the counted number of pores. Figure 3.4.1 shows the effect of the counted number of pores on the randomization of the measured membrane pore size distribution (MPSD) represented by the accumulative frequency, in which “ $d_{10}$ ” means 10% number of pores have equal or smaller diameters than the parameter so as “ $d_{50}$ ”, “ $d_{90}$ ” and the ordinate in Figure 3.4.1.b. As illustrated in Figure 3.4.1.a and Figure 3.4.1.b, collecting more than 500 pores had a limited effect on measuring MPSD in considering confidence and precision. Figure 3.4.1 displays that the measurement of equivalent pore diameters on SEM images is a reliable technique to evaluate MPSD affected by

temperatures, and being consistent with the previous study (Tikka et al. 2019), 700 pores were counted for each sample.

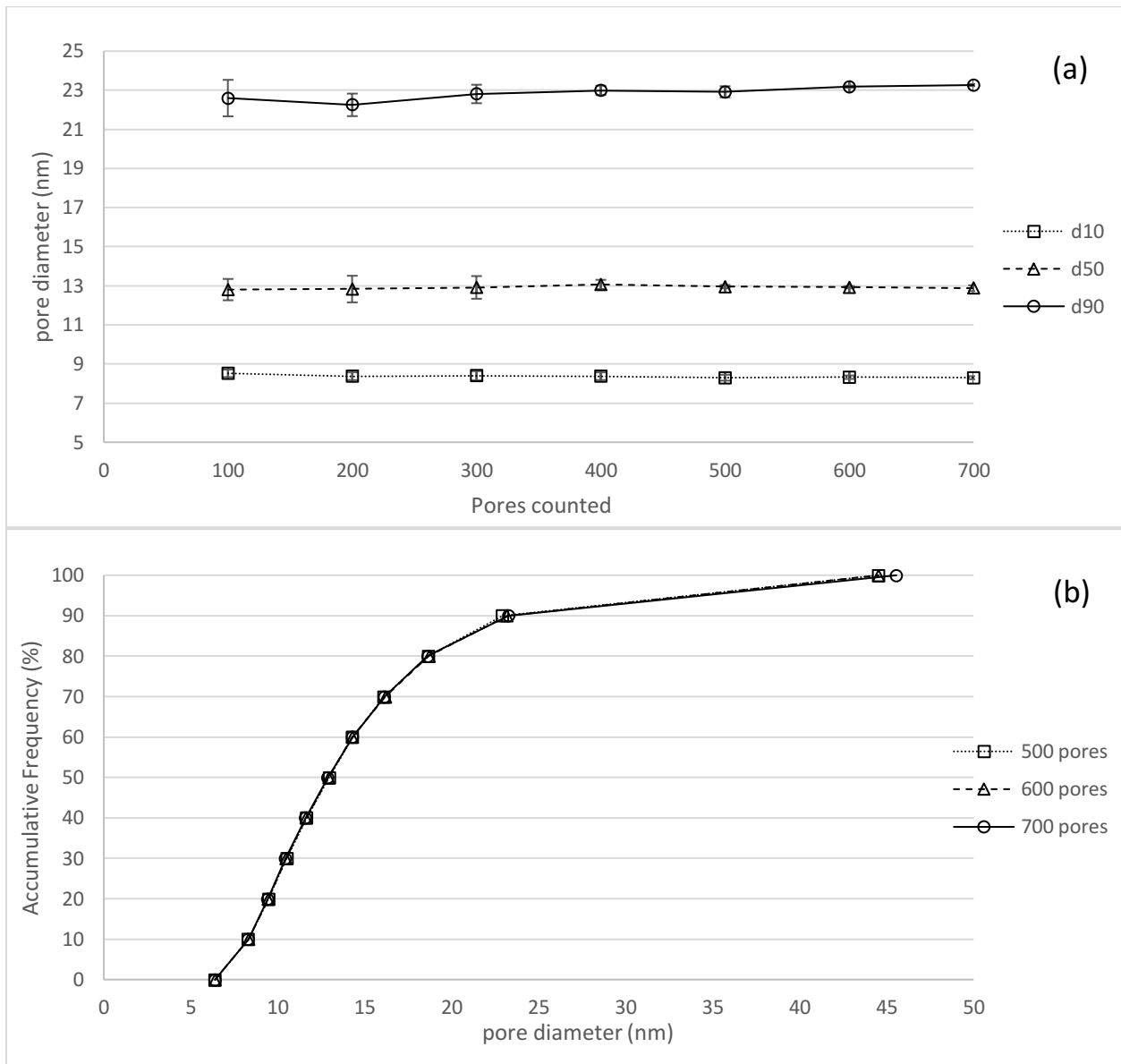


Figure 3.4.1 Effect of the counted number of pores on the randomization of the measured MPSD. (a) percentile pore diameters d10, d50 and d90 expressed as “average  $\pm$  standard deviation for three data sets” and (b) accumulated frequency of pore diameters (sample origin from 5CT-ET-24h).

In this study, each treatment period had two pieces of membrane segments for SEM testing, and a total of 2100 membrane pores were measured from these two SEM specimens. The 2100 pore size data were then randomized and divided into three groups. First, the equivalent diameters

for the membrane pores were analyzed. After sorting the diameters in order, each pore group had  $d_{10}$ ,  $d_{50}$  and  $d_{90}$  as the percentile particle sizes, which represent “small pore diameter”, “medium pore diameter” and “large pore diameter”, respectively, on the sampled membrane surface. Next, the percentile particle sizes for every identical treatment condition were expressed as the average values of  $d_{10}$ ,  $d_{50}$  and  $d_{90}$  among the three groups, with the standard deviations as the uncertainties.

The average changing rates during the first five hours of the treatment were calculated and compared to analyze the initial period’s variations of different temperature treatments regarding membrane pore sizes. In addition, analysis of variance (ANOVA) and student t-test were implemented to evaluate the temperature effects on long-time stabilized pore sizes.

After collecting the time series data of  $d_{10}$ ,  $d_{50}$  and  $d_{90}$ , the dynamic changes of percentile membrane pore diameters were modelled. Cold temperature treatments included three treatment conditions, which were at  $0.3^{\circ}\text{C}$  (0.3CT),  $5^{\circ}\text{C}$  (5CT) and  $10^{\circ}\text{C}$  (10CT). Each temperature treatment condition had the unique virgin membrane testing at the beginning of each batch run. Thus, the data of  $d_{10}$ ,  $d_{50}$  and  $d_{90}$  must be scaling normalized based on the percentile diameter of the virgin membrane in each run to unify the benchmark for across-run data analysis, in which the normalized  $d_{10}$ ,  $d_{50}$  and  $d_{90}$  ( $Nd_{10}$ ,  $Nd_{50}$  and  $Nd_{90}$ ) for virgin membranes were always “1”. Furthermore, recovery treatment was the subsequent procedure of the cold temperature treatment. Each CT treatment had its independent recovery processes, and the longest time point for the CT treatment was the beginning (time = 0) for the respective recovery treatment. The recovery data were still required to be scaling normalized based on the virgin membrane profile from each CT treatment to process the cross-CT-group analysis. Then, the normalized data were modelling fitted versus treatment time.

The modelling fitting, modelling plots and post-modelling calculations were done by MATLAB (R2022a Update 4). After several trials of different models, the natural exponential model was optimal for modelling both cold temperature and recovery temperature treatments. The model is shown in Function (1).

$$y = ae^{bx} + c \quad (1)$$

Where:  $y$  — Scaling normalized percentile diameters (Nd10, Nd50 or Nd90);

$x$  — Treatment time, hour;

$a, b, c$  — Parameters of models.

## CHAPTER 4 Results

### 4.1 Temperature impacts on membrane pore size distribution

Temperature effects on membrane pore sizes and size distribution were examined in this study. SEM images were taken for membrane morphology analysis. Change in membrane pore size distribution under various cold operating temperatures and subsequent recovery of the membrane pores after warm water treatments were analyzed.

#### 4.1.1 Morphology of membrane surface from SEM images

##### 4.1.1.1 Comparison of virgin membrane and membranes after cold temperature operation

Figure 4.1.1(a and b) is side-by-side comparisons of the SEM images of the virgin membrane (4.1.1.a, 0.3CT-VM) and the membrane treated at 0.3°C for 14 days (4.1.1.b, 0.3CT-14d). The morphology changes can be visually compared among these images with the magnification of 100 thousand times for the membrane surfaces. Figure 4.1.1.a obviously has larger pores than Figure 4.1.1.b, which indicates the shrinkage of membrane pores after two weeks' cooling at 0.3°C.

Figure 4.1.1 (c, d, e and f) shows similar images for the experimental runs with cold temperature treatments at 5°C (5CT) and 10°C (10CT). Figures 4.1.1.c and 4.1.1.d show the SEM images for the 5CT run with a virgin membrane (4.1.1.c, 5CT-VM), the membrane treated at 5°C for 15 days (4.1.1.d, 5CT-15d). Figures 4.1.1.e and 4.1.1.f present the images for 10CT run, which are from 10CT-VM (4.1.1.e), 10CT-14d (4.1.1.f). The Figures for 5CT and 10CT treatments are comparable to those for 0.3CT, and the images from the membranes at the end of cold temperature treatments have smaller pore sizes than those for virgin membranes in their groups, indicating the membrane pore size decrease induced by the cold temperatures (5°C and 10°C).

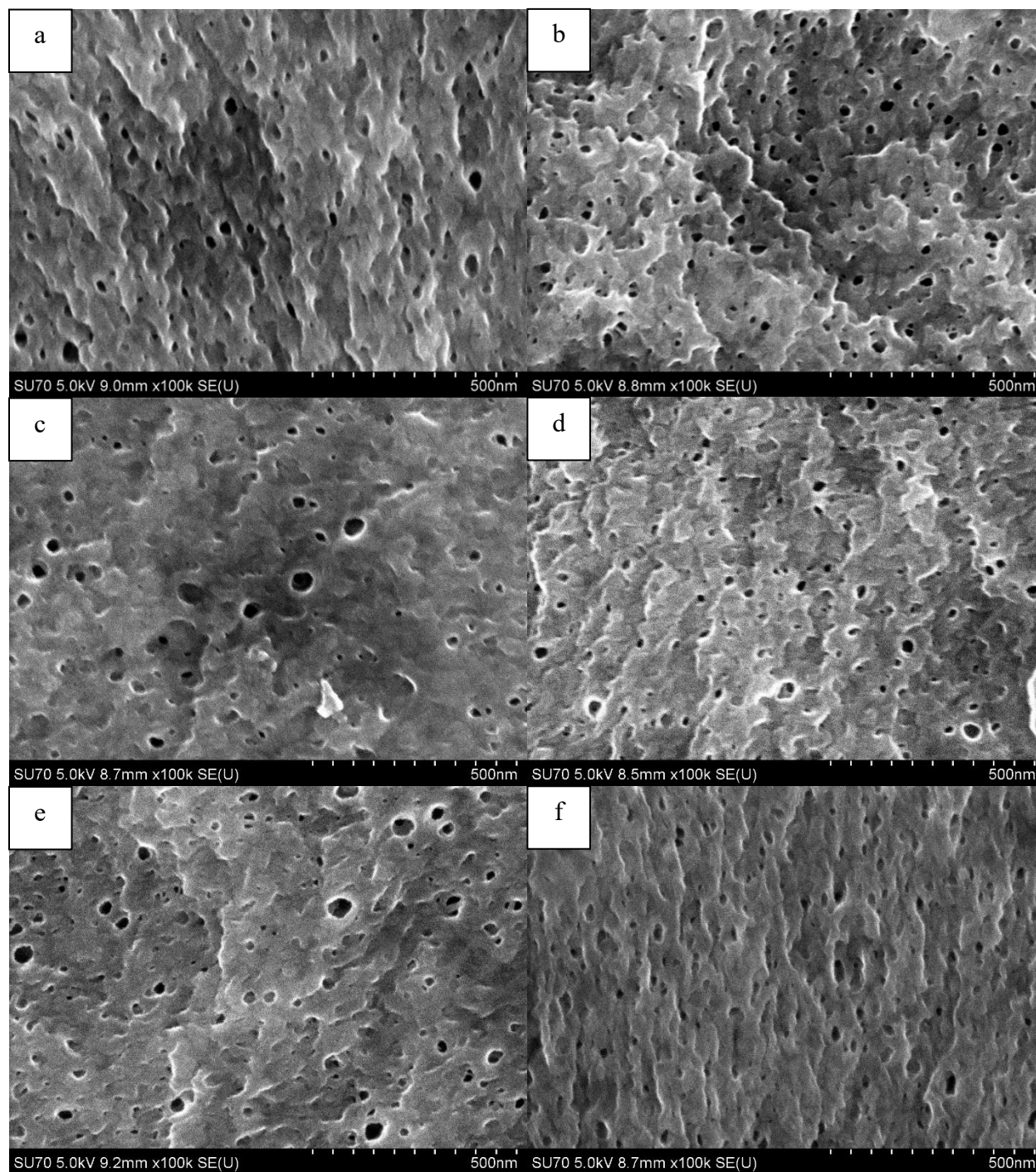


*Figure 4.1.1 SEM images of membranes: a) 0.3CT-VM, b) 0.3CT-14d, c) 5CT-VM, d) 5CT-15d, e) 10CT-VM and e) 10CT-14d.*

#### 4.1.1.2 Comparison of virgin membrane and recovered membranes after warm temperature operation

After two weeks of cooling conditioning at 0.3°C, the pictures of the membranes which were treated at room temperature (RT) for four days (Figure 4.1.2.b, 0.3CT-RT-4d) and elevated temperature (ET, 35°C) for four days (Figure 4.1.2.c, 0.3CT-ET-4d) are shown in Figure 4.1.2. The elevated temperature induced the membrane pore size expansions with the largest pore sizes from the cold temperature shrinkage, while the warming treatment at room temperature enlarged the membrane pore to a similar size to the virgin membranes (Figure 4.1.2.a). The results suggest that room and elevated temperatures can recover the membrane pore size shrinkage induced by the extremely cold temperature (0.3°C).

Figure 4.1.2 (e, f, h, and i) also presents the images for the membranes treated in 5CT-RT-6d (4.1.2.e), 5CT-ET-6d (4.1.2.f), 10CT-RT-4d (4.1.2.h) and 10CT-ET-4d (4.1.2.i). The membranes after RT treatments (Figure 4.1.2) tended to have larger pore sizes than the ones after CT treatments (Figure 4.1.1) but were still smaller than the virgin membranes (Figure 4.1.2). By contrast, the membranes after ET treatments (Figure 4.1.2) had similar pore sizes as those of the virgin membranes. Depending on the warm water temperature, the recovery treatments could partially or fully recover the membrane pore sizes reduced by cold temperatures (5°C and 10°C).

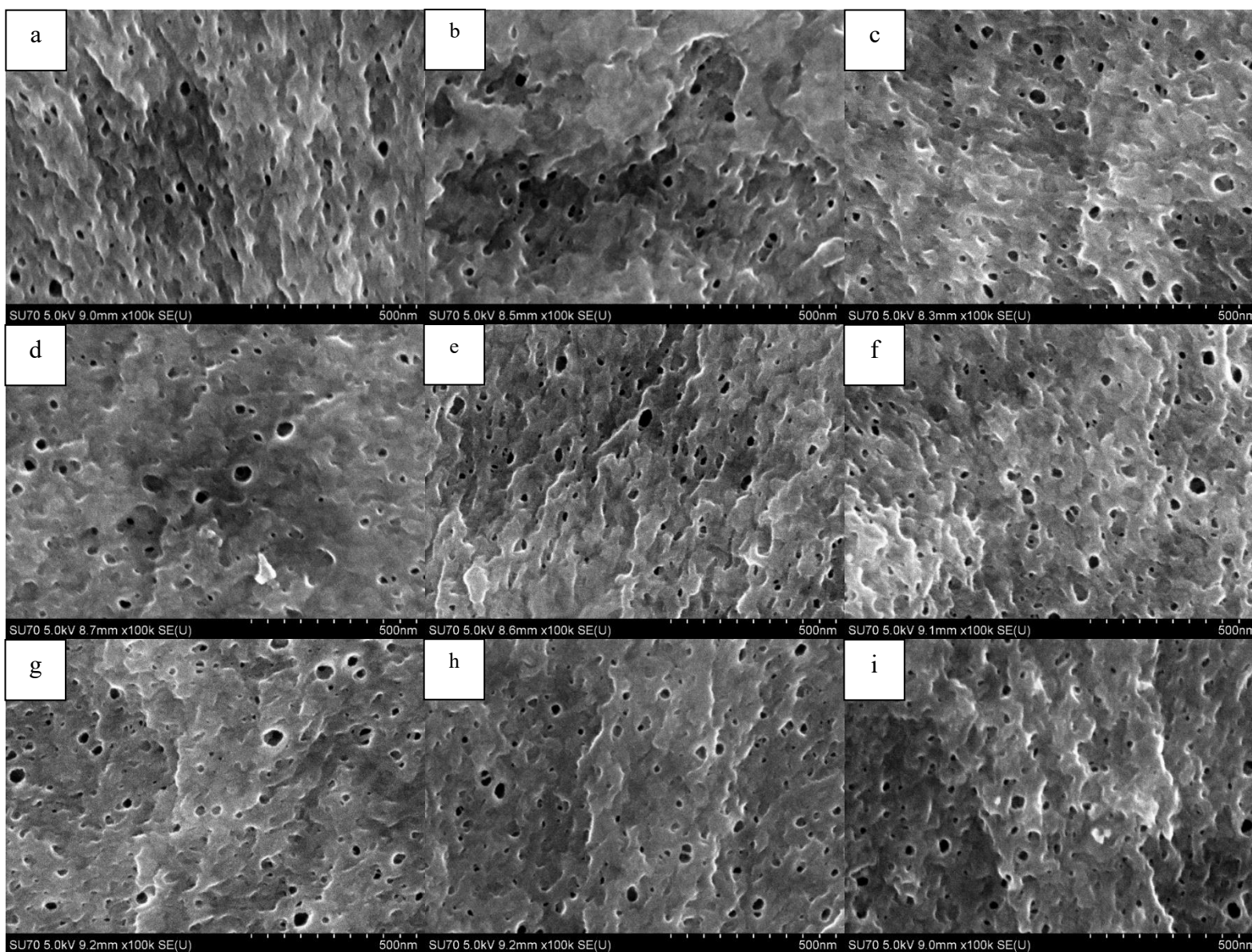


Figure 4.1.2 SEM images of membranes: a) 0.3CT-VM, b) 0.3CT-RT-4d, c) 0.3CT-ET-4d, d) 5CT-VM, e) 5CT-RT-6d, f) 5CT-ET-6d, g) 10CT-VM h)10CT-RT-4d and i)10CT-ET-4d.

#### 4.1.2 Temperature effects on membrane pore size and size distribution

Figure 4.1.3 (a, b, and c) compares the accumulative frequencies of membrane pore sizes for the membranes treated under different operating temperatures. Figure 4.1.3 show the pore size distributions of the membranes treated at 0.3°C (0.3CT-14d) and 10°C (10CT-14d) for 14 days in comparison with the virgin membranes (0.3CT-VM, 10CT-VM), while Figure 4.1.3 clarifies the pore size distribution of the membrane treated at 5°C for 15 days (5CT-15d). The relatively high temperature at 10°C caused minimal pore diameter loss at the steady state while cooling at 0.3°C and 5°C could significantly shrink the membrane pores during a long-term operation.

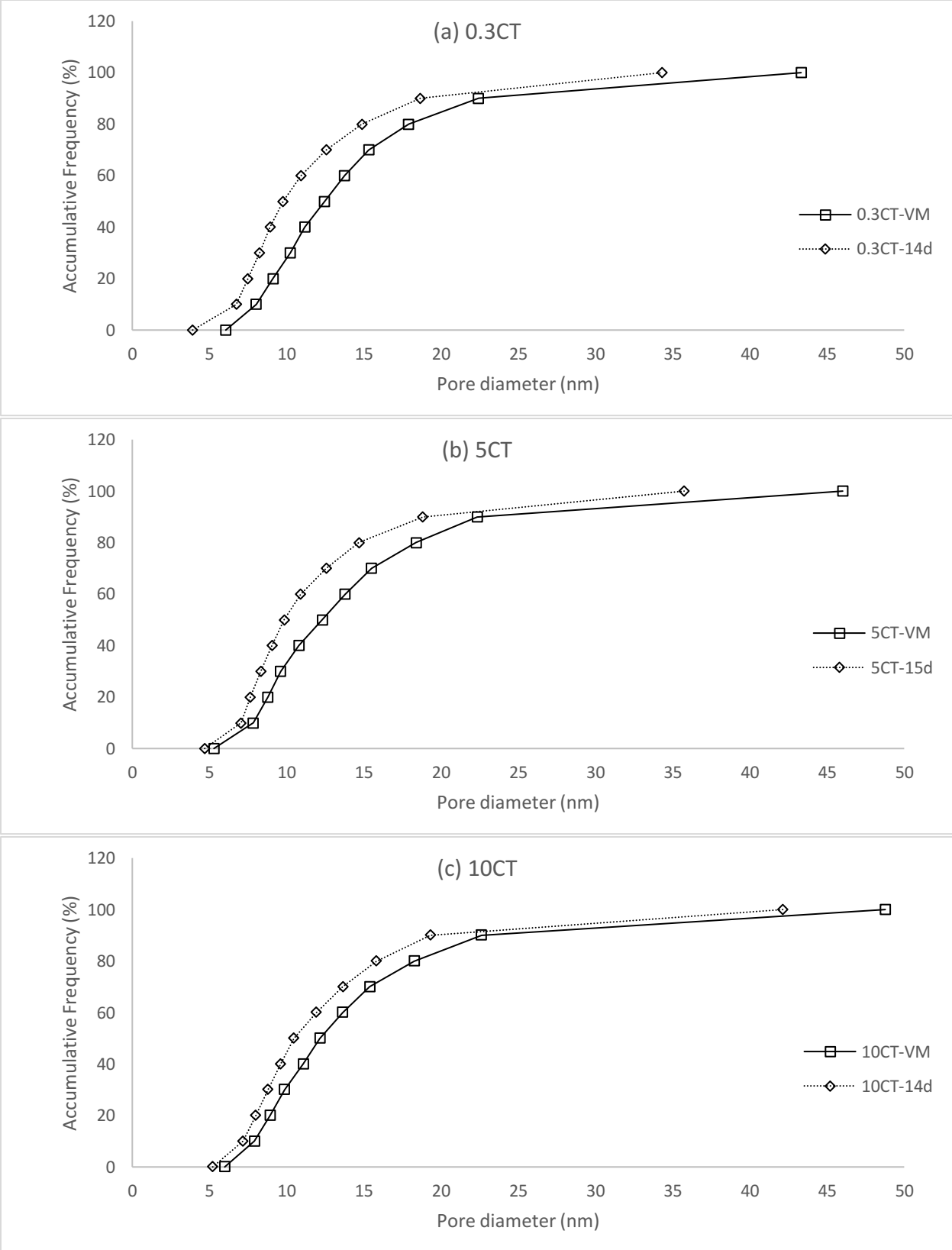


Figure 4.1.3 Membrane pore size distributions (accumulative frequencies) in the steady states of cold temperature treatments (0.3CT, 5CT and 10CT)

#### 4.1.3 Effects of recovery temperature on membrane pore size and size distribution

However, warm temperatures exhibited similar performance during recovery processes regardless of the cold treatment temperatures. Figure 4.1.4 show the pore size distributions of the membranes recovered after four to six days of warm water recovery treatment following cold temperature treatments at 0.3°C (0.3CT-RT/ET-4d), 5CT (5CT-RT/ET-6d) and 10°C (10CT-RT/ET-4d) in comparison with the virgin membranes (0.3CT-VM, 10CT-VM). Despite several days of recovery, RT was not able to fully recover membrane pores to the level of virgin membranes as the smaller pore diameters always presented in pore diameter accumulative frequencies. On the other hand, ET recovery efficiently expanded the membrane pores. The membrane recovered at ET treatment even had larger pore sizes than those of the virgin membrane in the steady states. It can be concluded that warm temperatures are sufficient to recuperate the membrane structure deteriorated by extremely low temperatures, and the recovery at ET was much more effective than at RT.

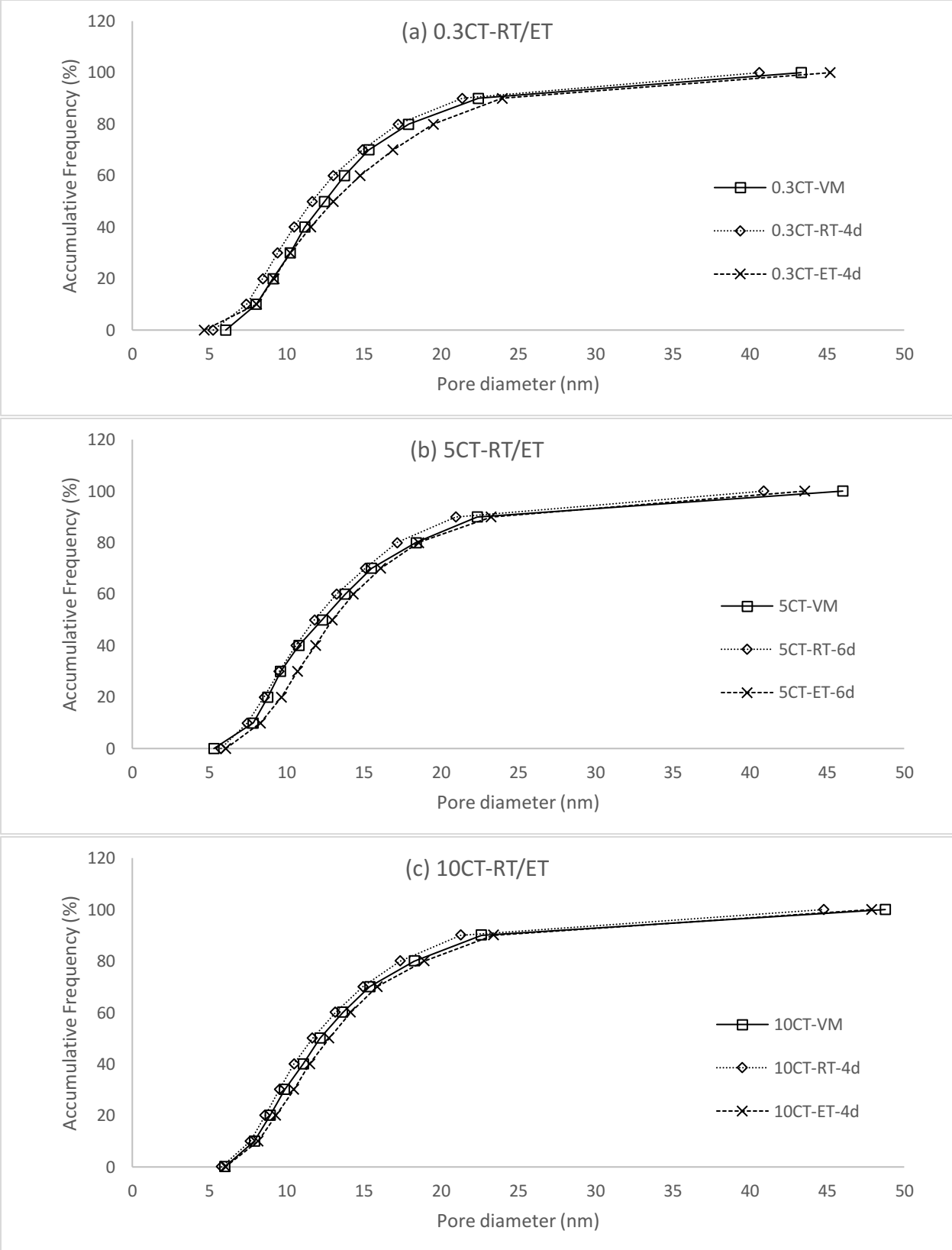


Figure 4.1.4 Membrane pore size distributions (accumulative frequencies) in the steady states of recovery treatments (0.3CT-RT/ET, 5CT-RT/ET and 10CT-RT/ET)

## 4.2 Dynamic changes in membrane pore sizes

Membrane pore sizes with respect to three cold temperature treatment conditions (0.3CT, 5CT and 10CT) and treatment time have been examined and will be presented in this section.

### 4.2.1 Dynamic changes in membrane pore sizes during cold temperature treatment

Figure 4.2.1 (a, b, and c) shows the changes in membrane pore sizes vs. time during the treatments at 0.3°C (0.3CT), 5°C (5CT) and 10°C (10CT). Percentile pore size d10, d50 and d90 are used for comparison. As the duration of exposure to cold temperatures during the initial 12 hours, membrane pores shrank rapidly. As shown in the figure, the membrane pores became stabilized with their structure after 24 hours for all three temperatures (0.3°C, 5°C and 10°C). Regardless of the treatment temperature, 24 hours seem to be the ending point of the decline of membrane pore sizes and the beginning of the steady states. In most time points, d10, d50 and d90 had similar changing trends. However, the considerable fluctuations of d90 occurred after 96 hours in membranes treated at 0.3°C and 5°C, respectively. Comparing these CT treatments, 0.3°C caused a more accelerated decrement at the early stage of the treatments and smaller pore size at the steady states than 5°C and 10°C.

Table 4.2.1 summarizes d10, d50 and d90 of the membrane after control/0, 5, and 24 hours treatments at 0.3°C, 5°C and 10°C. It was obvious that the dramatic declines of membrane pore diameters occurred between control/0 and 5 hours in all experimental conditions. Furthermore, pore size shrinkage slowed down after five hours of the CT treatments.

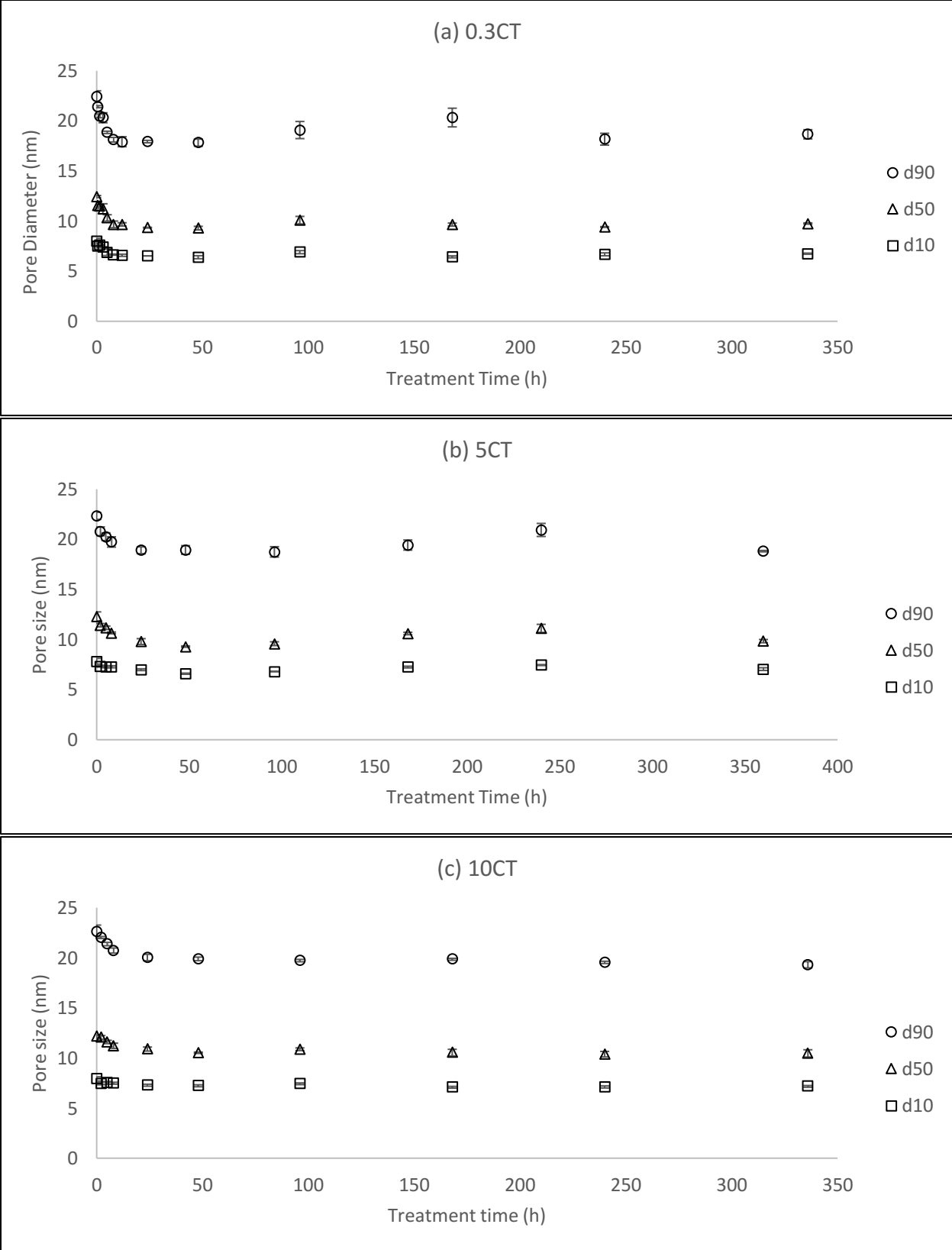


Figure 4.2.1 Dynamic changes in membrane pore size during 0.3°C (0.3CT), 5°C (5CT) and 10°C (10CT) cold temperature treatments.

Table 4.2.1 Summary of the d10, d50, and d90 in different cold temperature treatment conditions at 0h, 5h and 24h.

Treatment temperature	d10 (nm)		
	0h	5h	24h
0.3CT	8.0±0.25	6.9±0.33	6.5±0
5CT	7.8±0.28	7.3±0.10	7.0±0.09
10CT	7.9±0.21	7.5±0.15	7.3±0.10

Treatment temperature	d50 (nm)		
	0h	5h	24h
0.3CT	12.4±0.10	10.3±0.32	9.3±0.04
5CT	12.3±0.45	11.2±0.17	9.8±0.29
10CT	12.2±0.14	11.6±0.17	10.9±0.20

Treatment temperature	d90 (nm)		
	0h	5h	24h
0.3CT	22.4±0.57	18.9±0.12	17.9±0.12
5CT	22.3±0.35	20.3±0.38	18.9±0.34
10CT	22.6±0.64	21.4±0.17	20.0±0.32

The results are expressed as “mean of three measurements ± standard deviation.”

As shown in Table 4.2.1, the membrane pore size changing rates were calculated using the pore sizes between the virgin membranes and the membranes treated after initial five hours with the cold water presented in Table 4.2.2. Table 4.2.2 reveals that the membrane pore sizes of d10 decreased twice the speed at 0.3°C than those at 5°C and 10°C at the beginning of the cold-water treatment. The cold temperature treatment at 0.3°C had twice the pore size decreasing rate for d50 than that of the treatment at 5°C during the initial five hours, while the rate at 5°C was twice as it at 10°C. The pore size changing rates of d90 were -0.7 nm/h in cold water at 0.3°C, -0.4 nm/h at 5°C and -0.24 nm/h at 10°C during the initial period of cold temperature treatments.

Table 4.2.2 Membrane pore size changing rates during initial 5 hours of cold temperature treatment

Treatment temperature	d10 changing rate (nm/h)	d50 changing rate (nm/h)	d90 changing rate (nm/h)
0.3CT	-0.22	-0.42	-0.7
5CT	-0.1	-0.22	-0.4
10CT	-0.08	-0.12	-0.24

After 24 hours of cold temperature treatments, the membrane pore sizes seemed stable. Thus, the membrane pore sizes of d10, d50 and d90 after 24-hour treatments were grouped and distinguished by different cold temperatures. Table 4.2.3 displays the results of ANOVA for the single factor of treatment temperature and student t-test for the comparisons among the temperatures. According to Table 4.2.3, the *p*-values of ANOVA tests are all smaller than 0.001, and the null hypotheses of no significant difference between virgin membrane pore size and the pore sizes in cold temperature treatments were rejected at a 95% confidence interval with the cold temperatures at 0.3, 5 and 10°C. For the comparisons among different cold temperatures, only the membrane pore sizes of d10 and d90 treated after 24 hours between 5°C and 10°C had no significant difference, with the *p*-values equaling 0.050 and 0.077, while 0.3°C cold temperature treatment after 24 hours induced the distinguished membrane pore sizes compared to the treatments at 5°C and 10°C.

*Table 4.2.3 ANOVA and student t-test results (p-values) of d10, d50 and d90 for temperature factor after 24h treatment at cold temperatures*

d10					
Temperature condition	Virgin membrane	0.3CT	5CT	10CT	ANOVA
0.3CT	< 0.001	-	-	-	
5CT	< 0.001	< 0.001	-	-	< 0.001
10CT	< 0.001	< 0.001	0.050	-	
d50					
Temperature condition	Virgin membrane	0.3CT	5CT	10CT	ANOVA
0.3CT	< 0.001	-	-	-	
5CT	< 0.001	0.005	-	-	< 0.001
10CT	< 0.001	< 0.001	0.006	-	
d90					
Temperature condition	Virgin membrane	0.3CT	5CT	10CT	ANOVA
0.3CT	< 0.001	-	-	-	
5CT	< 0.001	0.049	-	-	< 0.001
10CT	< 0.001	< 0.001	0.077	-	

#### 4.2.2 Dynamic changes in membrane pore size during recovery treatments

Figure 4.2.2 to Figure 4.2.4 show the dynamic changes in membrane pore size recovery after treatment in warm water for various time periods in comparison with corresponding virgin membranes. Figure 4.2.2 presents the recovery of the membrane treated at 0.3CT for 336 hours. Figure 4.2.3 is the recovery of the membrane treated at 5CT for 360 hours, while Figure 4.2.4 is the recovery for 10CT for 336 hours. The recovery treatment for each cold temperature treated membrane consisted of two warm water temperatures – room (RT) and elevated (ET). In those figures, the d10, d50 and d90 of the virgin membrane form the based lines, marked as “VM d10”, “VM d50” and “VM d90”. According to the figures, both RT and ET are capable of recovering the geometrical structure of the membranes, and different cold temperature treatments did not influence the trend of recovery treatment. The membrane pore sizes reached the plateaus after 24 hours of treatment with both RT and ET rehabilitations. However, RT and ET recoveries were accompanied by distinctive results. Membrane pore sizes present a higher-order growth at elevated temperature (35°C) than at room temperature during the initial period of recovery treatments. Furthermore, the membrane pore size could be fully recovered to that of virgin membranes at 35°C within 12 hours, while the room temperature treatment is deficient in perfectly restoring membrane pore structure to initial status (virgin membrane) even in prolonging treatment time.

The data for d10, d50 and d90 in 0, 5 and 24 hours of recovery treatments are revealed in Table 4.2.1. There were remarkable differences between 0h and 5h in both RT and ET treatments for d10, d50 and d90, which validated the effectiveness of recovery treatments. The ET treatments led to larger pore sizes than RT treatments, regardless of the CT conditions, indicating that the ET recovery was more efficient compared to the RT recovery. The pore sizes were still increased from 5h to 24h of the ET treatments though the increasing rates were lower than the beginning five

hours. RT performed much worse after the same duration than ET in expanding the membrane pores, as d10 had no change during this period.

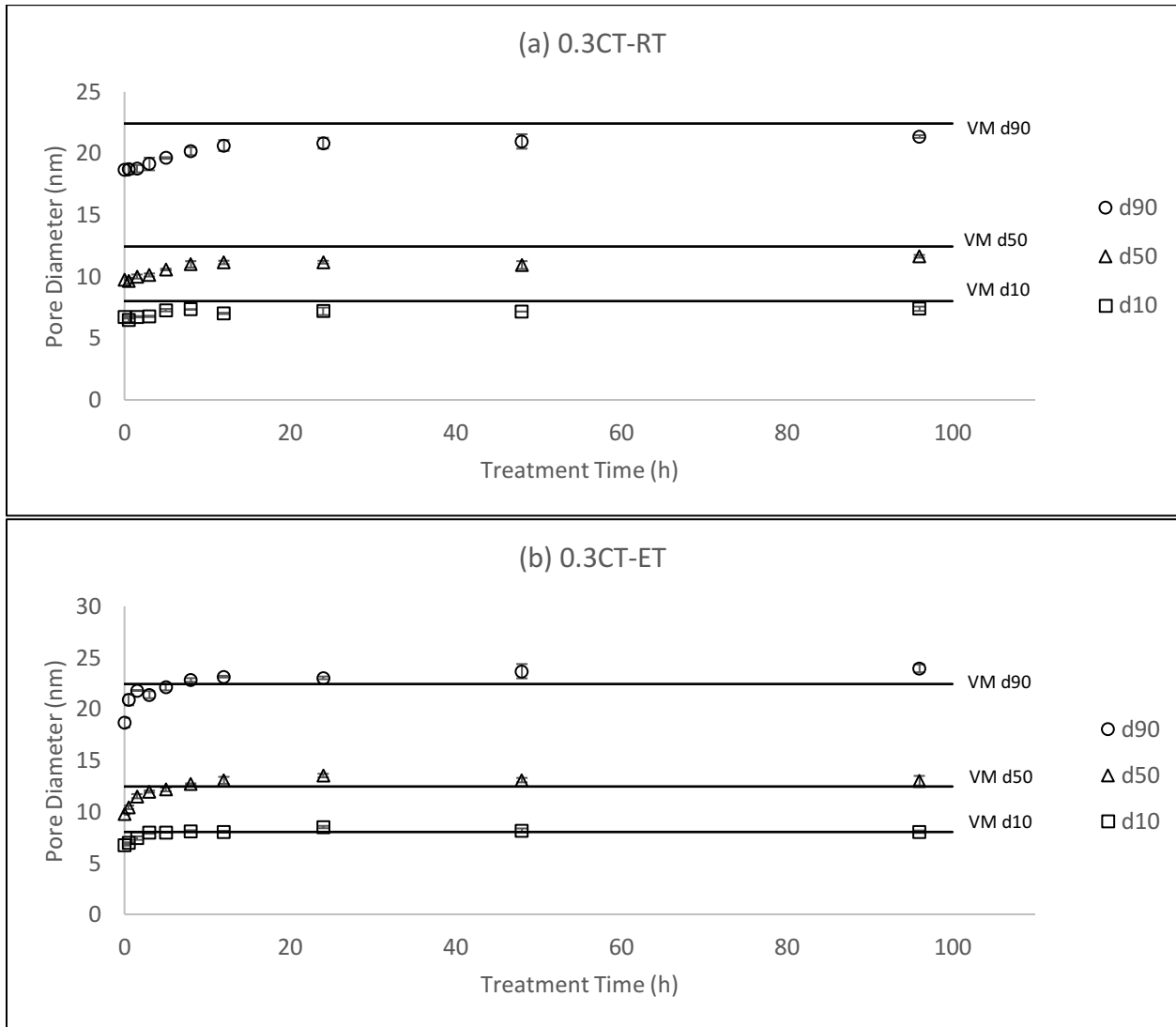
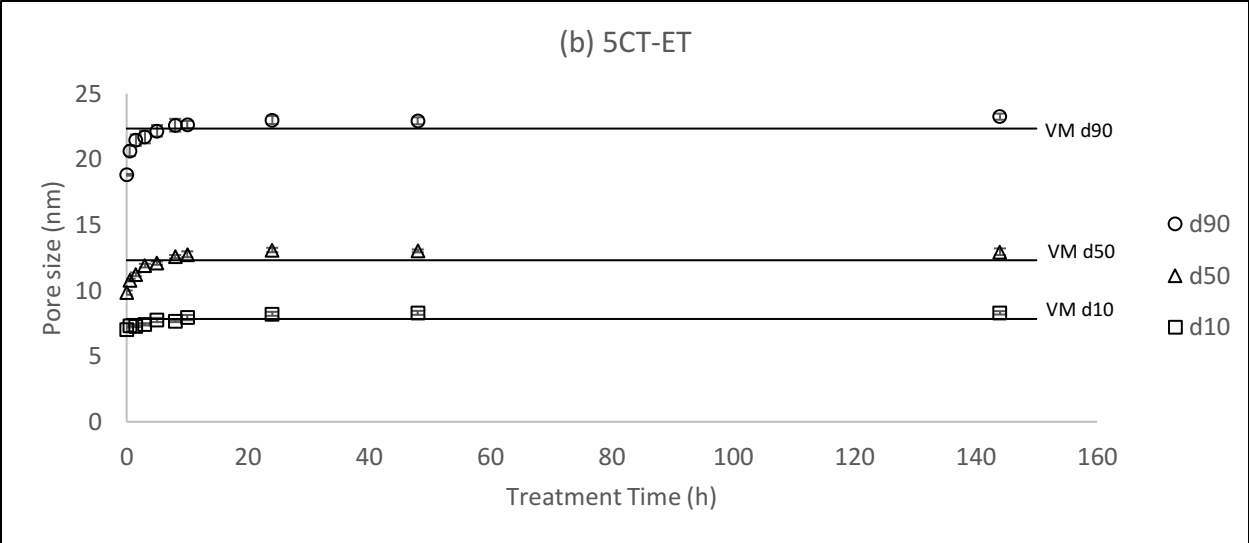
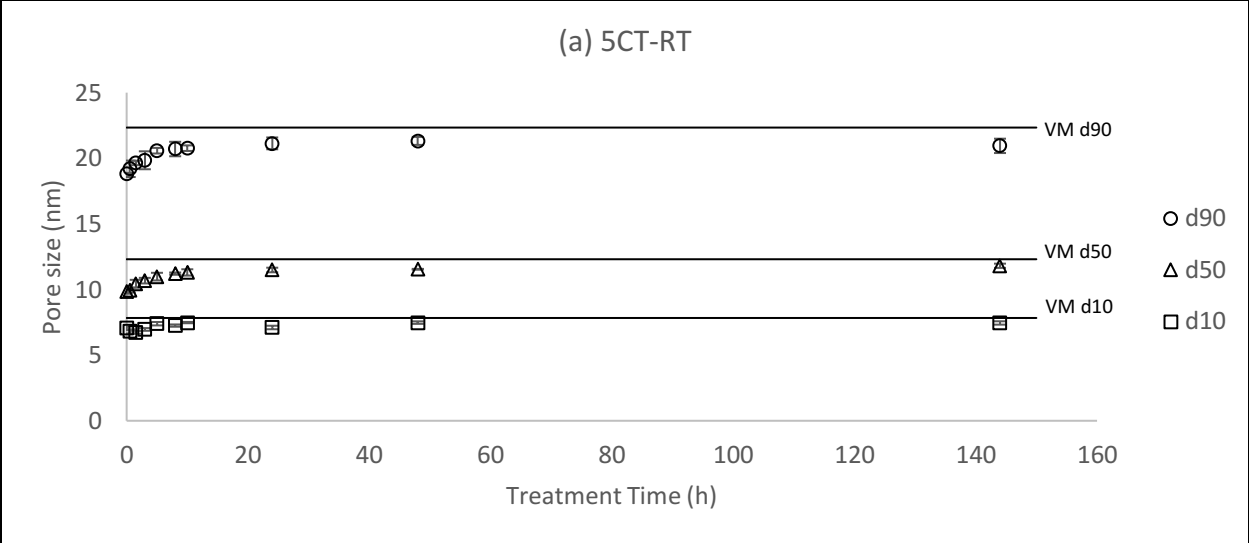


Figure 4.2.2 Recovery of membrane pore sizes at room temperature (RT) and 35 °C (ET) following 0.3 °C cold temperature



*Figure 4.2.3 Recovery of membrane pore sizes at room temperature (RT) and 35°C (ET) following 5°C cold temperature*

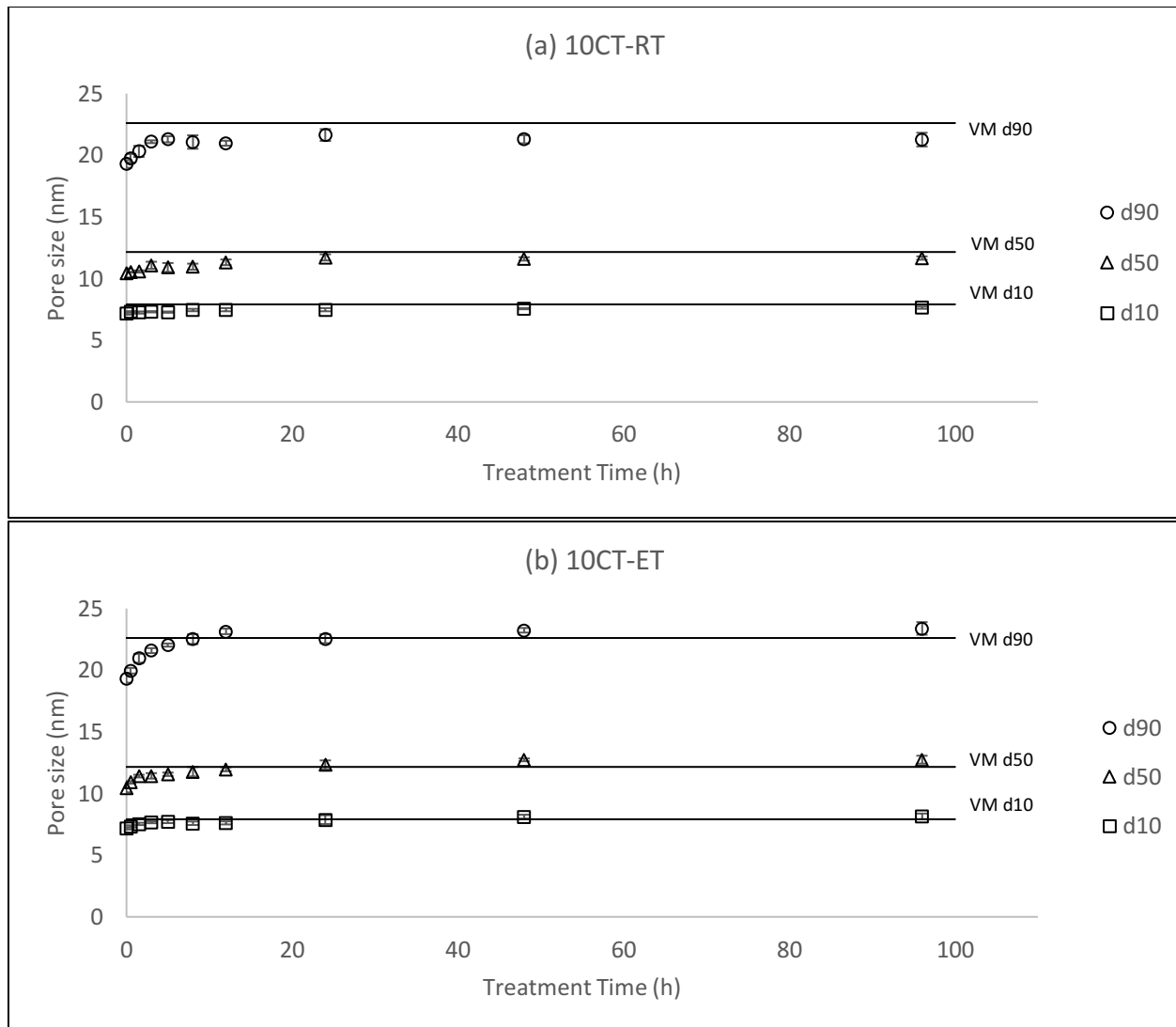


Figure 4.2.4 Recovery of membrane pore sizes at room temperature (RT) and 35°C (ET) following 10°C cold temperature

Table 4.2.4 Recovery of d10, d50, and d90 after 0, 5h and 24h with warm water (room temperature and 35°C) treatments

Treatment condition	d10 (nm)		
	0h	5h	24h
0.3CT-RT	6.7±0.05	7.3±0.1	7.2±0.31
0.3CT-ET	6.7±0.05	8.0±0	8.5±0.11
5CT-RT	7.0±0.14	7.4±0.13	7.1±0.13
5CT-ET	7.0±0.14	7.8±0.16	8.2±0.15
10CT-RT	7.2±0.09	7.3±0.05	7.5±0.13
10CT-ET	7.2±0.09	7.7±0.12	7.9±0.36

Table 4.2.4 Recovery of d10, d50, and d90 after 0, 5h and 24h with warm water (room temperature and 35°C) treatments

Treatment temperature	d50 (nm)		
	0h	5h	24h
0.3CT-RT	9.8±0.06	10.6±0.07	11.2±0.12
0.3CT-ET	9.8±0.06	12.2±0.18	13.5±0.17
5CT-RT	9.8±0.16	11.0±0.29	11.5±0.17
5CT-ET	9.8±0.16	12.1±0.13	13.1±0.17
10CT-RT	10.5±0.36	10.9±0.36	11.7±0.25
10CT-ET	10.5±0.36	11.6±0.14	12.3±0.36
Treatment temperature	d90 (nm)		
	0h	5h	24h
0.3CT-RT	18.7±0.46	19.6±0.07	20.8±0.44
0.3CT-ET	18.7±0.46	22.1±0.3	23.0±0.13
5CT-RT	18.8±0.07	20.6±0.21	21.1±0.45
5CT-ET	18.8±0.07	22.2±0.43	23.0±0.32
10CT-RT	19.3±0.31	21.3±0.25	21.6±0.48
10CT-ET	19.3±0.31	22.0±0.13	22.6±0.36

The results are expressed as “mean of three measurements ± standard deviation.”

Table 4.2.5 shows the changing rates of the membrane pore sizes of d10, d50 and d90 at the beginning of five hours of room temperature and 35°C treatments. The results from Table 4.2.5 present that the initial five-hour recovery treatment at 35°C had much larger pore size increasing rates than room temperature recovery. The membrane pore size increasing rates at the beginning five hours of 35°C recovery were double or more than double compared to those of room temperature recovery, except the d90 increasing rates were 0.4 nm/h at RT recovery and 0.54 nm/h at ET recovery. The membrane pore size recovering speeds at ET recovery were five times as at RT recovery with d10 at 10CT batch, three times with d50 at 0.3CT batch and four times with d90 at 0.3CT batch.

Table 4.2.5 Membrane pore size changing rates during initial 5 hours of warm water (room temperature and 35°C) treatments

Treatment temperature	d10 changing rate (nm/h)	d50 changing rate (nm/h)	d90 changing rate (nm/h)
0.3CT-RT	0.12	0.16	0.18
0.3CT-ET	0.26	0.48	0.68
5CT-RT	0.08	0.24	0.36
5CT-ET	0.16	0.46	0.68
10CT-RT	0.02	0.08	0.4
10CT-ET	0.1	0.22	0.54

The ANOVA and student t-test results of membrane pore sizes in the comparisons of recovery temperature influences after 24 hours are shown in Table 4.2.6. The ANOVA results indicate significantly different membrane pore sizes of d10, d50 and d90 among room and elevated temperature recoveries above 24 hours and virgin membranes. Most of the null hypotheses for the student t-test were rejected at a 95% confidence interval, while insignificant differences in membrane pore sizes only were found between the virgin membranes and the membranes at 35°C recoveries for d10 and d50 with the p-values for t-tests larger than 0.05.

Table 4.2.6 ANOVA and student t-test results (p-values) of d10, d50 and d90 for temperature factor after 24h treatment at warm temperatures

d10 at 0.3CT	Temperature condition	Virgin membrane	0.3CT-RT	0.3CT-ET	ANOVA
	0.3CT-RT	< 0.001	-	-	< 0.001
	0.3CT-ET	0.011	< 0.001	-	< 0.001
d10 at 5CT	Temperature condition	Virgin membrane	5CT-RT	5CT-ET	ANOVA
	5CT-RT	< 0.001	-	-	< 0.001
	5CT-ET	< 0.001	< 0.001	-	< 0.001
d10 at 10CT	Temperature condition	Virgin membrane	10CT-RT	10CT-ET	ANOVA
	10CT-RT	< 0.001	-	-	< 0.001
	10CT-ET	0.278	< 0.001	-	< 0.001
d50 at 0.3CT	Temperature condition	Virgin membrane	0.3CT-RT	0.3CT-ET	ANOVA
	0.3CT-RT	< 0.001	-	-	< 0.001
	0.3CT-ET	< 0.001	< 0.001	-	< 0.001
d50 at 5CT	Temperature condition	Virgin membrane	5CT-RT	5CT-ET	ANOVA
	5CT-RT	< 0.001	-	-	< 0.001

Table 4.2.6 ANOVA and student t-test results (p-values) of d10, d50 and d90 for temperature factor after 24h treatment at warm temperatures

	5CT-ET	< 0.001	< 0.001	-	
d50 at 10CT	Temperature condition	Virgin membrane	10CT-RT	10CT-ET	ANOVA
	10CT-RT	< 0.001	-	-	< 0.001
	10CT-ET	0.051	< 0.001	-	
d90 at 0.3CT	Temperature condition	Virgin membrane	0.3CT-RT	0.3CT-ET	ANOVA
	0.3CT-RT	< 0.001	-	-	< 0.001
	0.3CT-ET	< 0.001	< 0.001	-	
d90 at 5CT	Temperature condition	Virgin membrane	5CT-RT	5CT-ET	ANOVA
	5CT-RT	< 0.001	-	-	< 0.001
	5CT-ET	0.005	< 0.001	-	
d90 at 10CT	Temperature condition	Virgin membrane	10CT-RT	10CT-ET	ANOVA
	10CT-RT	< 0.001	-	-	< 0.001
	10CT-ET	0.020	< 0.001	-	

### 4.3 Modelling of dynamic changes in membrane pore sizes

#### 4.3.1 Modelling for cold temperature treatment

Changes in membrane percentile pore size, which d10, d50 and d90 represented, were modelled versus treatment time. To present the comparisons among different CT treatments, the data sets of d10, d50 and d90 were scaling normalized and are marked as “Nd10”, “Nd50” and “Nd90”, respectively. Nd10, Nd50 and Nd90 were curves fitted versus time and grouped regarding the cold temperatures. Figure 4.3.1 to Figure 4.3.3 show the modelling curves for 0.3CT, 5CT and 10CT, respectively, versus treatment time. Due to the abnormal fluctuations after one week of the cold temperature treatments, only the initial 50 hours of CT treatments were curve fitted.

For each cold treatment temperature, Nd10, Nd50 and Nd90 presented a comparable changing tendency with the rapid decrement at the beginning of the tests. However, the stable stages were at different levels with Nd10, Nd50 and Nd90. For example, all the cold temperature treatments had a larger Nd10 than Nd90, while the Nd50 was the smallest at the stable phase. At the stable stages, i.e., after around 24 hours, the Nd90 in 0.3CT and 5CT was similar to the Nd10.

For 10CT, the curve of Nd50 was comparable to the Nd90. Furthermore, the decreasing rates of pore sizes in 5CT and 10CT were much lower than those in 0.3CT, and the membrane in 0.3CT was faster in reaching the steady stages than in 5CT and 10CT.

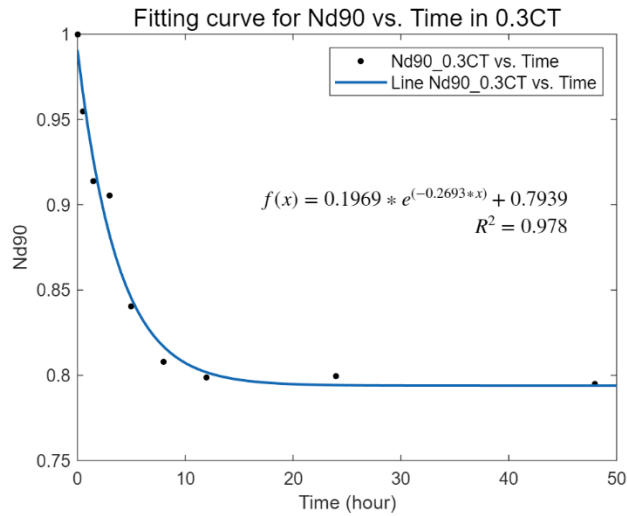
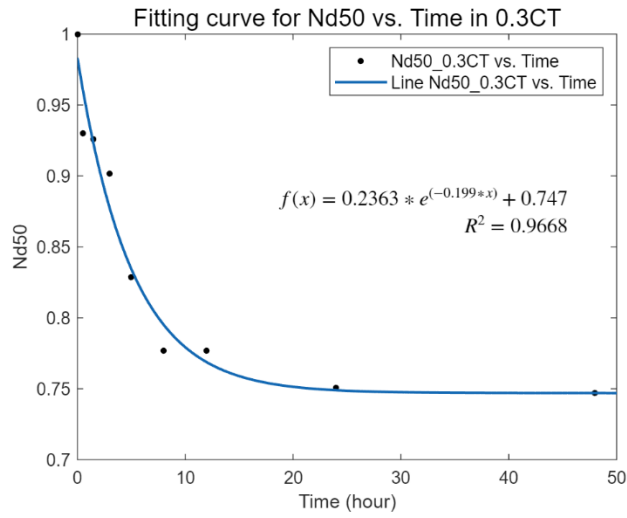
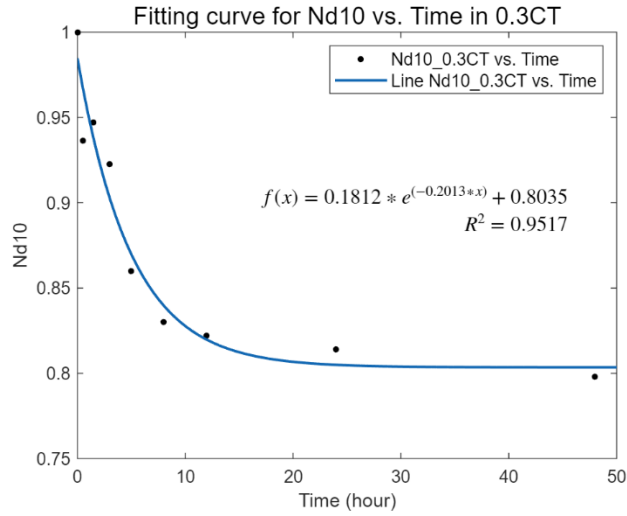


Figure 4.3.1 Fitting curves for Nd10, Nd50 and Nd90 versus time in 0.3°C cold temperature treatment

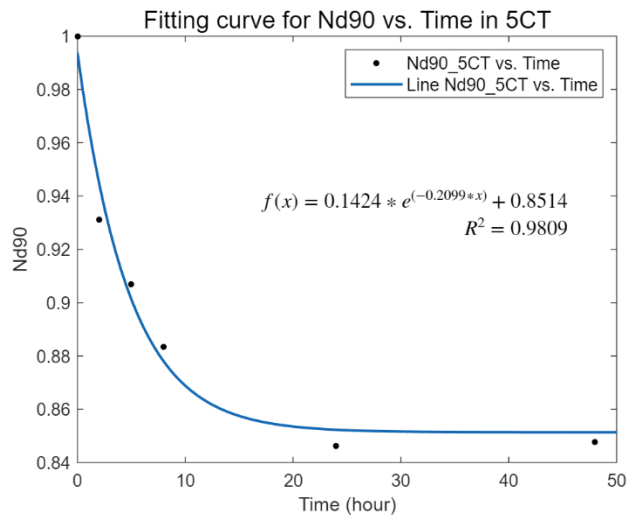
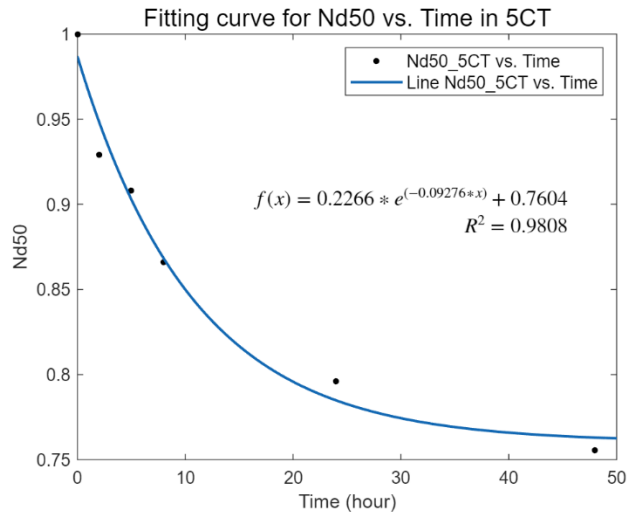
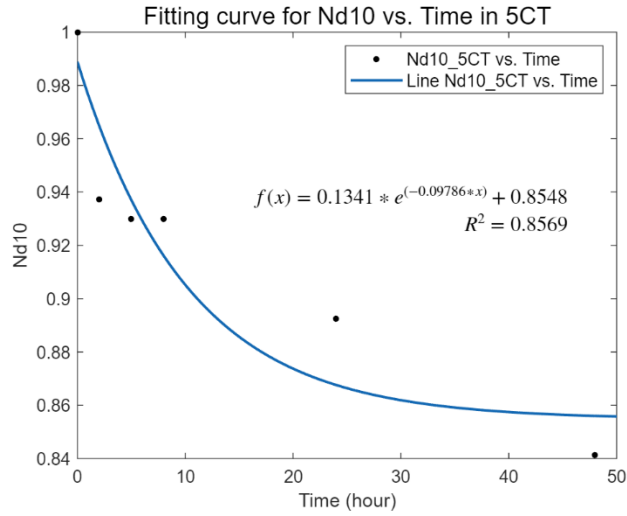


Figure 4.3.2 Fitting curves for Nd10, Nd50 and Nd90 versus time in 5°C cold temperature treatment

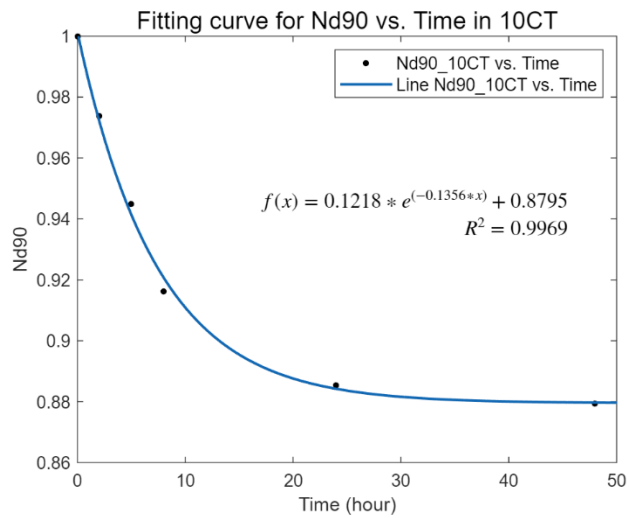
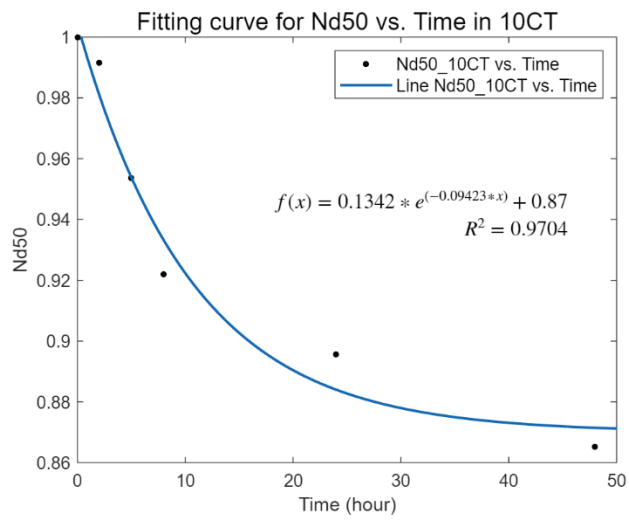
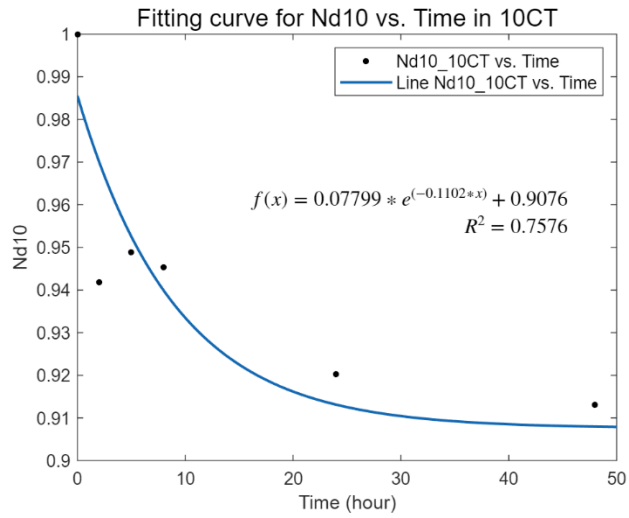


Figure 4.3.3 Fitting curves for Nd10, Nd50 and Nd90 versus time in 10°C cold temperature treatment

The comparisons of CT effects on d10, d50 and d90 are presented in Figure 4.3.4 to Figure 4.3.6. These figures were plotted based on the modelling functions fitted by MATLAB and presented in Figure 4.3.1 to Figure 4.3.3. Figure 4.3.4 shows the modelling changes of Nd10 in different cold temperatures. It is clear that 0.3CT decreased the Nd10 much faster than 5CT and 10CT, and Nd10 was much earlier to become stable in 0.3CT at 12 hours than 5CT and 10CT both at around 24 to 30 hours. Furthermore, the Nd10 in 0.3CT reached the stable stage at 0.81 compared to the 5CT at 0.86 and 10CT at 0.91.

The changes of Nd50 versus time in the model are shown in Figure 4.3.5. The difference between Nd50 of the membrane treated at 5°C and that of the membrane treated at 0.3°C was much smaller after 30 hours, which was different from the figure for Nd10. The stabilized Nd50 was at 0.75 for 0.3CT, 0.77 for 5CT and 0.87 for 10CT, which were all lower than Nd10 at the stable states. In addition, Figure 4.3.6 compares the effects of three cold temperatures on Nd90. The differences among the three curves are more even compared to the graphs of Nd50 but less than those for Nd10. Although 5CT and 10CT induced a comparable decreasing trend on Nd90, the Nd90 in 10CT had larger pore sizes than that of 5CT all the time. Nd90 in both 0.3CT and 5CT reached the smallest pore size compared to virgin membranes at 12 hours, while it took 24 hours for Nd90 in 10CT to the lowest level. 0.3CT, 5CT and 10CT could shrink the d90 to 79%, 85% and 88% of the virgin membranes, respectively, after 24-hour treatment.

In general, the membrane treated with a lower temperature tended to have a greater pore size decreasing rate, a faster speed to reach a stable pore structure and a smaller pore size in the steady state.

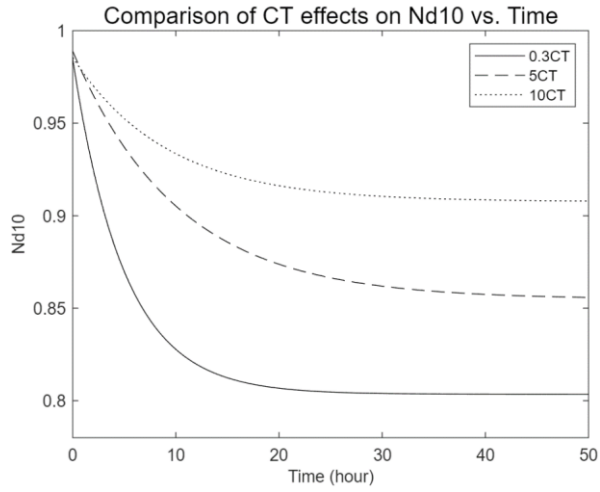


Figure 4.3.4 Comparison of CT effects on Nd10 vs. Time

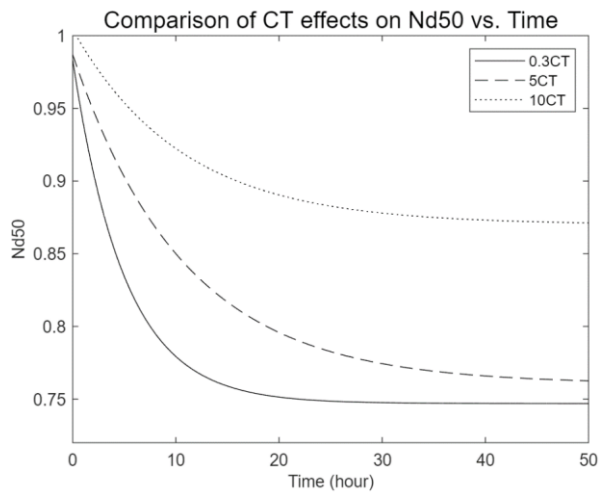


Figure 4.3.5 Comparison of CT effects on Nd50 vs. Time

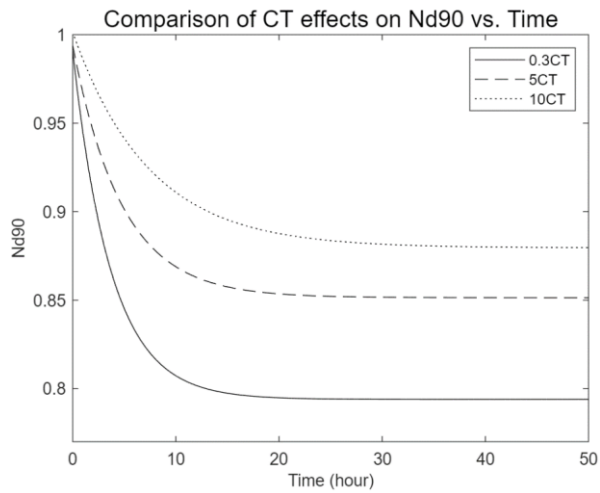


Figure 4.3.6 Comparison of CT effects on Nd90 vs. Time

#### 4.3.2 Modelling for recovery treatment

After cold temperature treatments, the recovery treatments were introduced with warm water temperatures at room temperature (RT) and 35°C (elevated temperature, ET) treatments. The data of d10, d50 and d90 were also scaling normalized as Nd10, Nd50 and Nd90 for modelling fitting. The fitting curves were categorized based on the cold temperature treatments.

The fitting curves for recovery treatment at RT and ET following 0.3CT treatment were presented in Figure 4.3.7. The elevated temperature recovered the membrane pore sizes much faster and to larger magnitudes than the recovery treatment at room temperature. The Nd10, Nd50 and Nd90 at the stable status after around 24 hours for RT treatment reached about 0.9 to 0.94, while they can be larger than 1 for ET treatment. In addition, Figure 4.3.8 and Figure 4.3.9 illustrate the modelling curves of the recovery treatments following 5CT and 10CT treatments. At the periods with flat curves, warm water at room temperature recovered the membrane pore to the larger Nd10, Nd50 and Nd90 at about 0.93 to 0.96 in the 5CT and 10CT runs than in the 0.3CT run. Although there were differences in the ending points of membrane pore sizes among CT batches, the ET recovery treatments prompted the normalized membrane pore sizes to the same horizon between 1.02 and 1.06, i.e., the pore sizes were larger than those of virgin membranes. No matter what cold temperature was used for treatment, 35°C/elevated temperature treatment was able to enlarge the membrane pores to above the pore sizes of the virgin membranes, while the room temperature treatment deficiently expanded the membrane pore to its original status.

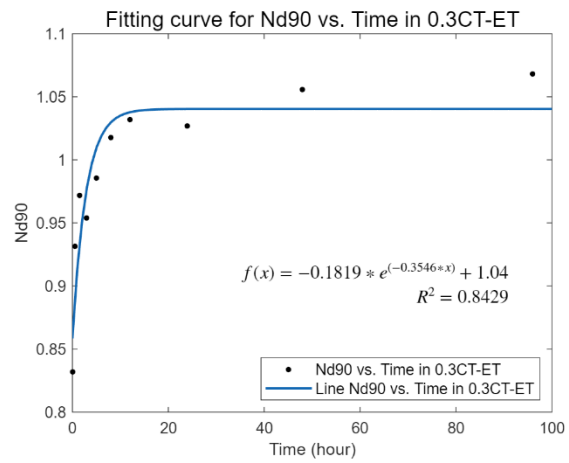
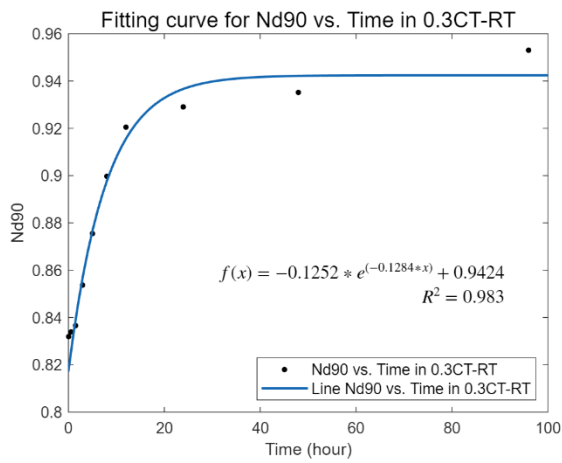
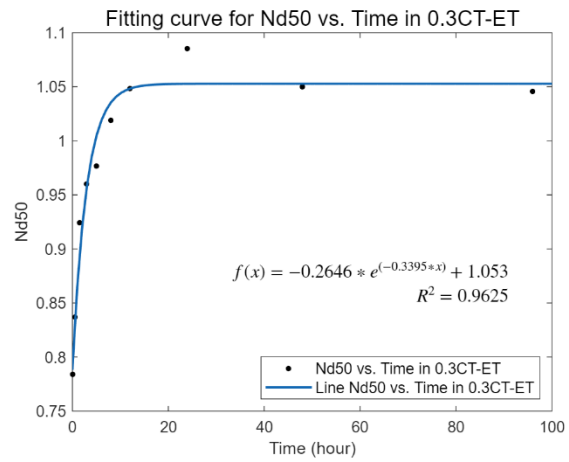
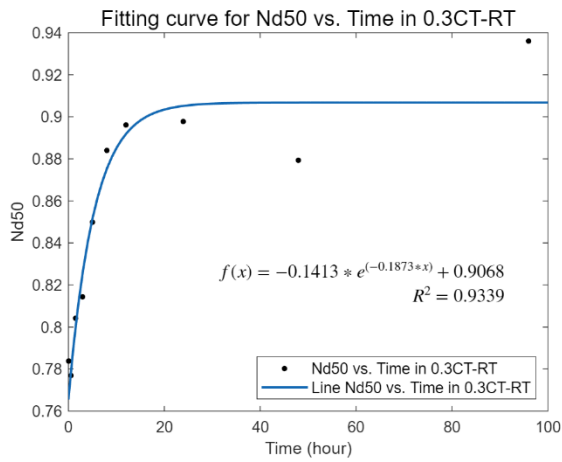
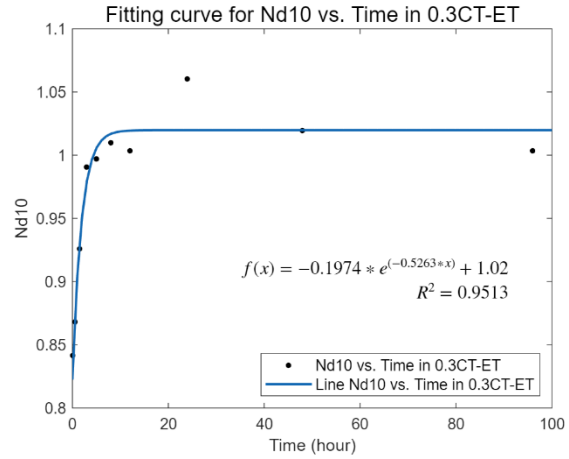
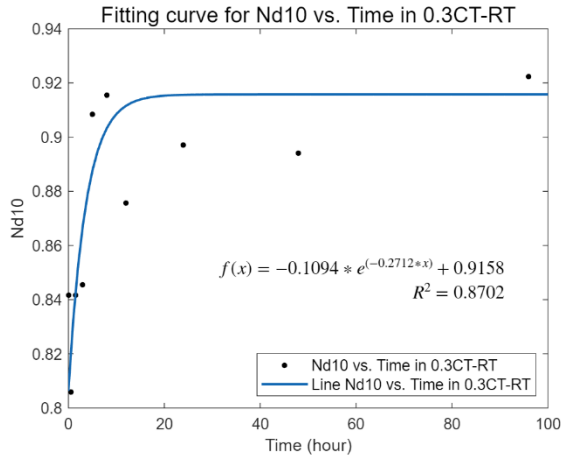


Figure 4.3.7 Fitting curves for Nd10, Nd50 and Nd90 versus time in recovery treatments in the subsequence of 0.3CT treatment

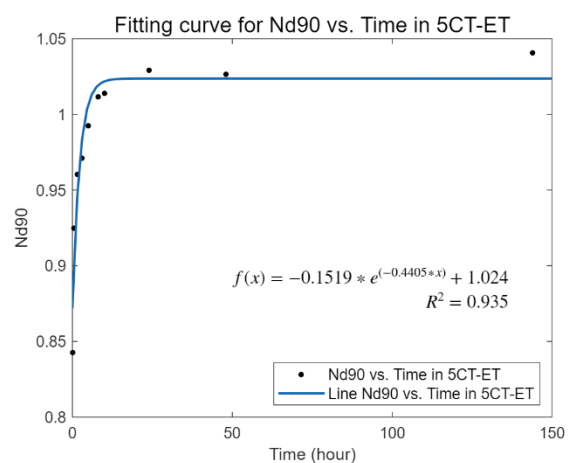
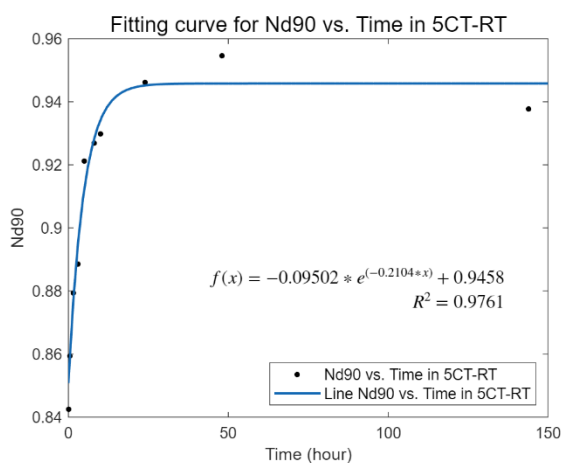
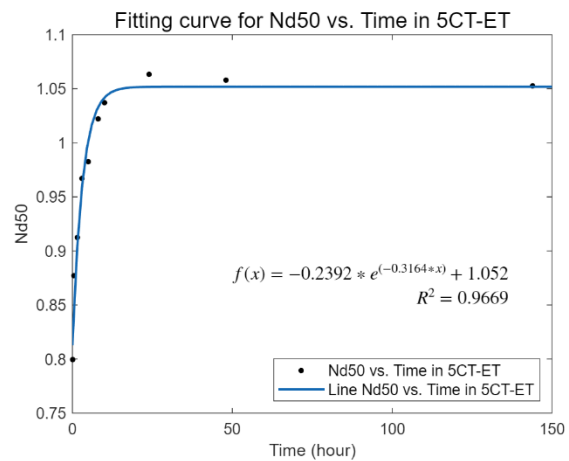
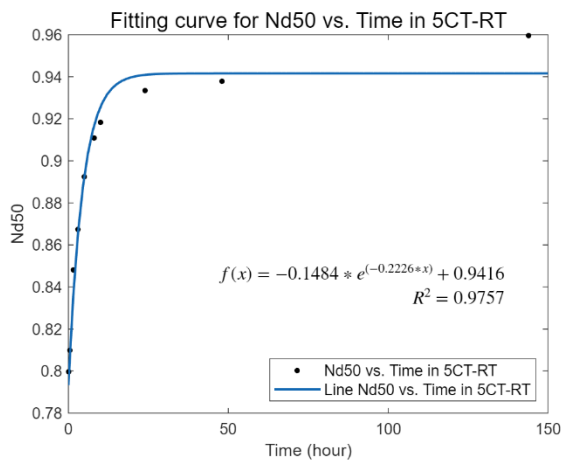
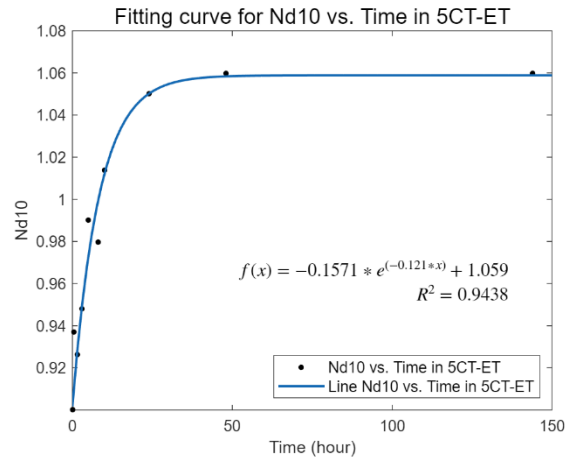
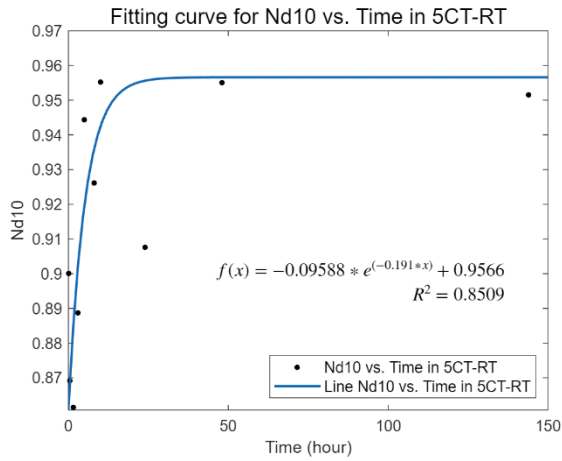


Figure 4.3.8 Fitting curves for Nd10, Nd50 and Nd90 versus time in recovery treatments in the subsequence of 5CT treatment

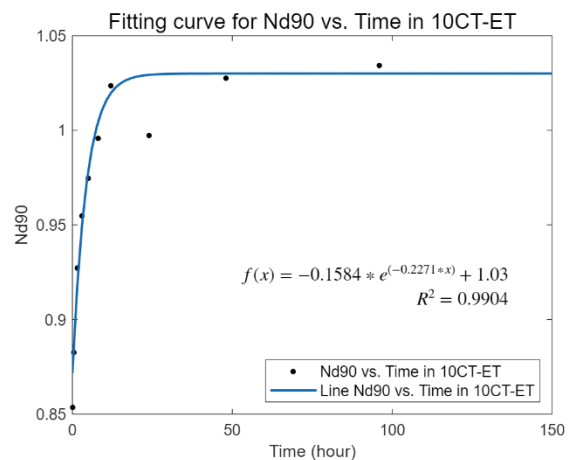
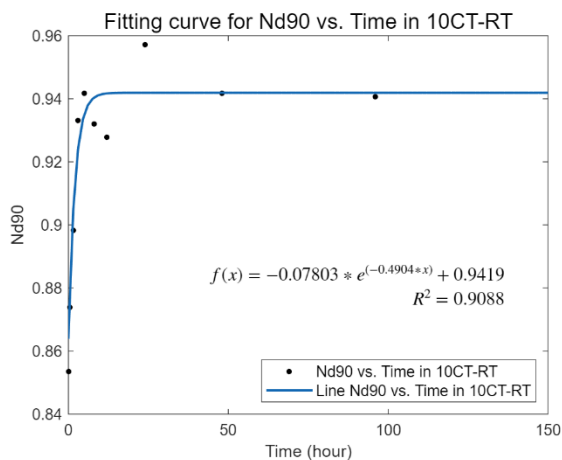
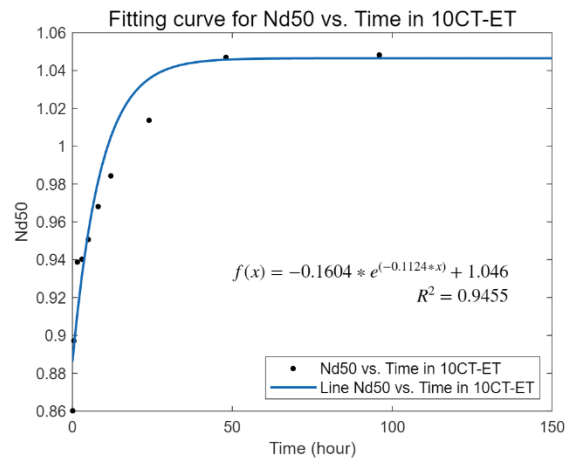
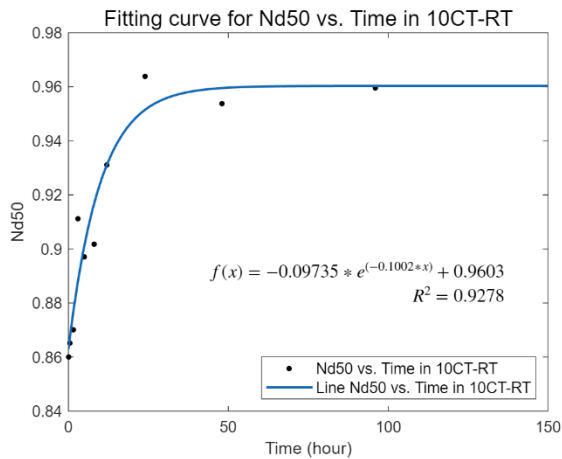
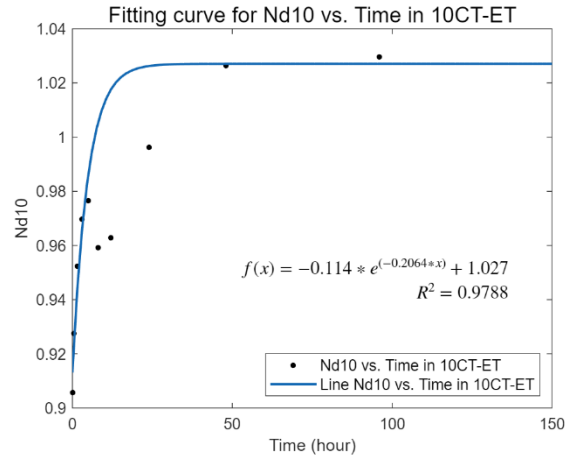
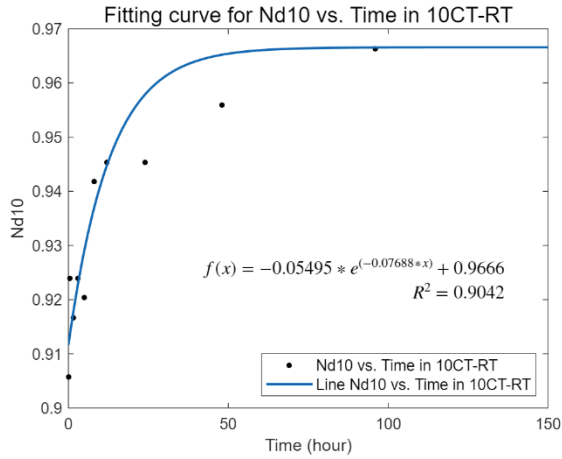


Figure 4.3.9 Fitting curves for Nd10, Nd50 and Nd90 versus time in recovery treatments in the subsequence of 10CT treatment

Warmwater treatments of the membrane following the cold temperature treatments were performed to investigate the recovery of membrane pore sizes. Figure 4.3.10 to Figure 4.3.12 present the comparisons of recovery temperature effects on Nd10, Nd50 and Nd90, respectively, of membrane treated under various cold temperatures. The duration of treatment time (x-axis) was chosen between 0 and 50 hours as there was no apparent fluctuation in pore size after 50 hours. In all the circumstances, the ET recovery treatments, i.e., submerging the membranes in 35°C water, were much more effective than the room temperature/RT (around 23°C) treatments, in which the membrane pore sizes were retrieved with higher recovering rates and maximum recovered pore sizes. Even after 50 hours of recovery treatment, the pore sizes of those membranes treated at room temperature/RT were unable to return to the original status, while in ET recovery treatment, it was found that some membrane pores were even larger than those of the virgin membranes. Figure 4.3.10 shows that the recovery treatments for those treated at 0.3CT had the smallest stable Nd10 than those after 5CT and 10CT treatments. However, after 0.3CT treatment, the increasing/recovery rates of Nd10 in the recovery treatment were larger, and the stabilization point occurred earlier than those treated at 5CT and 10CT. As shown in Figure 4.3.11, Nd10 of the membranes treated at 5°C and 10°C had comparable initial recovery rates during 35°C/ET treatment, but the stabilized membrane pore sizes at 0.3°C and 10°C had a similar Nd10, smaller than those treated at 5°C and larger than that of virgin membranes. While RT only recovered a few Nd10 for 10CT compared to those of 5CT, they incurred similar Nd10 after a long time of treatment.

Figure 4.3.11 revealed that the recovery treatments for 10CT always had lower recovery rates for Nd50 than those treated at 0.3CT and 5CT, and the stabilization points of pore sizes of ET treatments for 0.3CT, 5CT and 10CT were the same. In addition, the recovering rates and

plateau reaching speeds of Nd50 for 0.3CT and 5CT were close. The curves of 0.3CT-ET and 5CT-ET overlapped, though the curve of 5CT-RT was parallel and higher than that of 0.3CT-RT. Furthermore, Figure 4.3.12 shows a consistent ET recovering curve for Nd90 of 0.3CT, 5CT and 10CT. A similar pore size increasing rate, stable phase reaching time and stabilized pore size for Nd90 were found in the retrieving treatment of ET. Although the Nd90 was at the same level after prolonged time stabilizing, the retrieving rates and the time to reach the stabilization points were in the ascending orders of 0.3CT-RT, 5CT-RT and 10CT-RT.

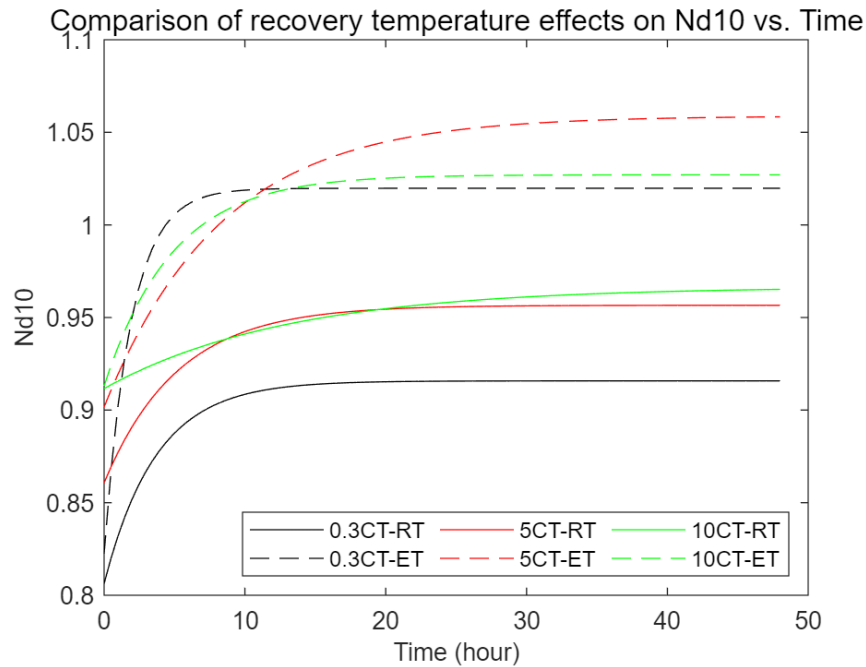


Figure 4.3.10 Comparison of recovery temperature effects on Nd10 vs. Time

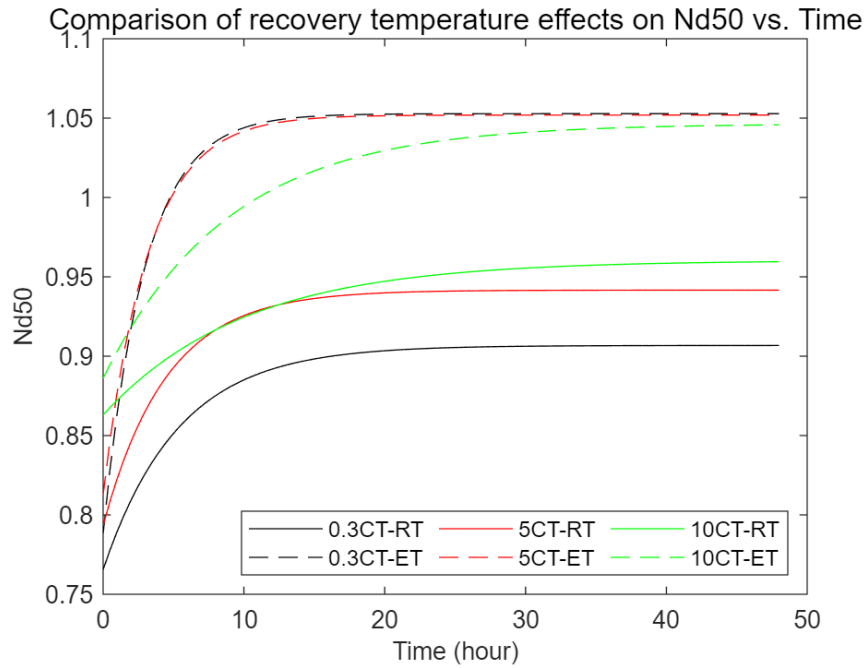


Figure 4.3.11 Comparison of recovery temperature effects on Nd50 vs. Time

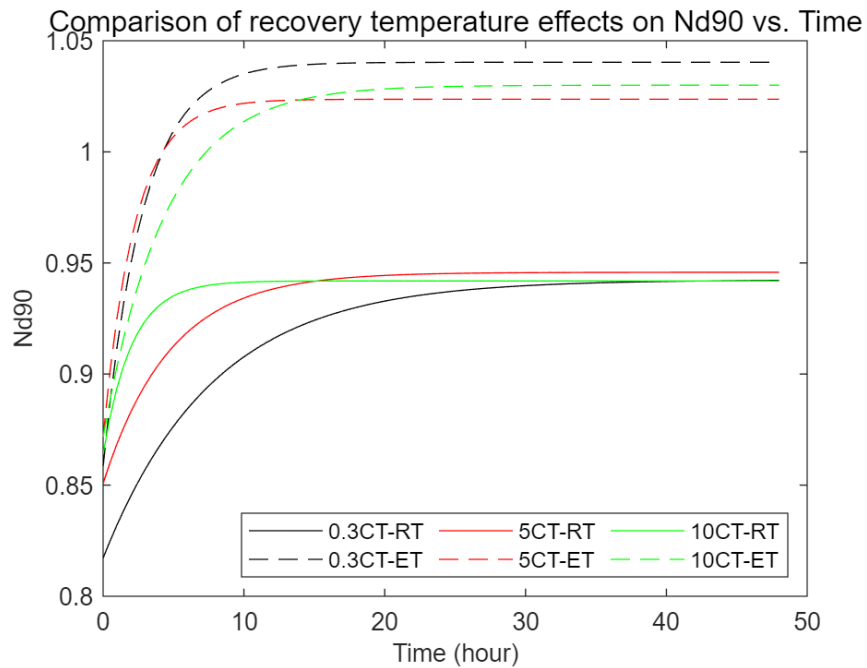


Figure 4.3.12 Comparison of recovery temperature effects on Nd90 vs. Time

## CHAPTER 5 Discussion

Experimental results from this study indicate that water temperature affected membrane pore sizes. Generally, temperature decrement incurs the declined membrane pore sizes, and increasing temperature counteracts it (Sharma et al. 2003, Dang et al. 2014, Xiao et al. 2014, Cui et al. 2017, Tikka et al. 2019, Xu et al. 2020). The morphology images shown in Figure 4.1.1 and Figure 4.1.2 of the membrane surfaces treated under different temperatures reveal the effects of temperatures on the membrane structure. The proportion of different pore sizes on an SEM image is the basis for comparing the distributions of membrane pore sizes. The visual reflection of the membrane surface submerged in the cold water with fewer large pores than the virgin membrane indicates that the cold temperature decreases the membrane pore sizes. On the contrary, fewer tiny pores on the membrane surface after warm water treatment at room temperature and 35°C (elevated temperature) imply that membrane pores shrank after cold temperature treatment could be remediated. However, the recovery treatment at room temperature insufficiently retrieved the membrane pores to the original sizes, while the membrane pore sizes after elevated temperature/35°C treatment were able to recover to or even surpass virgin membrane pore sizes. These conclusions accord with the thermal expansion with increasing temperature (Hughes et al. 2020).

The accumulative curves in Figure 4.1.3 and Figure 4.1.4 present the MPSD of each treatment condition on the last day of the treatment. It reveals that the treatments at 0.3°C and 5°C shrank the membrane pores more than 10°C. Although various cold temperatures led to different membrane pore size shrinkages, the recovery treatments tend to have a similar recovery efficiency after long-term treatments. The ET recovery had enlarged the membrane pore sizes above those of the virgin membrane, while the deficient remediation/recovery was observed with the RT recovery treatment. Thus, the warm water temperature used for recovery treatment is the primary factor for

the membrane in deciding MPSD. It suggests that room temperature cleaning for water treatment plants with cold source water would insufficiently restore the membrane pores to the original sizes, while cleaning and conditioning of membrane with warm water at 35°C could fully remediate the membrane pores to those of the virgin membrane or larger, which was also informed previously (Cui et al. 2017, Tikka et al. 2019).

Figure 4.2.1 elucidates the trend of how cold temperatures influence membrane pore sizes. The dramatic loss of membrane pore structure in the initial stage of CT treatments was disclosed through these plots. After 24 hours of cold temperature treatment, the membrane pore size change started stabilizing. However, some fluctuations in membrane pore sizes emerged after the 50 hours of treatments at 0.3°C and 5°C, which were potentially induced by the solute ( $\text{Na}_2\text{S}_2\text{O}_5$ ) precipitation on the membrane surface then unevenly covering the tiny pores during the long-period standing still (Tikka et al. 2019).

Additionally, Table 4.2.1 presents brief comparisons of the percentile pore sizes ( $d_{10}$ ,  $d_{50}$  and  $d_{90}$ ) after 5 and 24 hours of cold temperature treatments. After 24 hours of the cold temperature treatments, the medium membrane pore diameters of  $d_{50}$  decreased 25%, 20% and 11% for 0.3CT, 5CT and 10CT, respectively. Dang et al. (2014) reported a 13% of increment of a nanofiltration membrane pore size with increasing temperature from 20°C to 40°C, while Xu et al. (2020) claimed that changing temperatures from 25°C to 5°C would decrease 10% to 14% of average pore sizes with two kinds of nanofiltration membranes. The decreasing rates of the membrane pore diameters in the initial five hours of 0.3CT and 5CT treatments were twice those during 5 to 24 hours, while for 10CT, the decreasing rates of the membrane pore diameters between 0 to 5 hours and 5 to 24 hours were the same. This phenomenon indicates that the initial five hours of cold temperature treatments contributed primarily to the membrane pore shrinkage and had

higher decreasing rates than the subsequent 19 hours of treatment time. Both Figure 4.2.1 and Table 4.2.1 explain that the decreasing rates of membrane pore sizes were reduced over the treatment time.

The correlation between the pore sizes and operating conditions of membrane filtration could be explained by Darcy's Law (Atangana 2018):

$$Q = \frac{-kA(p_b - p_a)}{\mu L} \quad (2)$$

Where Q — Total discharge flow, m<sup>3</sup>/s;

k — Intrinsic permeability, m<sup>2</sup>;

A — Cross-sectional area, m<sup>2</sup>;

(p<sub>b</sub> - p<sub>a</sub>) — Total pressure drop, Pa;

μ — Dynamic water viscosity, Pa × s;

L — Thickness of the membrane, m.

Song et al. (2022) indicated that although some early studies claimed that the intrinsic membrane permeability “k” was proportional to the square of the membrane average diameter, these studies dramatically overestimated “k” for asymmetric membranes, and “k” is only about the linear correlation with the pore diameter on membrane surfaces. Changing in membrane temperatures from 23°C to below 10°C, the membrane cross-sectional area “A” and the membrane thickness “L” stay unchanged; the dynamic water viscosity “μ” is a specific value in a fixed temperature; the intrinsic permeability of the membrane “k” however is decreasing caused by the decreasing membrane pore diameters. Therefore, to maintain the total discharge flow “Q”, the filtration pressure “-(p<sub>b</sub> - p<sub>a</sub>)” must be increased. In this situation, the water treatment plant with the cold-source water would have to consume more energy to elevate the filtration pressure and guarantee the water supply due to the membrane pore shrinkage. In addition, “μ” will increase to 190% at

0.3°C, 163% at 5°C and 140% at 10°C compared to at 23°C, which causes “Q” to be 52%, 61% and 71%, respectively, with unchanged filtration pressure. When the cold-water treatment had been in progress for 24 hours, “k” was 75%, 80% and 89% of that in the room temperature for 0.3CT, 5CT and 10CT, respectively, according to the linear relationship between “k” and the average pore diameter. Thus, combining the effects of the decreasing water viscosity and membrane pore size, membrane filtration would encounter 61%, 51% and 36% of flow rate reductions with the influent temperatures at 0.3°C, 5°C and 10°C, respectively, as compared to the summertime if the same trans-membrane pressure is applied. The loss of membrane structure in cold regions during winter is still a crucial problem in elevating membrane filtration pressure, though the viscosity increment of influent water plays a dominant role.

In Table 4.2.2, the changing rates of the membrane pore sizes in the initial five hours of cold treatments reveal that the lower water temperatures caused the faster membrane pore size decrements at the beginning of the treatments. Additionally, the ANOVA test presented in Table 4.2.3 shows that cold temperature treatments at various cold temperatures had different effects on membrane pore sizes at a 95% confidence interval. Most of the student t-test results in Table 4.2.3 indicated significant differences among diverse cold temperature effects, including the comparison with virgin membrane, while the membrane pore sizes of d10 and d90 were not significantly distinctive in the treatments at 5°C and 10°C.

While the viscosity of the influent water could not be altered resulting from that changing influent temperature is implausible, it is essential to control the membrane properties to the optimal condition. Therefore, cleaning the membrane with warm water is likely to be a sound approach to counteract and recover the membrane structure loss in cold temperatures. Figure 4.2.2 to Figure 4.2.4 show the effects of different recovery temperatures on the membrane pore sizes following

various cold temperature treatments. The recoveries in room temperature (RT) and elevated temperature (ET) were validated in offsetting the membrane pore shrinkage induced by cold temperatures. The membrane pore sizes in recovering processes performed an inverse propensity as the cooling processes. According to the plots, a period of 24 hours was needed for membrane pore sizes to stabilize. ET recovery was performed with extraordinarily high efficiency than RT recovery. The membrane pore sizes in ET remediations could surpass the threshold of virgin membranes within a 12-hour treatment, while RT recovery insufficiently retrieved the membrane pore sizes to their original status even with prolonged treatment time.

The particular time points chosen in Figure 4.2.4 present the features of the recovery treatments. The initial five hours of the recovery treatments were dramatically efficient and recovered more pore diameters than the following 19 hours. The beginning periods of the recovery treatments were similar to the reverse of cold temperature treatments. The fast membrane pore size changing rates at the initial few hours of cold or recovering treatments were potentially due to the significant temperature differences in the early stage of the treatments. Based on Fourier's law of Heat Conduction (Arfken et al. 1984), the higher temperature gradient caused higher heat transfer and pore deformation rates on the membrane surface. Furthermore, the recovery treatments with ET retrieved higher proportions of membrane pore sizes than with RT because ET was higher than RT and created higher temperature differences toward post-cooling samples. Therefore, according to Fourier's law, recovery at ET acquired more significant temperature gaps leading to faster pore size increment and larger stable pore sizes than RT.

According to recovery data listed in Figure 4.2.4, the medium membrane pore sizes of d50 for 0.3CT, 5CT and 10CT were 85%, 89% and 89% of the virgin membranes after five hours of RT recovery treatments and 90%, 93% and 96% after 24 hours of the treatments. The d50 for ET

recoveries following 0.3CT, 5CT and 10CT treatments were 98%, 98% and 95% at five hours and 109%, 107% and 101% at 24 hours compared to the virgin membranes' pore sizes. Therefore, referring to Darcy's Law in Equation (2) and the correlation between medium pore diameter and permeability, the proportions of medium membrane pore size to the virgin membrane are exactly the flow recovery rates for the water treatment plants. RT recovery only could restore about 93% of the filtration efficiency after five-hour treatment, and extended recovering time only had a minor contribution to increasing membrane performance. However, almost complete recovery of the membrane structures was reached after five hours of 35°C treatment, and extending treatment time to 24 hours could lead to extra productivity than the virgin membrane.

The increasing rates of membrane pore sizes in the initial five hours of recovery treatments shown in Table 4.2.5 present the drastic distinction in pore size remediation between room temperature and 35°C treatments. The twice or higher pore size expending rates with ET treatment than RT treatment at the initial period indicated that the recovery treatment at 35°C was significantly more effective than at room temperature. Furthermore, Table 4.2.6 shows the ANOVA results among the membrane pore sizes of virgin membranes and recoveries at room temperature and 35°C, and recovery temperatures had significant influences on membrane pore sizes at a 95% confidence interval. The student t-test results in Table 4.2.6 discloses that room temperature recovery had different effectiveness compared to 35°C recovery. In combining Figure 4.2.2 to Figure 4.2.4, it could be concluded that recovery at 35°C was significantly more effective than at room temperature. In addition, Table 4.2.6 shows that the null hypotheses with all the t-tests in comparing virgin membrane pore sizes and the membrane pore sizes after room temperature recovery indicated the non-negligible gaps for RT treatment to enlarge membrane pore size to the original state. In testing the differences between the membrane pore sizes of d10,

d50 and d90 at 35°C recovery and virgin membrane, besides the rejected alternative hypotheses of student t-test for d10 and d50 at 10CT-ET, other accepted alternative hypotheses illustrate that the ET recovery treatment either retrieved the shrinking membrane pore sizes to the same level as virgin membranes or expended the pore sizes to larger than the original sizes.

According to the scatter diagrams, the membrane pore sizes versus treatment time could be curve fitted and modelled. After the scaling normalization and modelling for the membrane pore sizes of d10, d50 and d90, the data could be compared across treatment groups. The exponential correlation was selected as the optimal model, though the exponential function has no minimum and maximum value. Thus, this study only implemented the model as curve predictions for the initial periods of different temperature treatments. If future studies require the extremums, the exponential model has a convergence value that could seem like the minimum/maximum/stabilized pore sizes with an infinite treatment time. Figure 4.3.4 to Figure 4.3.6 show a tendency in which colder temperatures decreased the membrane pore sizes at higher rates to smaller pore sizes. In addition, cold source water temperatures could alter membrane pore size distribution, and the extent of decrease of membrane pore sizes was not linearly correlated to the source water temperatures.

The models for recovery treatments shown in Figure 4.3.10 to Figure 4.3.12 predicted a significant distinction between the room and elevated temperature recoveries. The ET recovery at 35°C performed dramatically higher efficiencies than the RT recovery. ET could expand the membrane pore sizes to the virgin membrane status, while RT could not fully recover the membrane structure. The beginning points of recovery treatment following 0.3CT, 5CT and 10CT were in ascending order. For RT recovery, Nd10 and Nd50 presented a similar trend: the increasing rates for the membrane pore size during the initial treatment period were in descending order of

0.3CT-RT, 5CT-RT and 10CT-RT, and the stable values were in ascending order of them. However, the situation for Nd90 was slightly different, in which 0.3CT-RT, 5CT-RT and 10CT-RT had the same increasing rate of membrane pore sizes and reached the same plateau pore size. For ET recovery, the pore size increasing rates of Nd50 and Nd90 were close for 0.3CT-ET and 5CT-ET and larger than those for 10CT-ET, though 0.3CT-ET, 5CT-ET and 10CT-ET recoveries elevated membrane pore sizes of Nd10, Nd50 and Nd90 to the same level with extended treatment time. Except for the Nd10 in the 5CT-ET treatment, the results for other recovering conditions could be explained by the thermal expansion caused by temperature differences. For the Nd10 in 5CT-ET treatment, the pore size in the stable phase was larger than 0.3CT-ET and 10CT-ET, which could result from the microbial growth and tiny pore plugging by extracellular substances after a long time (20 hours) of the elevated temperature (35°C) warming environment.

In general, the membrane pore sizes declined rapidly during the beginning of the cold temperatures, which is not ideal for membrane water treatment plants operating in cold climates. Fortunately, warm water recovery treatments could effectively remediate the lost membrane structure. An elevated temperature is recommended for the recovery procedure since it is much more efficient than room temperature in rebuilding membrane structures.

## CHAPTER 6 Conclusion

This study researched the dynamic change of membrane pore size distribution in cold water treatment and warm water recovery processes. The primary conclusions are summarized as follows:

1. Cold temperatures could affect membrane pore sizes;
2. The colder water temperatures, the faster the membrane pores shrank, and the more magnitudes of membrane pore sizes decreased;
3. 0.3°C, 5°C and 10°C caused the membrane medium diameter losses of 25%, 20% and 11%, respectively, after 24 hours compared to the virgin membranes at room temperature;
4. The recovery treatment at 35°C induced a more significant membrane pore size increasing rate than at room temperature;
5. Room temperature was not able to fully recover the membrane pore structure with prolonged time, while elevated temperature recovery could retrieve the membrane pore sizes close to the virgin membrane states after six hours.

Although this study provided new information regarding the dynamic changes in the membrane surface's structure in cold temperatures, the structure variation inside the membrane has not been explored yet. Besides, how the dynamic membrane structure changes affect the permeability in cold environments also needs to be examined. Such research could provide valuable information for designing and operating membrane plants in cold regions.

## REFERENCE

- Ahmad, A.L., Mat Yasin, N.H., Derek, C.J.C., and Lim, J.K. 2014. Chemical cleaning of a cross-flow microfiltration membrane fouled by microalgal biomass. *Journal of the Taiwan Institute of Chemical Engineers*, **45**(1): 233–241. doi:10.1016/j.jtice.2013.06.018.
- Al-Amoudi, A., and Lovitt, R.W. 2007. Fouling strategies and the cleaning system of NF membranes and factors affecting cleaning efficiency. *Journal of Membrane Science*, **303**(1–2): 4–28. doi:10.1016/j.memsci.2007.06.002.
- Al-Amoudi, A., Williams, P., Mandale, S., and Lovitt, R.W. 2007. Cleaning results of new and fouled nanofiltration membrane characterized by zeta potential and permeability. *Separation and Purification Technology*, **54**(2): 234–240. doi:10.1016/j.seppur.2006.09.014.
- Al-Amoudi, A.S. 2010. Factors affecting natural organic matter (NOM) and scaling fouling in NF membranes: A review. *Desalination*, **259**(1–3): 1–10. doi:10.1016/j.desal.2010.04.003.
- Al-Amri, A., Salim, M.R., and Aris, A. 2010. The effect of different temperatures and fluxes on the performance of membrane bioreactor treating synthetic-municipal wastewater. *Desalination*, **259**(1–3): 111–119. doi:10.1016/j.desal.2010.04.023.
- Almecija, M.C., Martinez-Ferez, A., Guadix, A., Paez, M.P., and Guadix, E.M. 2009. Influence of the cleaning temperature on the permeability of ceramic membranes. *Desalination*, **245**(1–3): 708–713. doi:10.1016/j.desal.2009.02.041.
- Alresheedi, M.T., and Basu, O.D. 2019. Effects of feed water temperature on irreversible fouling of ceramic ultrafiltration membranes. *Journal of Water Process Engineering*, **31**: 100883. doi:10.1016/j.jwpe.2019.100883.
- Alresheedi, M.T., and Basu, O.D. 2020. Interplay of water temperature and fouling during ceramic ultrafiltration for drinking water production. *Journal of Environmental Chemical Engineering*, **8**(5): 104354. doi:10.1016/j.jece.2020.104354.
- Arfken, G.B., Griffing, D.F., Kelly, D.C., and Priest, J. 1984. chapter 23 - HEAT TRANSFER. *In International Edition University Physics. Edited by G.B. Arfken, D.F. Griffing, D.C. Kelly, and J. Priest. Academic Press. pp. 430–443.*
- Ashfaq, M.Y., Al-Ghouti, M.A., Da'na, D.A., Qiblawey, H., and Zouari, N. 2020. Investigating the effect of temperature on calcium sulfate scaling of reverse osmosis membranes using FTIR, SEM-EDX and multivariate analysis. *Science of The Total Environment*, **703**: 134726. doi:10.1016/j.scitotenv.2019.134726.
- Atangana, A. 2018. Chapter 2 - Principle of Groundwater Flow. *In Fractional Operators with Constant and Variable Order with Application to Geo-Hydrology. Edited by A. Atangana. Academic Press. pp. 15–47.*
- Bassyouni, M., Abdel-Aziz, M.H., Zoromba, M.Sh., Abdel-Hamid, S.M.S., and Drioli, E. 2019. A review of polymeric nanocomposite membranes for water purification. *Journal of Industrial and Engineering Chemistry*, **73**: 19–46. doi:10.1016/j.jiec.2019.01.045.
- van den Brink, P., Satpradit, O.-A., van Bentem, A., Zwijnenburg, A., Temmink, H., and van Loosdrecht, M. 2011. Effect of temperature shocks on membrane fouling in membrane bioreactors. *Water Research*, **45**(15): 4491–4500. doi:10.1016/j.watres.2011.05.046.
- Bruggen, B.V.D., Vandecasteele, C., Gestel, T.V., Doyen, W., and Leysen, R. 2003. A review of pressure-driven membrane processes in wastewater treatment and drinking water production. *Environmental Progress*, **22**(1): 46–56. doi:10.1002/ep.670220116.

- Canada, H. 2004. From Source To Tap - The Multi-Barrier Approach To Safe Drinking Water. navigation page. Available from <https://www.canada.ca/en/health-canada/services/environmental-workplace-health/reports-publications/water-quality/source-multi-barrier-approach-safe-drinking-water-health-canada.html>. [accessed 24 August 2022].
- Chae, S.R., and Shin, H.S. 2007. Characteristics of simultaneous organic and nutrient removal in a pilot-scale vertical submerged membrane bioreactor (VSMBR) treating municipal wastewater at various temperatures. *Process Biochemistry*, **42**(2): 193–198. doi:10.1016/j.procbio.2006.07.033.
- Chen, J.P., Kim, S.L., and Ting, Y.P. 2003. Optimization of membrane physical and chemical cleaning by a statistically designed approach. *Journal of Membrane Science*, **219**(1–2): 27–45. doi:10.1016/S0376-7388(03)00174-1.
- Childress, A.E., Le-Clech, P., Daugherty, J.L., Chen, C., and Leslie, G.L. 2005. Mechanical analysis of hollow fiber membrane integrity in water reuse applications. *Desalination*, **180**(1–3): 5–14. doi:10.1016/j.desal.2004.12.026.
- Chun, Y., Mulcahy, D., Zou, L., and Kim, I. 2017. A Short Review of Membrane Fouling in Forward Osmosis Processes. *Membranes*, **7**(2): 30. doi:10.3390/membranes7020030.
- Cui, L., Goodwin, C., Gao, W., and Liao, B. 2017. Effect of cold water temperature on membrane structure and properties. *Journal of Membrane Science*, **540**: 19–26. doi:10.1016/j.memsci.2017.06.037.
- Cui, X., and Choo, K.-H. 2014. Natural Organic Matter Removal and Fouling Control in Low-Pressure Membrane Filtration for Water Treatment. *Environmental Engineering Research*, **19**(1): 1–8. doi:10.4491/eer.2014.19.1.001.
- Dang, H.Q., Price, W.E., and Nghiem, L.D. 2014. The effects of feed solution temperature on pore size and trace organic contaminant rejection by the nanofiltration membrane NF270. *Separation and Purification Technology*, **125**: 43–51. doi:10.1016/j.seppur.2013.12.043.
- Dashtban Kenari, S.L., and Barbeau, B. 2016. Understanding ultrafiltration fouling of ceramic and polymeric membranes caused by oxidized iron and manganese in water treatment. *Journal of Membrane Science*, **516**: 1–12. doi:10.1016/j.memsci.2016.06.003.
- Ding, J., Wang, S., Xie, P., Zou, Y., Wan, Y., Chen, Y., and Wiesner, M.R. 2020. Chemical cleaning of algae-fouled ultrafiltration (UF) membrane by sodium hypochlorite (NaClO): Characterization of membrane and formation of halogenated by-products. *Journal of Membrane Science*, **598**(117662): 1–10. doi:10.1016/j.memsci.2019.117662.
- Edzwald, J.K. 2011. *Water Quality & Treatment: A Handbook on Drinking Water*, Sixth Edition. McGraw-Hill Education.
- Elcik, H., Fortunato, L., Alpatova, A., Soukane, S., Orfi, J., Ali, E., AlAnsary, H., Leiknes, T., and Ghaffour, N. 2020. Multi-effect distillation brine treatment by membrane distillation: Effect of antiscalant and antifoaming agents on membrane performance and scaling control. *Desalination*, **493**: 114653. doi:10.1016/j.desal.2020.114653.
- Fan, G., Su, Z., Lin, R., Lin, X., Xu, R., and Chen, W. 2016. Influence of Membrane Materials and Operational Modes on the Performance of Ultrafiltration Modules for Drinking Water Treatment. *International Journal of Polymer Science*, **2016**: 1–8. doi:10.1155/2016/6895235.
- Farahbakhsh, K., and Smith, D.W. 2006. Membrane filtration for cold regions – impact of cold water on membrane integrity monitoring tests. *Journal of Environmental Engineering and Science*, **5**(Supplement 1): S69–S75. doi:10.1139/s06-037.

- Farhat, N.M., Vrouwenvelder, J.S., van Loosdrecht, M.C.M., Bucs, S.S., and Staal, M. 2016. Effect of water temperature on biofouling development in reverse osmosis membrane systems. *Water research*, **103**: 149–159. doi:10.1016/j.watres.2016.07.015.
- Gao, W., Liang, H., Ma, J., Han, M., Chen, Z., Han, Z., and Li, G. 2011a. Membrane fouling control in ultrafiltration technology for drinking water production: A review. *Desalination*, **272**(1–3): 1–8. doi:10.1016/j.desal.2011.01.051.
- Gao, W.J., Leung, K.T., Qin, W.S., and Liao, B.Q. 2011b. Effects of temperature and temperature shock on the performance and microbial community structure of a submerged anaerobic membrane bioreactor. *Bioresource Technology*, **102**(19): 8733–8740. doi:10.1016/j.biortech.2011.07.095.
- Gao, W.J., Qu, X., Leung, K.T., and Liao, B.Q. 2012. Influence of temperature and temperature shock on sludge properties, cake layer structure, and membrane fouling in a submerged anaerobic membrane bioreactor. *Journal of Membrane Science*, **421–422**: 131–144. doi:10.1016/j.memsci.2012.07.003.
- Ghosh, K., and Schnitzer, M. 1980. MACROMOLECULAR STRUCTURES OF HUMIC SUBSTANCES. *Soil Science*, **129**(5): 266–276. doi:10.1097/00010694-198005000-00002.
- Gu, Y., Wang, Y.-N., Wei, J., and Tang, C.Y. 2013. Organic fouling of thin-film composite polyamide and cellulose triacetate forward osmosis membranes by oppositely charged macromolecules. *Water Research*, **47**(5): 1867–1874. doi:10.1016/j.watres.2013.01.008.
- Hofs, B., Ogier, J., Vries, D., Beerendonk, E.F., and Cornelissen, E.R. 2011. Comparison of ceramic and polymeric membrane permeability and fouling using surface water. *Separation and Purification Technology*, **79**(3): 365–374. doi:10.1016/j.seppur.2011.03.025.
- Hong, S., and Elimelech, M. 1997. Chemical and physical aspects of natural organic matter (NOM) fouling of nanofiltration membranes. *Journal of Membrane Science*, **132**(2): 159–181. doi:10.1016/S0376-7388(97)00060-4.
- Howe, K., Marwah, A., Chiu, K., and Adham, S. 2007. Effect of membrane configuration on bench-scale MF and UF fouling experiments. *Water Research*, **41**(17): 3842–3849. doi:10.1016/j.watres.2007.05.025.
- Hube, S., Lee, S., Chong, T.H., Brynjólfsson, S., and Wu, B. 2022. Biocarriers facilitated gravity-driven membrane filtration of domestic wastewater in cold climate: Combined effect of temperature and periodic cleaning. *Science of The Total Environment*, **833**: 155248. doi:10.1016/j.scitotenv.2022.155248.
- Hube, S., Wang, J., Sim, L.N., Chong, T.H., and Wu, B. 2021. Direct membrane filtration of municipal wastewater: Linking periodical physical cleaning with fouling mechanisms. *Separation and Purification Technology*, **259**: 118125. doi:10.1016/j.seppur.2020.118125.
- Hughes, A.J., Mallick, T.K., and O'Donovan, T.S. 2020. Investigation of the Effects of Temperature on the Microstructure of PTFE Microfiltration Membranes Under Membrane Distillation Conditions. *Journal of Advanced Thermal Science Research*, **7**: 11–21. doi:10.15377/2409-5826.2020.07.2.
- Jackson, P.E. 2001. Determination of inorganic ions in drinking water by ion chromatography. *TrAC Trends in Analytical Chemistry*, **20**(6–7): 320–329. doi:10.1016/S0165-9936(01)00070-X.
- Jawor, A., and Hoek, E.M.V. 2009. Effects of feed water temperature on inorganic fouling of brackish water RO membranes. *Desalination*, **235**(1–3): 44–57. doi:10.1016/j.desal.2008.07.004.

- Jin, X., Jawor, A., Kim, S., and Hoek, E.M.V. 2009. Effects of feed water temperature on separation performance and organic fouling of brackish water RO membranes. *Desalination*, **239**(1–3): 346–359. doi:10.1016/j.desal.2008.03.026.
- Jönsson, C., and Jönsson, A.-S. 1995. Influence of the membrane material on the adsorptive fouling of ultrafiltration membranes. *Journal of Membrane Science*, **108**(1–2): 79–87. doi:10.1016/0376-7388(95)00144-X.
- Jung, C.-W., Son, H.-J., and Kang, L.-S. 2006. Effects of membrane material and pretreatment coagulation on membrane fouling: fouling mechanism and NOM removal. *Desalination*, **197**(1–3): 154–164. doi:10.1016/j.desal.2005.12.022.
- Karunakaran, A., Mungray, A.A., and Garg, M.C. 2021. Effects of temperature, pH, feed, and fertilizer draw solution concentrations on the performance of forward osmosis process for textile wastewater treatment. *Water Environment Research*, **93**(10): 2329–2340. doi:10.1002/wer.1607.
- Kim, K.-J., and Jang. 2016. Fouling characteristics of NOM during the ceramic membrane microfiltration process for water treatment. *Desalination and Water Treatment*, **57**(19): 9034–9042. doi:10.1080/19443994.2015.1057035.
- Kim, Y., Lee, S., Shon, H.K., and Hong, S. 2015. Organic fouling mechanisms in forward osmosis membrane process under elevated feed and draw solution temperatures. *Desalination*, **355**: 169–177. doi:10.1016/j.desal.2014.10.041.
- Krzeminski, P., Iglesias-Obelleiro, A., Madebo, G., Garrido, J.M., van der Graaf, J.H.J.M., and van Lier, J.B. 2012. Impact of temperature on raw wastewater composition and activated sludge filterability in full-scale MBR systems for municipal sewage treatment. *Journal of Membrane Science*, **423–424**: 348–361. doi:10.1016/j.memsci.2012.08.032.
- Laiarinandrasana, L., Besson, J., Lafarge, M., and Hochstetter, G. 2009. Temperature dependent mechanical behaviour of PVDF: Experiments and numerical modelling. *International Journal of Plasticity*, **25**(7): 1301–1324. doi:10.1016/j.ijplas.2008.09.008.
- Lee, A., Elam, J.W., and Darling, S.B. 2016. Membrane materials for water purification: design, development, and application. *Environmental Science: Water Research & Technology*, **2**(1): 17–42. The Royal Society of Chemistry. doi:10.1039/C5EW00159E.
- Lee, S., and Lee, C.-Ha. 2000. Effect of operating conditions on CaSO<sub>4</sub> scale formation mechanism in nanofiltration for water softening. *Water Research*, **34**(15): 3854–3866. doi:10.1016/S0043-1354(00)00142-1.
- Li, Y., Zhang, W., Zhang, X., Chen, C., and Wang, J. 2010. Characterization of fouling in immersed polyvinylidene fluoride hollow fibre membrane ultrafiltration by particles and natural organic matter. *Desalination and Water Treatment*, **18**(1–3): 309–314. doi:10.5004/dwt.2010.1814.
- Liao, B.Q., Bagley, D.M., Kraemer, H.E., Leppard, G.G., and Liss, S.N. 2004. A Review of Biofouling and its Control in Membrane Separation Bioreactors. *Water Environment Research*, **76**(5): 425–436. doi:10.2175/106143004X151527.
- Lintzos, L., Chatzikonstantinou, K., Tzamtzis, N., and Malamis, S. 2018. Influence of the Backwash Cleaning Water Temperature on the Membrane Performance in a Pilot SMBR Unit. *Water*, **10**(3): 238. doi:10.3390/w10030238.
- Liu, C., Chen, L., Zhu, L., Wu, Z., Hu, Q., and Pan, M. 2019. The effect of feed temperature on biofouling development on the MD membrane and its relationship with membrane performance: An especial attention to the microbial community succession. *Journal of Membrane Science*, **573**: 377–392. doi:10.1016/j.memsci.2018.12.003.

- Liu, D., Li, D., Du, D., Zhao, X., Qin, A., Li, X., and He, C. 2015. Antifouling PVDF membrane with hydrophilic surface of terry pile-like structure. *Journal of Membrane Science*, **493**: 243–251. doi:10.1016/j.memsci.2015.07.005.
- Liu, J., Yang, E., Huang, T., Wang, Z., and Dong, B. 2020. Correlation of chemically irreversible fouling with organic constituents of feed water during membrane filtration. *Colloids and Surfaces A: Physicochemical and Engineering Aspects*, **597**(124790): 1–8. doi:10.1016/j.colsurfa.2020.124790.
- Lyko, S., Wintgens, T., Alhalbouni, D., Baumgarten, S., Tacke, D., Drensla, K., Janot, A., Dott, W., Pinnekamp, J., and Melin, T. 2008. Long-term monitoring of a full-scale municipal membrane bioreactor—Characterisation of foulants and operational performance. *Journal of Membrane Science*, **317**(1–2): 78–87. doi:10.1016/j.memsci.2007.07.008.
- Ma, B., Ding, Y., Wang, B., Qi, Z., Bai, Y., Liu, R., Liu, H., and Qu, J. 2020. Influence of sedimentation with pre-coagulation on ultrafiltration membrane fouling performance. *Science of The Total Environment*, **708**: 134671. doi:10.1016/j.scitotenv.2019.134671.
- Ma, C., Yu, S., Shi, W., Heijman, S.G.J., and Rietveld, L.C. 2013a. Effect of different temperatures on performance and membrane fouling in high concentration PAC-MBR system treating micro-polluted surface water. *Bioresource technology*, **141**: 19–24. doi:10.1016/j.biortech.2013.02.025.
- Ma, Z., Wen, X., Zhao, F., Xia, Y., Huang, X., Waite, D., and Guan, J. 2013b. Effect of temperature variation on membrane fouling and microbial community structure in membrane bioreactor. *Bioresource Technology*, **133**: 462–468. doi:10.1016/j.biortech.2013.01.023.
- Madaeni, S.S., and Samieirad, S. 2010. Chemical cleaning of reverse osmosis membrane fouled by wastewater. *Desalination*, **257**(1–3): 80–86. doi:10.1016/j.desal.2010.03.002.
- Matyka, M., Khalili, A., and Koza, Z. 2008. Tortuosity-porosity relation in porous media flow. *Physical Review E*, **78**(2): 026306. doi:10.1103/PhysRevE.78.026306.
- Metsämuuronen, S., Sillanpää, M., Bhatnagar, A., and Mänttari, M. 2014. Natural Organic Matter Removal from Drinking Water by Membrane Technology. *Separation & Purification Reviews*, **43**(1): 1–61. doi:10.1080/15422119.2012.712080.
- Mi, B., and Elimelech, M. 2008. Chemical and physical aspects of organic fouling of forward osmosis membranes. *Journal of Membrane Science*, **320**(1–2): 292–302. doi:10.1016/j.memsci.2008.04.036.
- Moreau, A.A., Ratkovich, N., Nopens, I., and van der Graaf, J.H.J.M. 2009. The (in)significance of apparent viscosity in full-scale municipal membrane bioreactors. *Journal of Membrane Science*, **340**(1–2): 249–256. doi:10.1016/j.memsci.2009.05.049.
- Morrow, C.P., McGaughey, A.L., Hübel, S.R., and Childress, A.E. 2018. Submerged or sidestream? The influence of module configuration on fouling and salinity in osmotic membrane bioreactors. *Journal of Membrane Science*, **548**: 583–592. doi:10.1016/j.memsci.2017.11.030.
- Nguyen, T., Roddick, F., and Fan, L. 2012. Biofouling of Water Treatment Membranes: A Review of the Underlying Causes, Monitoring Techniques and Control Measures. *Membranes*, **2**(4): 804–840. doi:10.3390/membranes2040804.
- Nyström, M., Ruohomäki, K., and Kaipia, L. 1996. Humic acid as a fouling agent in filtration. *Desalination*, **106**(1): 79–87. doi:10.1016/S0011-9164(96)00095-1.
- Pearce, G. 2007. Introduction to membranes: Filtration for water and wastewater treatment. *Filtration & Separation*, **44**(2): 24–27. doi:10.1016/S0015-1882(07)70052-6.

- Peña, N., Gallego, S., del Vigo, F., and Chesters, S.P. 2013. Evaluating impact of fouling on reverse osmosis membranes performance. *Desalination and Water Treatment*, **51**(4–6): 958–968. doi:10.1080/19443994.2012.699509.
- Plevri, A., Mamais, D., and Noutsopoulos, C. 2021. Anaerobic MBR technology for treating municipal wastewater at ambient temperatures. *Chemosphere*, **275**: 129961. doi:10.1016/j.chemosphere.2021.129961.
- Pramanik, B.K., Pramanik, S.K., Sarker, D.C., and Suja, F. 2017. Impact of ozonation, anion exchange resin and UV/H<sub>2</sub>O<sub>2</sub> pre-treatments to control fouling of ultrafiltration membrane for drinking water treatment. *Environmental Technology*, **38**(11): 1383–1389. doi:10.1080/09593330.2016.1228701.
- Rabuni, M.F., Nik Sulaiman, N.M., Aroua, M.K., Yern Chee, C., and Awanis Hashim, N. 2015. Impact of in situ physical and chemical cleaning on PVDF membrane properties and performances. *Chemical Engineering Science*, **122**: 426–435. doi:10.1016/j.ces.2014.09.053.
- Randtke, S.J., and Horsley, M.B. 2012. *Water Treatment Plant Design, Fifth Edition*. McGraw-Hill Education.
- Rong, C., Wang, T., Luo, Z., Hu, Y., Kong, Z., Qin, Y., Hanaoka, T., Ito, M., Kobayashi, M., and Li, Y.-Y. 2022. Pilot plant demonstration of temperature impacts on the methanogenic performance and membrane fouling control of the anaerobic membrane bioreactor in treating real municipal wastewater. *Bioresource Technology*, **354**: 127167. doi:10.1016/j.biortech.2022.127167.
- Rosenberger, S., Laabs, C., Lesjean, B., Gnirss, R., Amy, G., Jekel, M., and Schrotter, J.-C. 2006. Impact of colloidal and soluble organic material on membrane performance in membrane bioreactors for municipal wastewater treatment. *Water Research*, **40**(4): 710–720. doi:10.1016/j.watres.2005.11.028.
- de la Rubia, Á., Rodríguez, M., León, V.M., and Prats, D. 2008. Removal of natural organic matter and THM formation potential by ultra- and nanofiltration of surface water. *Water Research*, **42**(3): 714–722. doi:10.1016/j.watres.2007.07.049.
- Sarihan, A., and Eren, E. 2017. Novel high performed and fouling resistant PSf/ZnO membranes for watertreatment. *Membrane Water Treatment*, **8**(6): 563–574. doi:10.12989/mwt.2017.8.6.563.
- Shao, S., Fu, W., Li, X., Shi, D., Jiang, Y., Li, J., Gong, T., and Li, X. 2019. Membrane fouling by the aggregations formed from oppositely charged organic foulants. *Water research*, **159**: 95–101. doi:10.1016/j.watres.2019.05.004.
- Sharma, R.R., Agrawal, R., and Chellam, S. 2003. Temperature effects on sieving characteristics of thin-film composite nanofiltration membranes: pore size distributions and transport parameters. *Journal of Membrane Science*, **223**(1–2): 69–87. doi:10.1016/S0376-7388(03)00310-7.
- Shirazi, S., Lin, C.-J., and Chen, D. 2010. Inorganic fouling of pressure-driven membrane processes — A critical review. *Desalination*, **250**(1): 236–248. doi:10.1016/j.desal.2009.02.056.
- Simon, A., Price, W.E., and Nghiem, L.D. 2013. Impact of chemical cleaning on the nanofiltration of pharmaceutically active compounds (PhACs): The role of cleaning temperature. *Journal of the Taiwan Institute of Chemical Engineers*, **44**(5): 713–723. doi:10.1016/j.jtice.2013.01.030.

- Song, S., Rong, L., Dong, K., Liu, X., Le-Clech, P., and Shen, Y. 2022. Pore-scale numerical study of intrinsic permeability for fluid flow through asymmetric ceramic microfiltration membranes. *Journal of Membrane Science*, **642**: 119920. doi:10.1016/j.memsci.2021.119920.
- Srisurichan, S., Jiratananon, R., and Fane, A.G. 2005. Humic acid fouling in the membrane distillation process. *Desalination*, **174**(1): 63–72. doi:10.1016/j.desal.2004.09.003.
- Sun, W., Liu, J., Chu, H., and Dong, B. 2013. Pretreatment and Membrane Hydrophilic Modification to Reduce Membrane Fouling. *Membranes*, **3**(3): 226–241. doi:10.3390/membranes3030226.
- Tao, C., Parker, W., and Bérubé, P. 2021. Assessing the role of cold temperatures on irreversible membrane permeability of tertiary ultrafiltration treating municipal wastewater. *Separation and Purification Technology*, **278**: 119556. doi:10.1016/j.seppur.2021.119556.
- Tao, C., Parker, W., and Bérubé, P. 2022. Evaluation of the impact of SBR operating temperature and filtration temperature on fouling of membranes used for tertiary treatment. *Separation and Purification Technology*, **294**: 121194. doi:10.1016/j.seppur.2022.121194.
- Tikka, A., Gao, W., and Liao, B. 2019. Reversibility of membrane performance and structure changes caused by extreme cold water temperature and elevated conditioning water temperature. *Water research*, **151**: 260–270. doi:10.1016/j.watres.2018.12.047.
- Wan, P., Zhang, Z., and Deng, B. 2019. Photocatalytic Polysulfone Hollow Fiber Membrane with Self-Cleaning and Antifouling Property for Water Treatment. *Industrial & Engineering Chemistry Research*, **58**(8): 3339–3348. doi:10.1021/acs.iecr.8b05783.
- Wang, H., Ma, D., Shi, W., Yang, Z., Cai, Y., and Gao, B. 2021. Formation of disinfection by-products during sodium hypochlorite cleaning of fouled membranes from membrane bioreactors. *Frontiers of Environmental Science & Engineering*, **15**(5): 102. doi:10.1007/s11783-021-1389-3.
- Wang, L., Wang, X., and Fukushi, K. 2008. Effects of operational conditions on ultrafiltration membrane fouling. *Desalination*, **229**(1–3): 181–191. doi:10.1016/j.desal.2007.08.018.
- Wang, Z., Wu, Z., and Tang, S. 2010. Impact of Temperature Seasonal Change on Sludge Characteristics and Membrane Fouling in a Submerged Membrane Bioreactor. *Separation Science and Technology*, **45**(7): 920–927. doi:10.1080/01496391003656974.
- Woo, Y.C., Lee, J.J., Oh, J.S., Jang, H.J., and Kim, H.S. 2013. Effect of chemical cleaning conditions on the flux recovery of fouled membrane. *Desalination and Water Treatment*, **51**(25–27): 5268–5274. doi:10.1080/19443994.2013.768754.
- Xiao, L., Isner, A., Waldrop, K., Saad, A., Takigawa, D., and Bhattacharyya, D. 2014. Development of bench and full-scale temperature and pH responsive functionalized PVDF membranes with tunable properties. *Journal of Membrane Science*, **457**: 39–49. doi:10.1016/j.memsci.2014.01.033.
- Xie, M., Price, W.E., Nghiem, L.D., and Elimelech, M. 2013. Effects of feed and draw solution temperature and transmembrane temperature difference on the rejection of trace organic contaminants by forward osmosis. *Journal of Membrane Science*, **438**: 57–64. doi:10.1016/j.memsci.2013.03.031.
- Xu, P., Bellona, C., and Drewes, J.E. 2010. Fouling of nanofiltration and reverse osmosis membranes during municipal wastewater reclamation: Membrane autopsy results from pilot-scale investigations. *Journal of Membrane Science*, **353**(1–2): 111–121. doi:10.1016/j.memsci.2010.02.037.

- Xu, R., Zhou, M., Wang, H., Wang, X., and Wen, X. 2020. Influences of temperature on the retention of PPCPs by nanofiltration membranes: Experiments and modeling assessment. *Journal of Membrane Science*, **599**: 117817. doi:10.1016/j.memsci.2020.117817.
- Yamamura, H., Okimoto, K., Kimura, K., and Watanabe, Y. 2014. Hydrophilic fraction of natural organic matter causing irreversible fouling of microfiltration and ultrafiltration membranes. *Water Research*, **54**: 123–136. doi:10.1016/j.watres.2014.01.024.
- Yang, Y., Qiao, S., Zhou, J., and Quan, X. 2019. A novel porous-carbon-based hollow fiber membrane with electrochemical reduction mediated by in-situ hydroxyl radical generation for fouling control and water treatment. *Applied Catalysis B: Environmental*, **255**(117772): 1–7. doi:10.1016/j.apcatb.2019.117772.
- Yoon, Y., Amy, G., Cho, J., and Her, N. 2005. Effects of retained natural organic matter (NOM) on NOM rejection and membrane flux decline with nanofiltration and ultrafiltration. *Desalination*, **173**(3): 209–221. doi:10.1016/j.desal.2004.06.213.
- Yuan, W., and Zydney, A.L. 1999. Humic acid fouling during microfiltration. *Journal of Membrane Science*, **157**(1): 12. doi:10.1016/s0376-7388(98)00329-9.
- Yuan, W., and Zydney, A.L. 2000. Humic Acid Fouling during Ultrafiltration. *Environmental Science & Technology*, **34**(23): 5043–5050. doi:10.1021/es0012366.
- Zhao, S., and Zou, L. 2011. Effects of working temperature on separation performance, membrane scaling and cleaning in forward osmosis desalination. *Desalination*, **278**(1–3): 157–164. doi:10.1016/j.desal.2011.05.018.
- Zheng, W., Wen, X., Zhang, B., and Qiu, Y. 2019. Selective effect and elimination of antibiotics in membrane bioreactor of urban wastewater treatment plant. *Science of The Total Environment*, **646**: 1293–1303. doi:10.1016/j.scitotenv.2018.07.400.
- Zhu, C., Liu, G., Han, K., Ye, H., Wei, S., and Zhou, Y. 2017. One-step facile synthesis of graphene oxide/TiO<sub>2</sub> composite as efficient photocatalytic membrane for water treatment: Crossflow filtration operation and membrane fouling analysis. *Chemical Engineering and Processing - Process Intensification*, **120**: 20–26. doi:10.1016/j.cep.2017.06.012.
- Zularisam, A.W., Ismail, A.F., and Salim, R. 2006. Behaviours of natural organic matter in membrane filtration for surface water treatment — a review. *Desalination*, **194**(1–3): 211–231. doi:10.1016/j.desal.2005.10.030.